Hydrodynamic lubrication of soft solids

Bennett, Alan

HYDRODYNAMIC LUBRICATION OF SOFT SOLIDS

by

ALAN BENNETT

Thesis submitted for the

Degree of Master of Science in the University of Durham

Engineering Science Department,
July 1969.

ABSTRACT

This investigation is concerned with the lubrication of soft solids under pure sliding.

The design of the experimental rig is described in detail. Very slight modification was required to ensure the correct functioning of the rig and the results obtained are compared with those of a fairly simple theory.

Particular reference is made to the functioning of human joints, and it is noted that even with severe deterioration of the articular cartilage, human joints can function satisfactorily for considerable periods of time.

The results of the investigation show clearly that the manner in which human joints behave can be applied to soft bearings generally. A soft bearing reduces friction drastically at low speeds and the frictional coefficients of human joints and those obtained from the experimental rig are comparable.

The soft layer, exceeding a minimum thickness, has little effect upon the performance of the bearing generally but enables hydrodynamic lubrication to persist to very low sliding speeds. The effect of the surface roughness of the compliant sliding surfaces is evident in the form of increased friction in the boundary and in the hydrodynamic lubrication regimes.

A major discrepancy between experimental results and theory has still to be satisfactorily explained but further experiments may solve this problem.

One achievement of the investigation was the successful application of the "backward method" of solving the elasto-hydrodynamic problem. It is hoped that this may be useful in other applications.

ACKNOWLEDGMENTS

I thank Professor G. R. Higginson, B.Sc., Ph.D., for his guidance and help during the last two years and for the benefit of his wealth of experience in the field of lubrication.

Thanks are also rendered to other members of the staff and the technicians for their valued assistance, in particular Mr. B. Scurr for his craftsmanship during the manufacture of the rig.

I am grateful to I.C.I. for furnishing free of charge the elastic specimens (E.V.A. Polythene Copolymer) used in my experiments.

I thank Mr. R. J. Boness for putting at my disposal results from his own thesis which is not yet published.

I thank the Ministry of Defence for allowing me leave and financial assistance over my period of research.

Lastly, thanks to Mr. R. Norman, B.Sc., for providing the initial step in the inspiration of the "backward solution to the elasto-hydrodynamic problem."

CONTENTS

CHAPTER 1

Introduction

The hydrodynamic lubrication of soft solids, or of a combination of hard and soft solids, occurs in a range of important situations: in journal bearings, from the long-established ships' stern tubes, to the compliant surfaces in gas bearings of recent origin; in a wide variety of seals, usually made of synthetic rubber; in human (and other animal) joints where the articular cartilage provides a much softer load-bearing surface than the bone on which it is mounted.

The mechanism known as elastohydrodynamic lubrication is active to some extent in all the above situations, but in a different manner from that in the more deeply-studied applications such as rolling-contact bearings, where load is transmitted between metal surfaces at very high pressure. The high pressure greatly increases the viscosity of the mineral oil normally used as the lubricant. This viscosity increase is decisive in effecting full-film lubrication. The pressures in the lubricant film are relatively small with soft surfaces, but, because of the low stiffness of the solids, elastic deformation dominates the lubrication mechanism. Pressure variations in the engineering applications do not sensibly affect the viscosity, although it is now thought that in human joints a quite different mechanism, solute enrichment, causes an increase in viscosity when high loads are applied.

The behaviour of soft journal bearings was first examined experimentally by Fogg and Hunswicks as far back as 1937. The first theoretical paper was by Higginson (1965), but since then a series of much more comprehensive papers has been published by Brighton, Hooke and O'Donoghue (1967). The mode of operation of the wide range of seals is still something of a mystery, but their mechanisms are receiving much attention (Jagger, 1967).

The mechanical behaviour of human joints has been the subject of study by the medical profession for many years, and has recently attracted the attention of members of other disciplines, notably engineers and physicists. The investigation described in this thesis arose from a contribution by Mr. J. Charnley, a Consultant Orthopaedic Surgeon, to the Symposium on Lubrication and Wear in Living and Artificial Human Joints held by the Institution of Mechanical Engineers in 1967. In the discussion Mr. Charnley noted that the surfaces in a human joint can degenerate significantly (down to about 1 mm thickness) and continue to function satisfactorily for long periods of time before they become painful and show arthritic symptons. The aim of the present investigation is to find out whether this persistance of correct functioning is peculiar to the extremely complex (and living) human joint, or general to bearings with soft surfaces.

It was decided at the outset that a simple two-dimensional model should be used, consisting of a rotating steel cylinder loaded against a stationary plane with a soft surface layer. No attempt was made to simulate the human joint, as articular cartilage is porous, with very non-linear stress/strain/liquid content relationships and synovial fluid is non-Newtonian and thixotropic. A simple soft solid was required for the surface layer, with a low modulus so that elastic effects would be present at low loads, and preferably transparent so that the appearance of the contact zone could be studied and possibly film thickness measured eventually.

I.C.I. Plastics Division suggested and generously supplied, free of any charge, enough samples of a suitable material for the investigation.

Serious deterioration of a joint will presumably show itself in increasing stiffness (i.e. friction) until the thickness of articular cartilage eventually reaches zero over a finite area, accompanied by severe pain.

The main feature of the experiments therefore was to measure friction variation with a decrease in the thickness of the surface layer. Rather than wearing the surface, the thickness was artificially reduced by using layers of different thickness.

The lubrication regime in human joints still retains a few of its secrets but it is clear that in a healthy joint the friction is of a magnitude associated with hydrodynamic lubrication in inanimate mechanisms. It was decided therefore to operate primarily in hydrodynamic conditions over a wide range of load and speed, and in particular to locate the lower limit of full-film lubrication. With a full film between the solids the only significant properties of the soft layer would be the mechanical (primarily stress/strain) and to a small extent the thermal properties. Considerations of surface adhesion and interfacial shear strength would not arise. Since the soft solid was to be stationary, and the experiment essentially steady-state, the hysteresis effects in the polymer would also be suppressed.

The frictional behaviour of polymers has received much attention, but in all the references consulted by the author either the specimens have been unlubricated or the rubbing speeds so low as to preclude full hydrodynamic lubrication.

Denny (1953) investigated the friction of rubber with lubrication at very low speed, 10^{-4} m/s. Pascoe and Tabor (1956) and King and Tabor (1953) looked into the friction of polymer on polymer (like on like) over a very wide range of loads, but again at low speeds. They found a characteristic coefficient of friction of roughly 0.5 for all the materials except P.T.F.E. which had a value of 0.1. Cohen and Tabor (1966) examined the effects of various lubricants on the friction of nylon and polythene at speeds below those necessary to establish full-film lubrication.

Watanabe, Karasawa and Matsubara (1968) measured the coefficient of friction of steel on nylon, without lubricant, over a range of loads and speeds (up to 1 m/s). They found the value rose above the characteristic 0.5 as load increased, to a maximum of about 2.0, before falling again to roughly 0.5. The load at which the maximum occurred depended on the rubbing speed. They attributed this behaviour to the rise in temperature due to frictional heating.

The experiments described in this thesis are therefore quite different from those above, except when hydrodynamic lubrication fails.

CHAPTER 2

Experimental Apparatus

The experimental apparatus was designed with two main purposes. Firstly to measure the tangential forces acting on the cylinder and plane and secondly to observe the pressure and cavitation zones at various loads and speeds.

A double roller and plane system was adopted to avoid any non-normal application of loads. The consequences of non-normal applied loads are shown in Fig. 2.1. The experimental rig and the layout of drive, gear-box and rig itself are shown in Figs. 2.2. and 2.3. respectively.

The rig as shown in Fig. 2.3. was suitable for measuring the tangential forces. In order to observe the pressure and cavitation zones it was necessary to modify the rig as shown in Fig. 2.4. It was possible to view the pressure and cavitation zones as the soft surface layer of the plane was manufactured from E.V.A./polythene copolymer which is reasonably transparent in thicknesses up to 0.2 inches.

The design of the rig and its important features will be described in detail in this section together with descriptions of other equipment used in the experimental work.

Friction-measuring Rig

A drawing of the rig is shown in Fig. 2.3. and two photographs showing front and rear views of the rig are shown in Figs. 2.5. and 2.6.

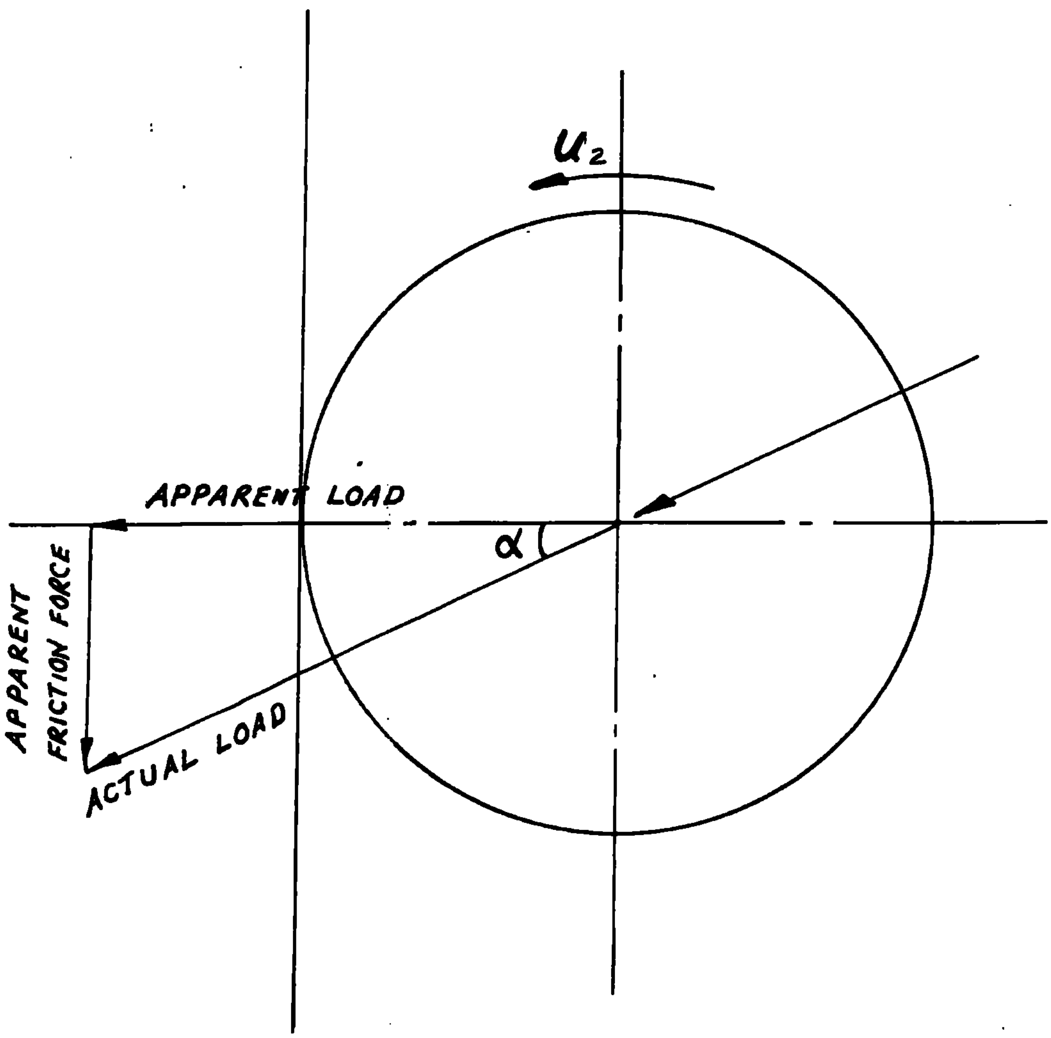

FIG. 2. 1. CONSEQUENCE OF NON-NORMAL APPLIED LOAD.

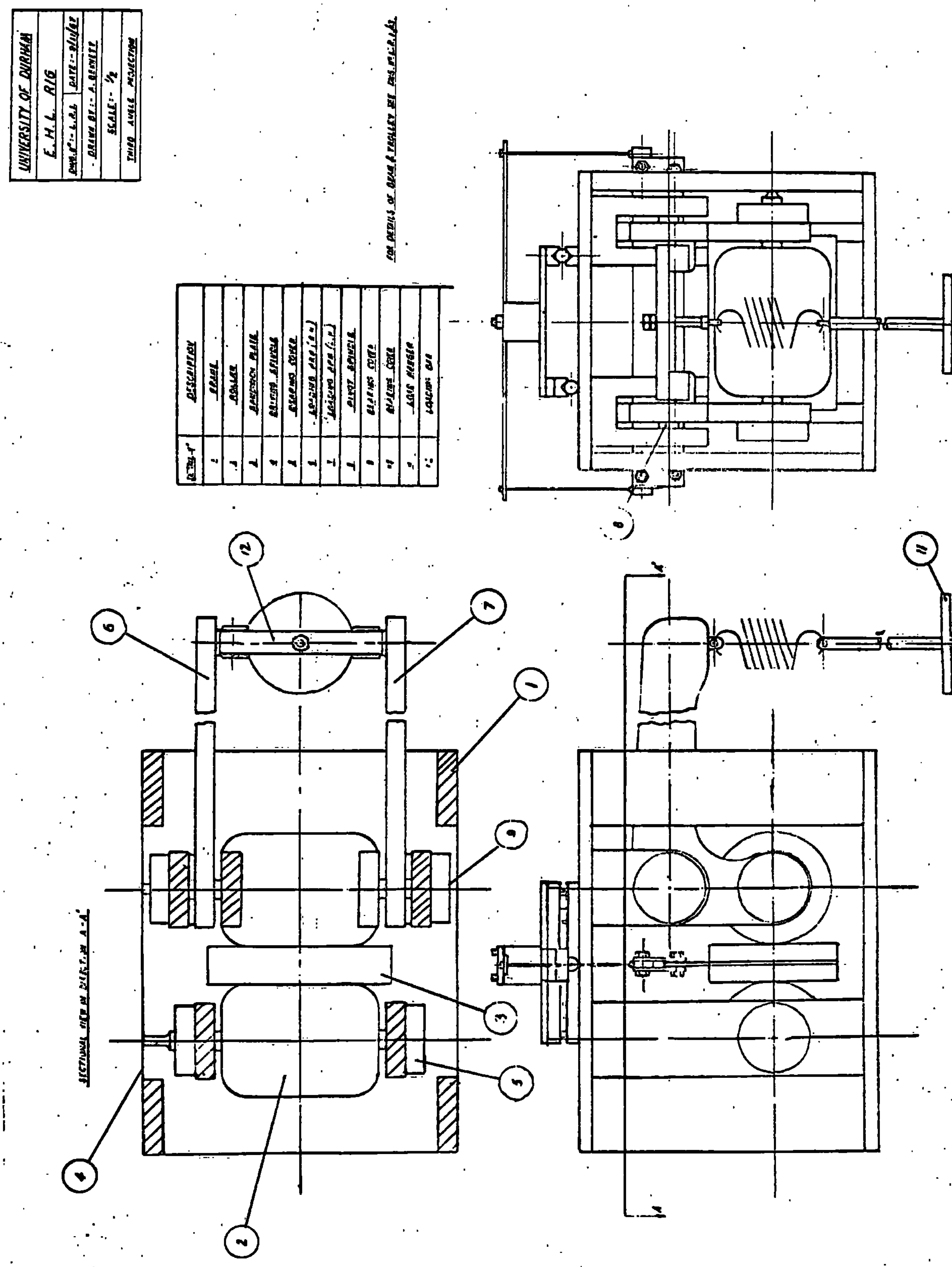

FIG. 2.2. RIG ASSEMBLY

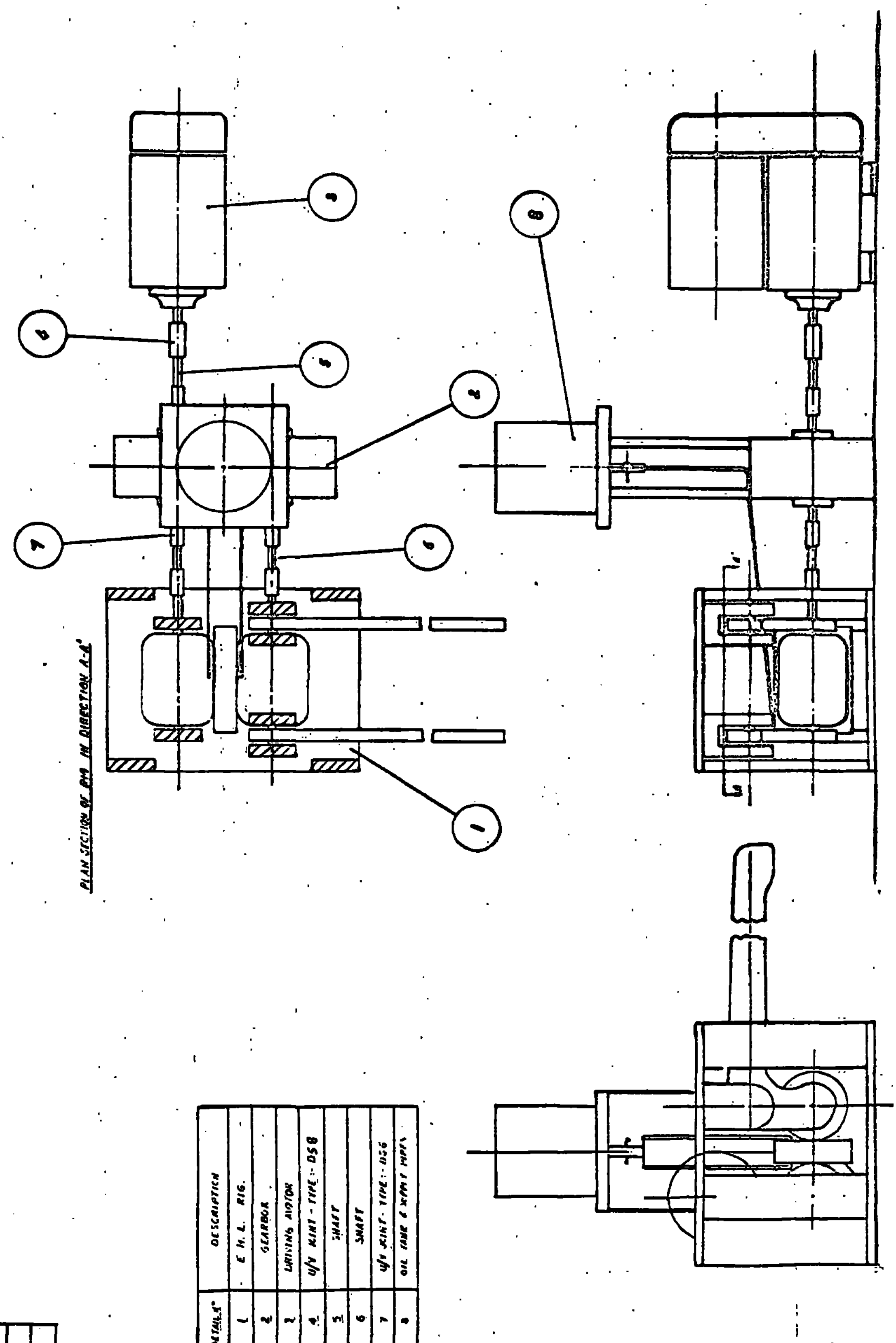

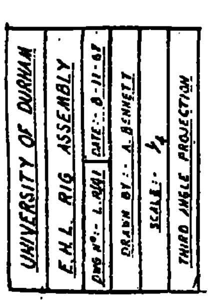

FIG. 2.3. LAYOUT OF RIG, GEARBOX AND DRIVE.

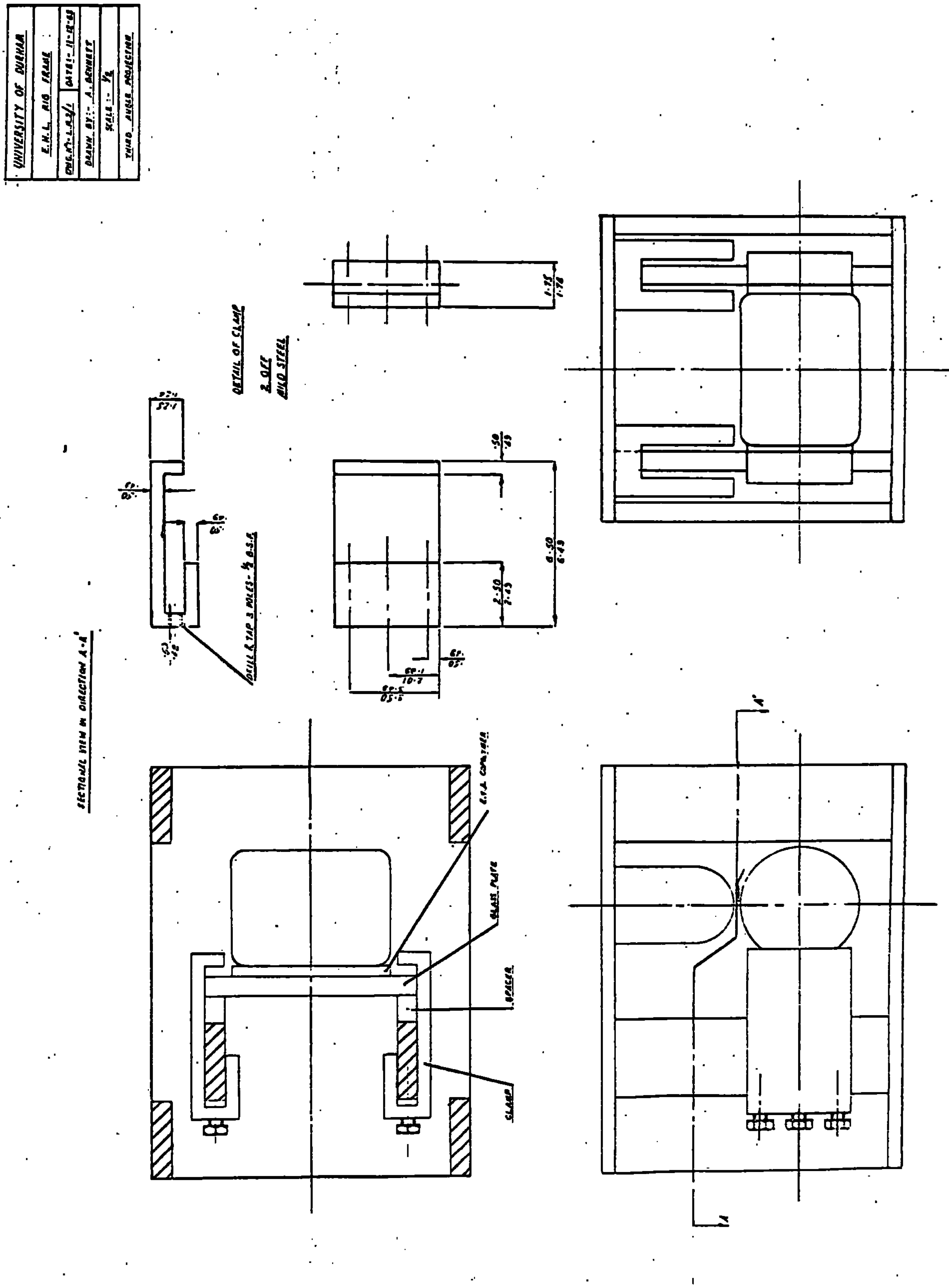

FIG. 2.4. MODIFIED RIG.

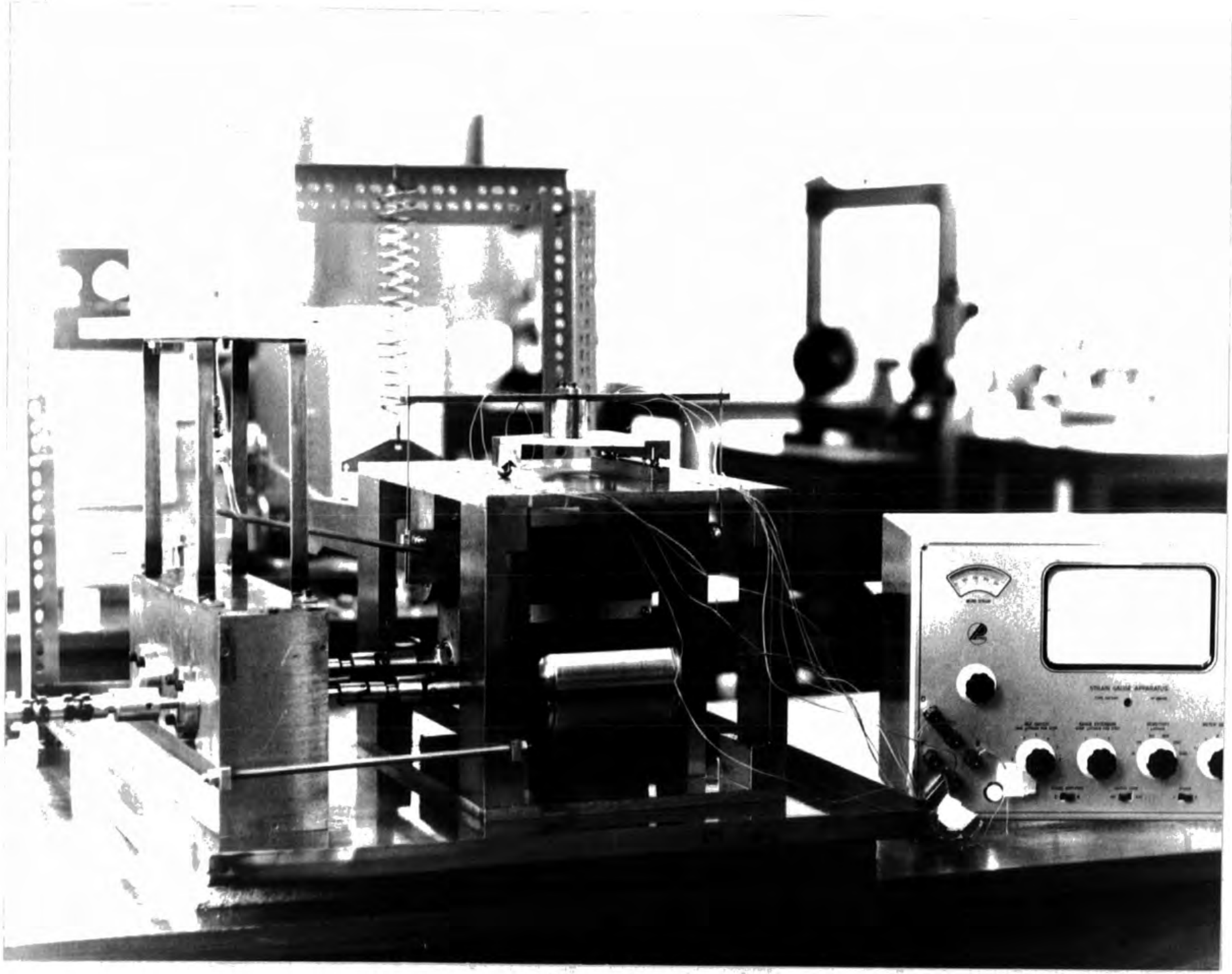

Fig. 2.5. FRONT VIEW OF EXPERIMENTAL RIG

Fig. 2.6. REAR VIEW OF EXPERIMENTAL RIG

The rig consisted of an upper and lower plate separated by six vertical pillars. The fixed axis roller was supported in rigid race bearings between the inner two pillars. The movable axis roller was supported in self-aligning bearings set in bell-crank arms. The bell-crank arms were themselves suspended from the upper plate by rigid race bearings set in suspension blocks.

Rollers and Planes

Fig. 2.7. shows a photograph of the rollers and planes and shows clearly the suspension of the movable-axis roller.

The rollers were manufactured from steel and accurately ground to a surface finish of 20 micro-inches C.L.A.

Apart from one test the soft surface layers were used as supplied by the manufacturers, that is, in the unmachined condition. The soft layers were bonded to rigid tufnol backing plates with araldite.

The tufnol used was type 6F/45 and had admirable machining and physical properties.

Plane Carrier and Measurement of Friction Force

A detailed drawing of the plane-carrier is shown in Fig. 2.8. A photograph showing the self-alignment system for the plane is shown in Fig. 2.9. This consisted of two vee-shaped tracks attached to a triangular plate and one vee-shaped track attached to the upper plate of the rig. Three balls were placed in these tracks

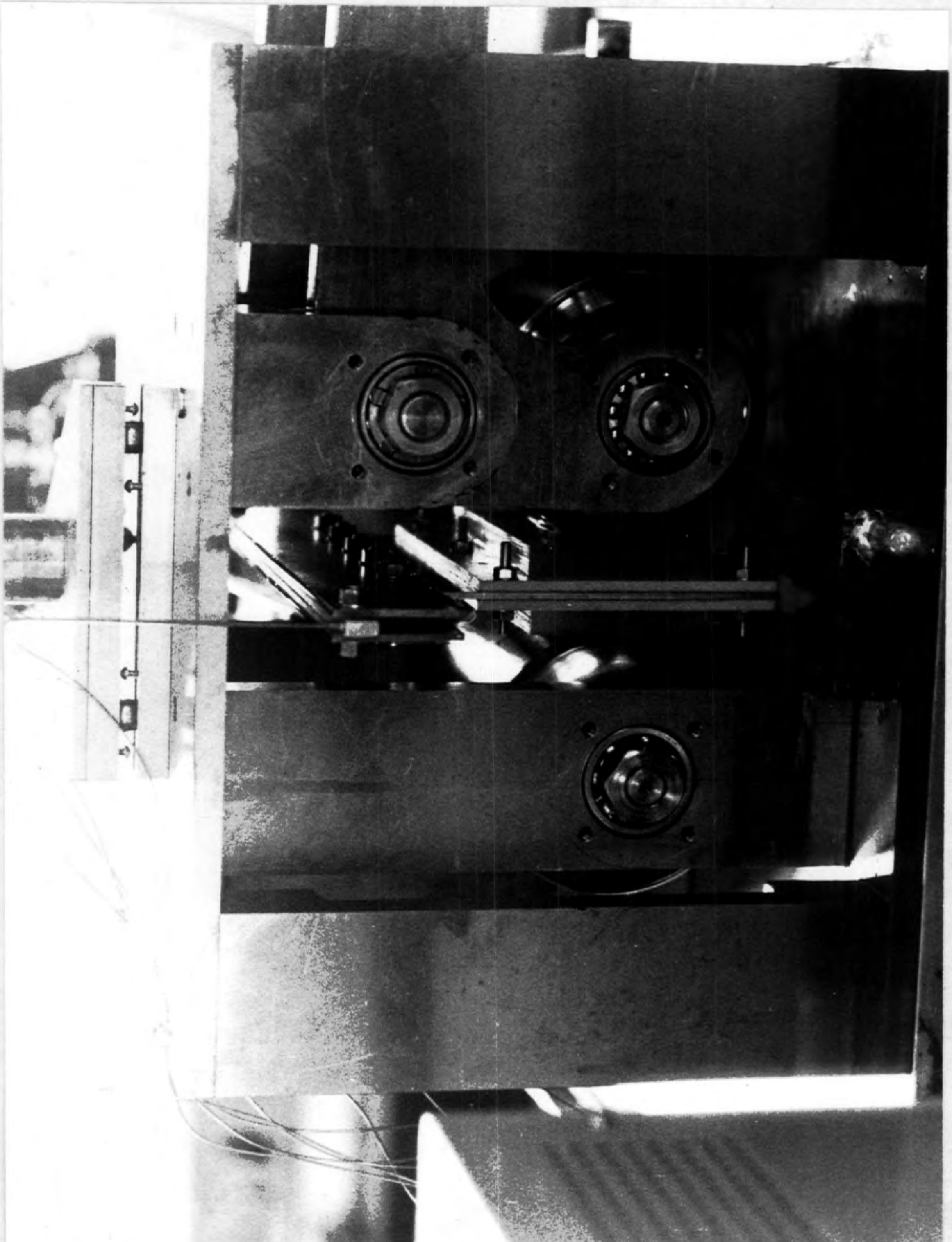

Fig. 2.7. ROLLERS AND PLANE SHOWING SUSPENSION OF MOVABLE-AXIS ROLLER

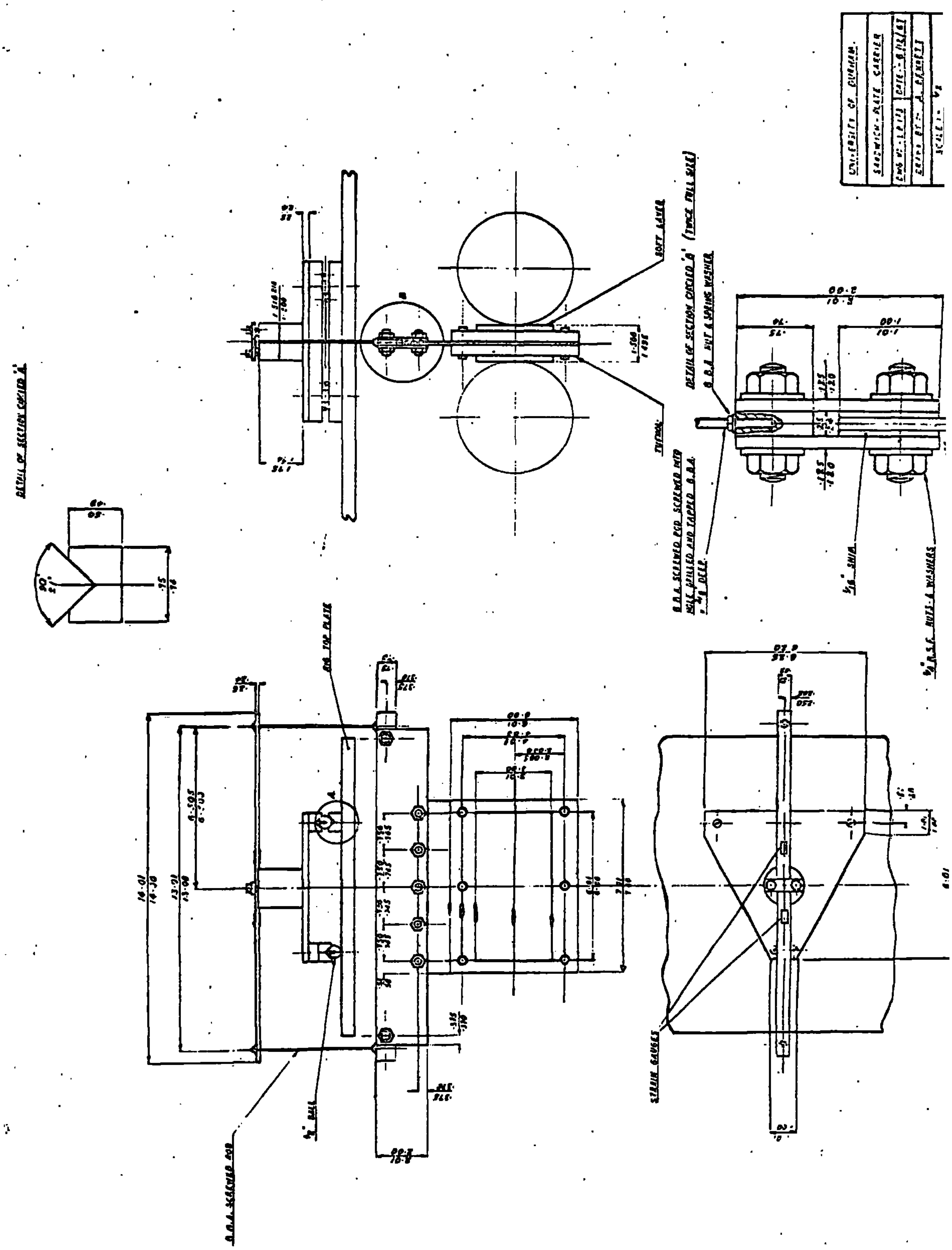

FIG. 2. PLANE CARRIER SYSTEM

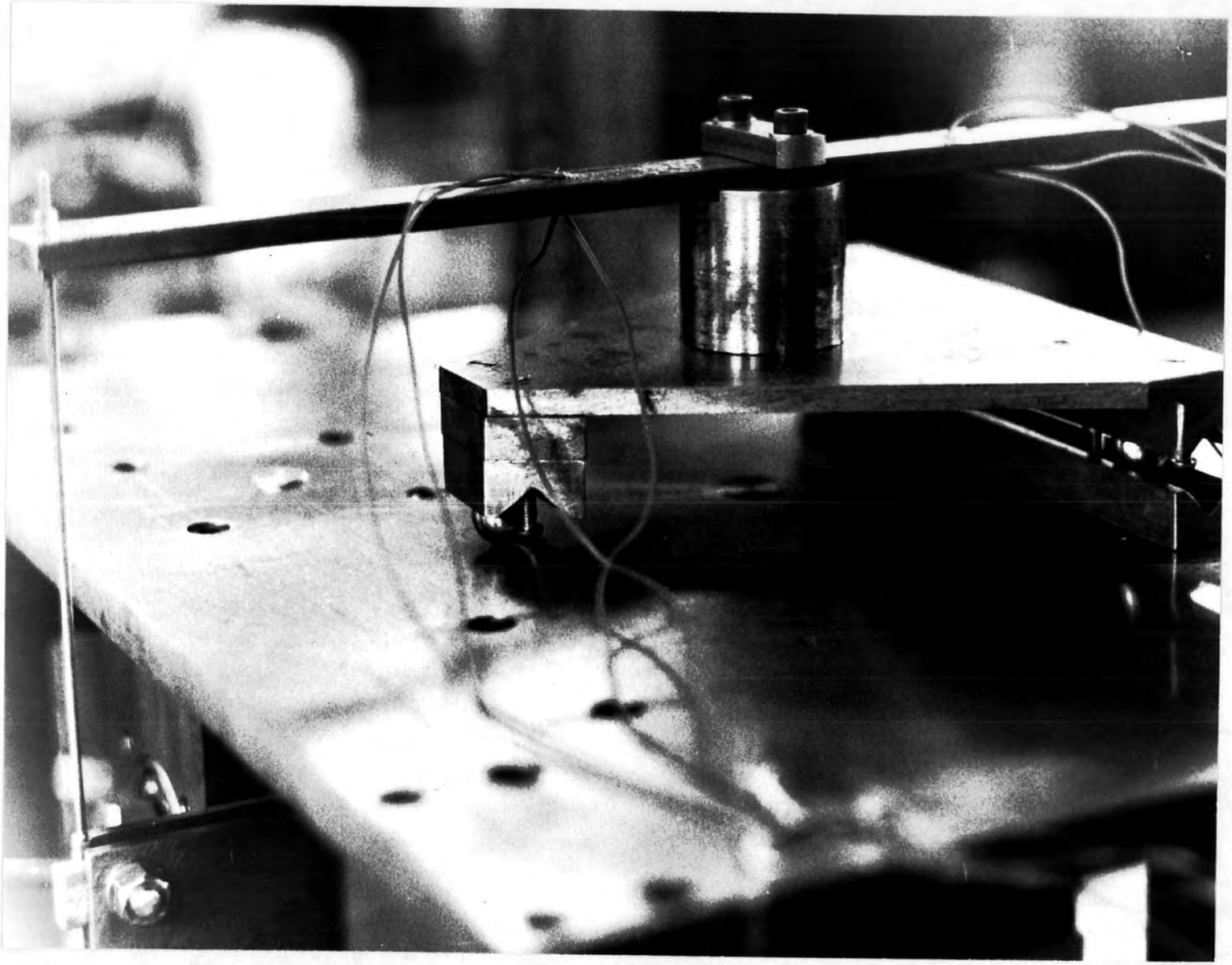

Fig. 2.9. SELF-ALIGNMENT SYSTEM FOR PLANES

allowing the plane carrier to move at right-angles to the roller-axis and the planes to hang vertically.

Attached to the triangular plate was a rectangular-section beam. The planes were suspended from this beam by two screwed rods and it was to this beam that strain-gauges were attached in order to measure friction forces.

Fig. 2.9. shows the plane-suspension and strain-gauges. The strain-gauges were of the etched-foil type.

A photograph of the rollers and planes under operating conditions is shown in Fig. 2.10.

Calibration of the beam took place using the following procedure:-

(i) The plane carrier was allowed to hang freely from the beam without any contact with the rollers.

(ii) Dead loads were applied to the plane and for each applied load the corresponding strain reading was noted.

The instrument used to measure the strain readings was the Peekel Electronic Strain Gauge Apparatus Type 540 DNH No. 66888.

(iii) Since the friction force for one face of the plane was required a graph of strain reading against half each corresponding dead load was plotted.

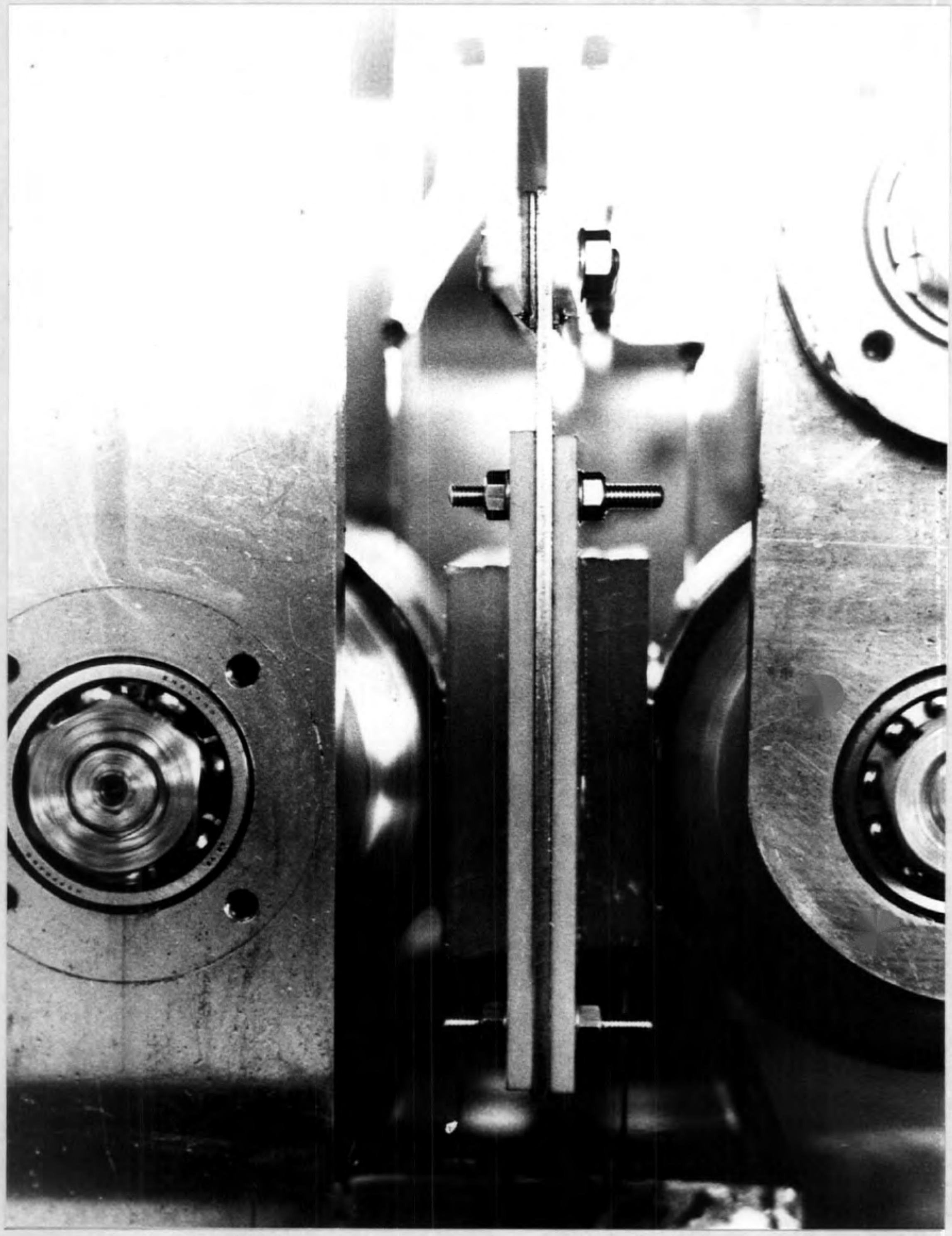

Fig. 2.10. ROLLERS AND PLANES UNDER OPERATING CONDITIONS

The strain reading for any combination of speed and load was simply converted to friction force by reference to the graph.

A typical plot of strain reading against applied dead load and friction force per roller width is shown in Fig. 2.11.

Application of Load and Balancing Arms

The load was applied to the planes from the rollers through bell crank arms. Two knife-edges were set in the ends of the arms and a loading bar sat on the knife-edges. The required loads were hung from a central point on the loading bar thus giving equal reactions in each arm.

The arms were balanced before loading to ensure that the roller and plane faces just met with zero applied load. A spring system hanging from a frame was used to balance the arms and this is shown in Figs. 2.5. and 2.6.

Drive for Rollers

A Carter variable speed gear driven by an English-Electric 3 phase-motor of 1 horse-power was used to drive the rollers.

The drive from the Carter gear was transmitted to the rollers via a specially designed gear-box. This gear-box had an input shaft connected to the Carter gear and had two output shafts. On these shafts were two equal inter-meshing gear-wheels thus giving contra-rotation of the two output shafts which were connected to the rollers. All the shafts were connected through universal couplings to allow for any mis-alignments.

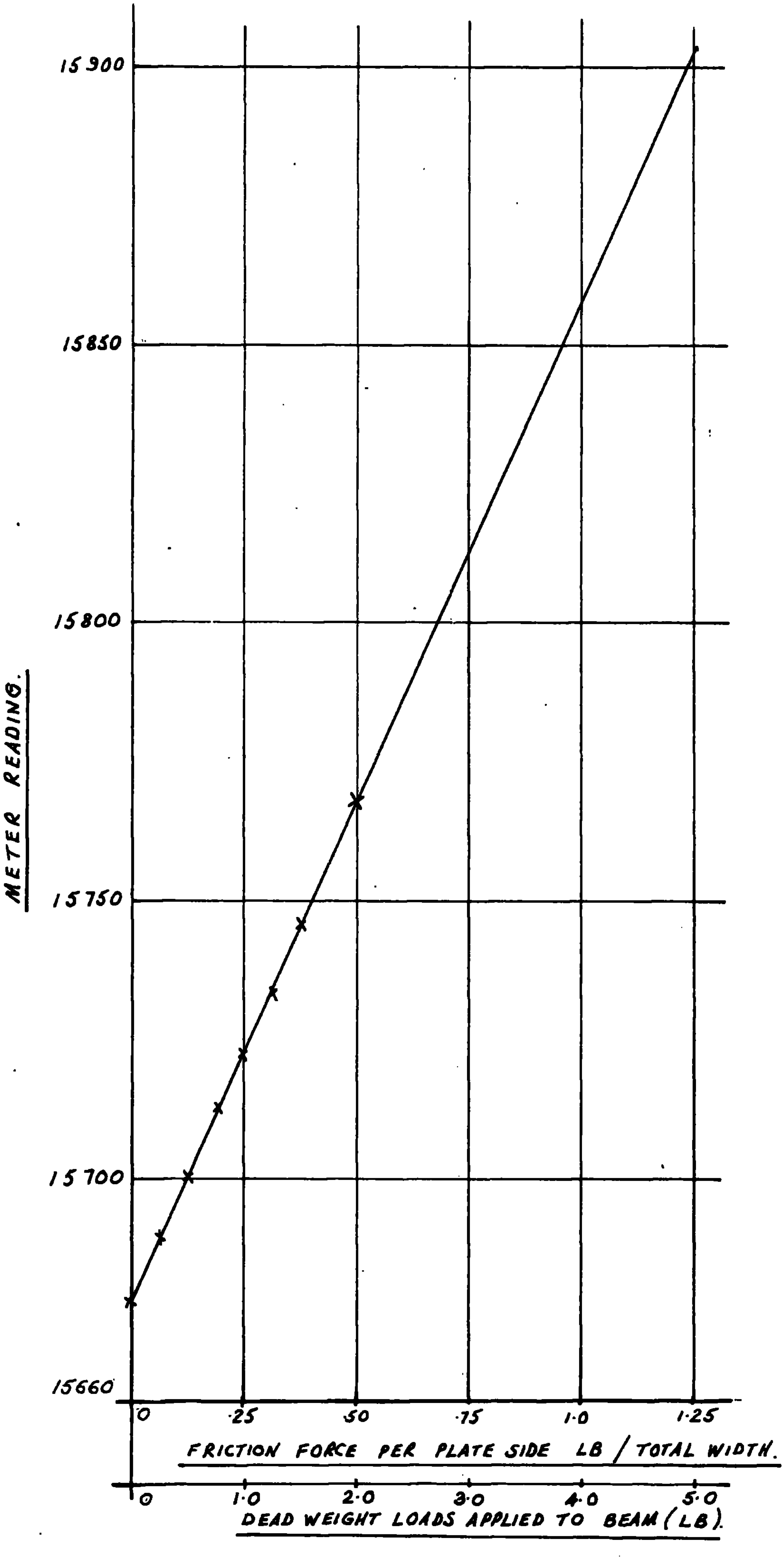

FIG. 2.11. CALIBRATION OF BEAM FOR ·03 INCH THICK SPECIMEN.

The spindle of the movable axis roller also had a key-way cut in it. A driving peg set in the universal coupling slotted into the key-way with a slight clearance fit allowing axial movement of the roller spindle in the universal coupling whenever the arms were raised or lowered.

A detailed drawing of the contra-rotating gear-box is shown in Fig. 2.12.

Speed control of the rollers was by a hand-wheel on the Carter-gear and speeds of zero to 940 revs/minute could be selected. An output torque and horse-power of 55 lb. in. and 0.8 h.p. respectively could be obtained.

Lubricant Supply and Collection

Lubricant to the rollers and planes was delivered through two pipes connected to an oil feed tank. The tank sat on top of the contra-rotating gear-box and a pipe fitted with a flow control-valve branched to give individual feeds to each set of rollers and planes.

A collection tray was located beneath the planes and a tube led from this to a tank similar in design to the feed tank.

Lubricant Viscosity Measurement

The viscosity of the lubricant used in the experiments was measured according to British Standard 188:1957 "Determination of the Viscosity of Liquids in C.G.S. Units."

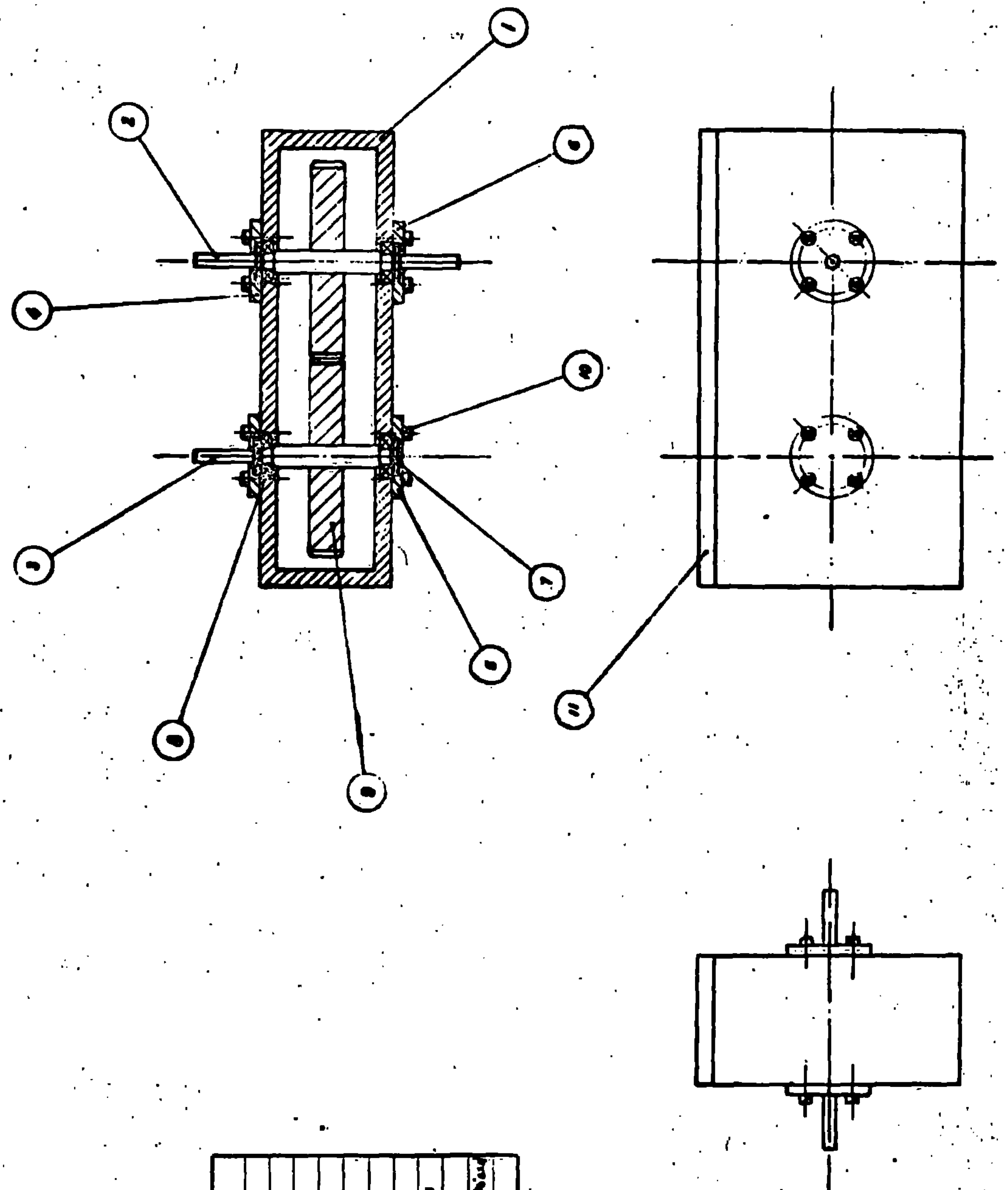

ITEM	DESCRIPTION
1	HOUSING
2	SHAFT (DRIVING)
3	SHAFT (DRIVEN)
4	COVER PLATE
5	COVER PLATE
6	COVER PLATE
7	LOCK NUT
8	BEARING TYPE:-UL59
9	SPUR GEAR
10	ALLEN CAP SCREW(¼BSF)
11	HOUSING COVER

UNIVERSITY OF DURHAM	
GEAR BOX ASSEMBLY	
DWG Nº:- GB1	DATE:- 25/10/62
DRAWN BY:- A.BENNETT	
SCALE - 1/2	
THIRD ANGLE PROJECTION	

FIG. 2. 12. CONTRA-ROTATING GEAR-BOX.

The apparatus used in measuring the viscosity consisted of a bridge controlled thermostat bath, appropriate U-tube viscometers and thermometers.

Photographs of the thermostat bath and a viscometer used in the tests are shown in Figs. 2.13. and 2.14. respectively.

According to the manufacturers of the thermostat bath (Townson and Mercer) the accuracy of the bath temperature was plus or minus 0.01°C.

The variation of viscosity of the lubricant against temperature is shown in Fig. 2.15. The lubricant in this case was Shell Tellus 29.

Modifications to Rig for Observation of Pressure and Cavitation Zones

The rig was modified very simply for observation tests. The fixed axis roller and oil feed tube to that roller were removed. A thick perspex plate with the required soft layer attached was clamped to the inner pillars of the rig. The assembly is shown in Fig. 2.4. and a photograph is shown in Fig. 2.16.

Observation of the pressure and cavitation zones could then be made using a travelling microscope and photographs taken if desired.

Fig. 2.13. BRIDGE CONTROLLED THERMOSTAT BATH

Fig. 2.14. U-TUBE VISCOMETER

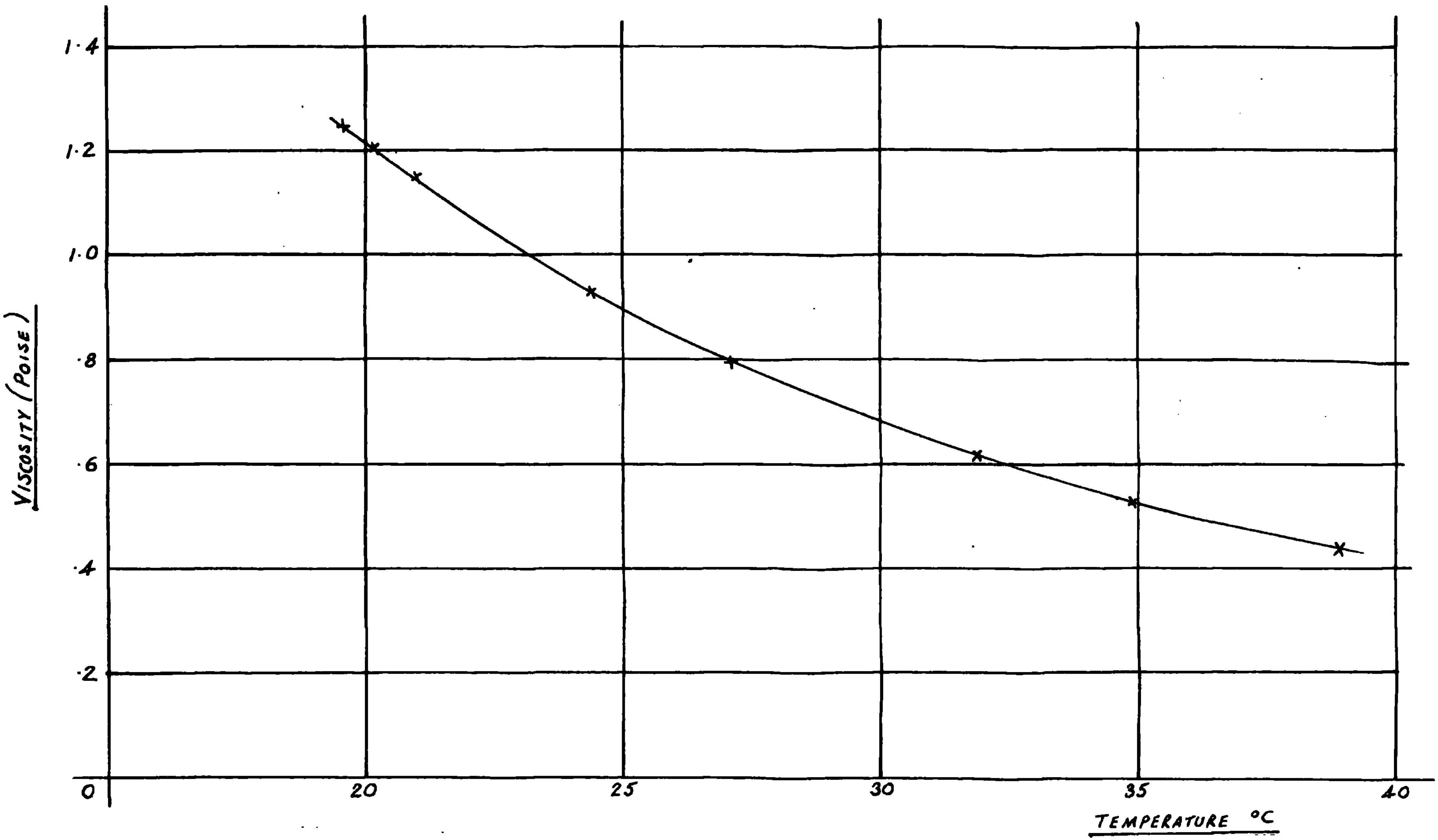

FIG. 2.15. VARIATION OF VISCOSITY (IN POISE) ~ TEMPERATURE (°C) FOR SHELL TELLUS 29.

Fig. 2.16. MODIFIED RIG FOR OBSERVATION TESTS

CHAPTER 3

Experimental Results

The experimental results of friction force against roller speed are tabulated in the following. Various figures in this section show graphs of friction force plotted against uη (roller speed in in./sec. x viscosity in Reyns).

TABLE 3.1. RIGID SPECIMEN 5 lbs LOAD

Roller Speed Rev./min.	Roller Speed - u - in./sec.	Friction Force Per Face	Friction Force, lbs, Per Inch Width	$\eta u \times 10^{-5}$ lb.wt./in.
25	5.89	1.525	0.305	9.31
40	9.43	.925	0.185	14.90
60	14.14	.550	0.110	22.35
85	20.03	.400	0.080	31.67
105	24.74	.400	0.080	39.11
125	29.44	.400	0.080	46.54
160	37.65	.450	0.090	59.52
210	49.45	.575	0.115	78.18
255	60.10	.625	0.125	95.02
300	70.60	.675	0.135	111.62
355	83.60	.750	0.150	132.17
440	103.69	.950	0.190	163.93
535	126.07	1.125	0.225	199.32
630	148.46	1.450	0.290	234.72
730	172.02	1.700	0.340	271.96

Lubricant Temperature Variations

	Start of Test	End of Test
Oil Feed °C	21.8	21.9
Oil Bath °C	21.3	21.7

Viscosity = 1.09 Poise = 1.581 x 10^{-5} Reyns

TABLE 3.2. RIGID SPECIMEN 10 lbs. LOAD

Roller Speed Rev./Min.	Roller Speed - u - in./sec.	Friction Force Per Face	Friction Force, lbs, Per Inch Width	$\eta u \times 10^{-5}$ lb.wt./in.
40	9.43	2.075	.415	14.81
60	14.14	1.100	.220	22.21
85	20.03	.700	.140	31.47
115	27.10	.550	.110	42.57
150	35.35	.550	.110	55.53
205	48.31	.700	.140	75.89
270	63.63	.750	.150	99.96
330	77.76	.925	.185	122.17
410	96.62	1.075	.215	151.78
465	109.58	1.225	.245	172.15
565	133.14	1.500	.300	209.17
665	156.71	1.900	.380	246.19
795	187.34	2.375	.495	294.31
945	222.69	2.775	.555	349.84
1025	241.54	3.200	.640	379.46

Lubricant Temperature Variations

	Start of Test	End of Test
Oil Feed °C	21.9	22.0
Oil Bath °C	21.5	22.3

Viscosity = 1.083 Poise = 1.571×10^{-5} Reyns

TABLE 3.3. RIGID SPECIMEN 15 lbs. LOAD

Roller Speed Rev./Min.	Roller Speed - u - in./sec.	Friction Force Per Face	Friction Force, lbs, Per Inch Width	$\eta u \times 10^{-5}$ lb.wt./in.
60	14.14	2.700	.540	21.93
80	18.85	1.700	.340	29.24
120	28.28	1.225	.245	43.86
165	38.88	.950	.190	60.31
220	51.84	1.000	.200	80.41
270	63.63	1.000	.200	98.68
350	82.48	1.100	.220	127.92
425	100.15	1.250	.250	155.33
510	120.18	1.450	.290	186.40
590	139.03	1.750	.350	215.64
685	161.42	2.300	.460	250.36
805	189.69	3.000	.600	294.22
1025	241.54	3.800	.760	374.63

Lubricant Temperature Variations

	Start of Test	End of Test
Oil Feed °C	22.1	22.2
Oil Bath °C	23.8	23.4

Viscosity = 1.07 Poise = 1.551×10^{-5} Reyns

TABLE 3.4. RIGID SPECIMEN 20 lbs. LOAD

Roller Speed Rev./Min.	Roller Speed - ū - in./sec.	Friction Force Per Face	Friction Force, lbs. Per Inch Width	$\eta \bar{u} \times 10^{-5}$ lb.wt./in.
90	21.21	2.260	.452	31.73
125	29.46	1.575	.315	44.07
165	38.88	1.250	.250	58.17
210	49.49	1.200	.240	74.03
265	62.45	1.200	.240	93.42
340	80.12	1.275	.255	119.86
420	98.97	1.470	.294	148.06
510	120.18	1.725	.345	179.79
595	140.21	2.000	.400	209.76
685	161.48	2.475	.495	241.48
770	181.45	2.925	.585	271.45
855	201.48	3.750	.750	301.42
1015	239.18	4.000	.800	357.82

Lubricant Temperature Variations

	Start of Test	End of Test
Oil Feed °C	22.6	22.9
Oil Bath °C	22.8	24.0

Viscosity = 1.032 Poise = 1.496×10^{-5} Reyns

TABLE 3.5. RIGID SPECIMEN 25 lbs. LOAD

Roller Speed Rev./Min.	Roller Speed - u - in./sec.	Friction Force Per Face	Friction Force, lbs, Per Inch Width	$\eta u \times 10^{-5}$ lb.wt./in.
105	24.74	3.000	.600	35.88
145	34.17	2.025	.405	49.55
170	40.06	1.725	.345	58.09
205	48.31	1.550	.310	70.05
260	61.27	1.550	.310	88.84
305	71.87	1.500	.300	104.22
350	82.48	1.550	.310	119.59
450	106.04	1.750	.350	153.76
535	126.07	2.000	.400	182.81
655	154.35	2.450	.490	223.81
760	179.09	3.300	.660	259.69

Lubricant Temperature Variations

	Start of Test	End of Test
Oil Feed °C	23.2	23.3
Oil Bath °C	25.0	25.0

Viscosity = 1.00 Poise = 1.45×10^{-5} Reyns

It will be noted at this stage that the graphs of friction force against ηu for the rigid specimen are plotted on different scales from those used on the elastic specimens. This is because the rigid case values of friction force and ηu extended much further than the corresponding elastic cases. However it will also be noted that graphs are drawn to the same scale wherever comparisons are made of rigid and elastic case results.

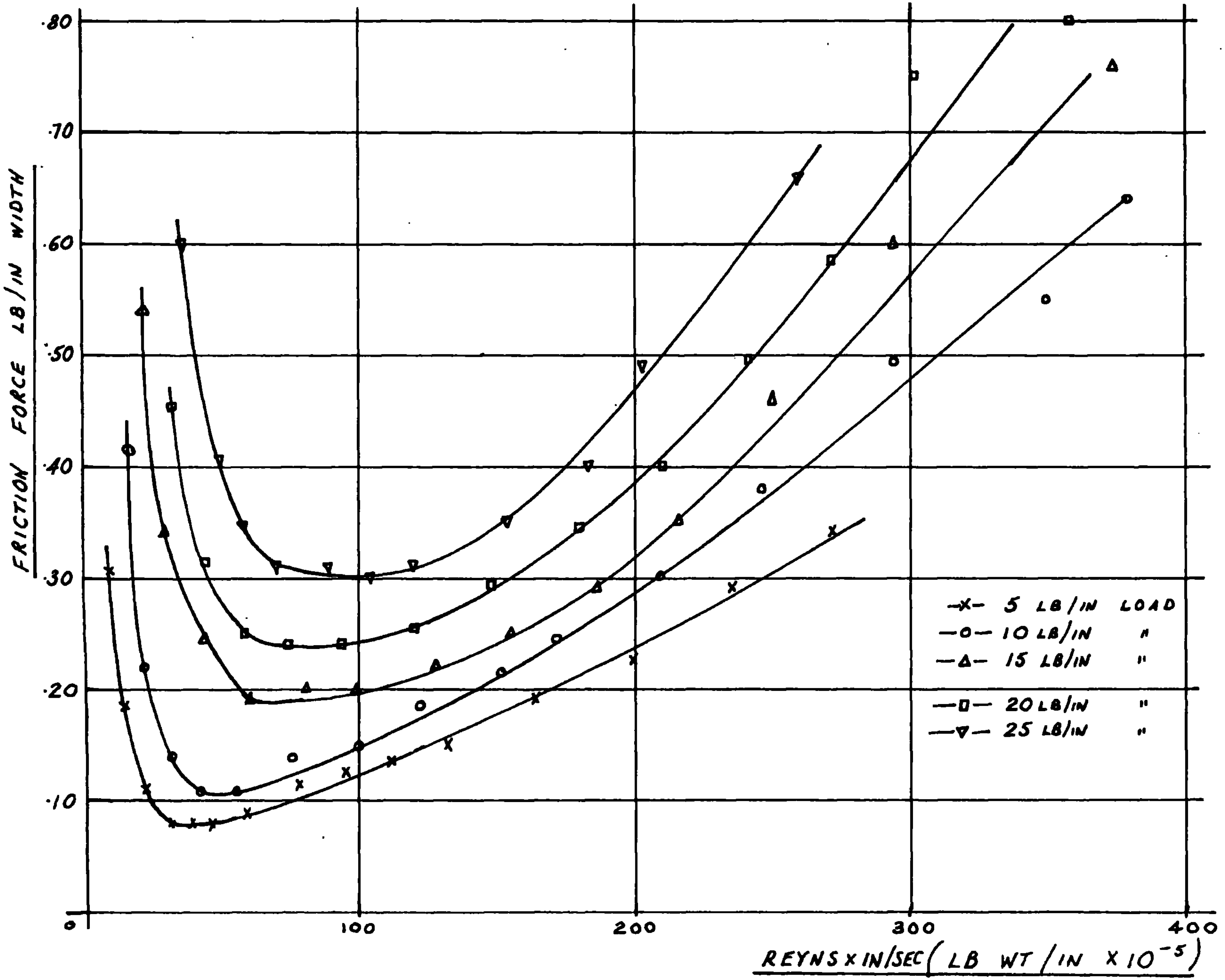

FIG. 3.1. FRICTION FORCE ~ ηU FOR RIGID SPECIMEN.

TABLE 3.6. ELASTIC SPECIMEN 0.1 INCHES THICK

5 lb. LOAD

Roller Speed Rev./Min.	Roller Speed - $\bar{u}$ - in./sec.	Friction Force Per Face	Friction Force, lbs, Per Inch Width	$\eta\bar{u} \times 10^{-5}$ lb.wt./in.
15	3.54	.120	.024	5.48
25	5.89	.120	.024	9.14
35	8.25	.120	.024	12.79
50	11.78	.125	.025	18.28
65	15.32	.125	.025	23.76
85	20.03	.150	.030	31.07
105	24.74	.175	.035	38.38
135	50.45	.200	.040	48.24
170	40.06	.240	.048	62.14
200	47.13	.300	.060	73.10
240	56.56	.340	.068	87.72
275	64.80	.400	.080	99.39
300	70.70	.420	.084	109.65
325	76.59	.450	.090	118.79
350	82.48	.480	.096	127.92
380	89.55	.500	.100	138.78
410	96.62	.575	.115	149.85

Lubricant Temperature Variations

	Start of Test	End of Test
Oil Feed °C	22.1	22.2
Oil Bath °C	21.6	22.2

Viscosity = 1.07 Poise = 1.551 x 10^{-5} Reyns

TABLE 3.7. ELASTIC SPECIMEN 0.1 INCHES THICK

10 lb. LOAD

Roller Speed Rev./Min.	Roller Speed - u - in./sec.	Friction Force Per Face	Friction Force, lbs, Per Inch Width	$\eta u \times 10^{-5}$ lb.wt./in.
25	5.89	.180	.036	8.67
40	9.43	.220	.044	13.88
60	14.14	.250	.050	20.81
85	20.03	.275	.055	29.48
120	28.28	.325	.065	41.63
160	37.70	.450	.090	55.50
190	44.77	.475	.095	65.91
230	54.20	.550	.110	79.78
260	61.27	.575	.115	90.19
285	67.16	.625	.125	98.86
315	74.23	.675	.135	109.27
345	81.30	.750	.150	119.67
375	88.37	.810	.162	130.08
410	96.62	.900	.180	142.22

Lubricant Temperature Variations

	Start of Test	End of Test
Oil Feed °C	22.2	22.3
Oil Bath °C	22.2	22.4

Viscosity = 1.015 Poise = 1.472×10^{-5} Reyns

TABLE 3.8. ELASTIC SPECIMEN 0.1 INCHES THICK

15 lb. LOAD

Roller Speed Rev./Min.	Roller Speed - ū - in./sec.	Friction Force Per Face	Friction Force, lbs, Per Inch Width	$\eta\bar{u} \times 10^{-5}$ lb.wt./in.
20	4.71	.300	.060	7.18
35	8.25	.275	.055	12.56
60	14.14	.325	.065	21.53
85	20.03	.375	.075	30.51
115	27.10	.450	.090	41.27
140	32.99	.520	.104	50.25
170	40.06	.570	.114	61.01
195	45.95	.650	.130	69.99
230	54.20	.740	.148	82.55
270	63.63	.780	.156	96.90
305	71.87	.880	.176	109.46
330	77.77	.940	.188	118.44
360	84.83	1.000	.200	129.20
395	93.08	1.120	.224	141.76
420	98.97	1.230	.246	150.74

Lubricant Temperature Variations

	Start of Test	End of Test
Oil Feed °C	22.3	22.6
Oil Bath °C	22.4	22.6

Viscosity = 1.05 Poise = 1.523×10^{-5} Reyns

TABLE 3.9. ELASTIC SPECIMEN 0.1 INCHES THICK

20 lb. LOAD

Roller Speed Rev./Min.	Roller Speed - u - in./sec.	Friction Force Per Face	Friction Force, lbs, Per Inch Width	$\eta u \times 10^{-5}$ lb.wt./in.
15	3.54	.375	.075	5.28
30	7.07	.340	.068	10.56
45	10.60	.375	.075	15.84
60	14.14	.400	.080	21.12
85	20.03	.425	.085	29.93
115	27.10	.500	.100	40.49
145	34.17	.600	.120	51.05
180	42.42	.700	.140	63.37
215	50.67	.800	.160	75.69
245	57.73	.840	.168	86.26
285	67.16	.950	.190	100.34
315	74.23	1.070	.214	110.90
350	82.48	1.150	.230	123.22
380	89.55	1.250	.250	133.78
400	94.26	1.375	.275	140.82

Lubricant Temperature Variations

	Start of Test	End of Test
Oil Feed °C	22.6	22.9
Oil Bath °C	22.6	23.0

Viscosity = 1.03 Poise = 1.494×10^{-5} Reyns

TABLE 3.10. ELASTIC SPECIMEN 0.1 INCHES THICK

25 lb. LOAD

Roller Speed Rev./Min.	Roller Speed - ū - in./sec.	Friction Force Per Face	Friction Force, lbs, Per Inch Width	$\eta u \times 10^{-5}$ lb.wt./in.
10	2.36	.425	.085	3.45
20	4.71	.400	.080	6.89
35	8.25	.400	.080	12.07
65	15.32	.450	.090	22.41
90	21.21	.500	.100	31.03
125	29.46	.625	.125	43.09
165	38.88	.750	.150	56.88
210	49.49	.875	.175	72.40
240	56.56	.975	.195	82.74
275	64.80	1.050	.210	94.81
295	69.52	1.150	.230	101.70
330	77.77	1.250	.250	113.77
355	83.66	1.325	.265	122.39
380	89.55	1.400	.280	131.01
400	94.26	1.530	.306	137.90

Lubricant Temperature Variations

	Start of Test	End of Test
Oil Feed °C	22.9	23.2
Oil Bath °C	23.0	23.3

Viscosity = 1.01 Poise = 1.463 x 10^{-5} Reyns

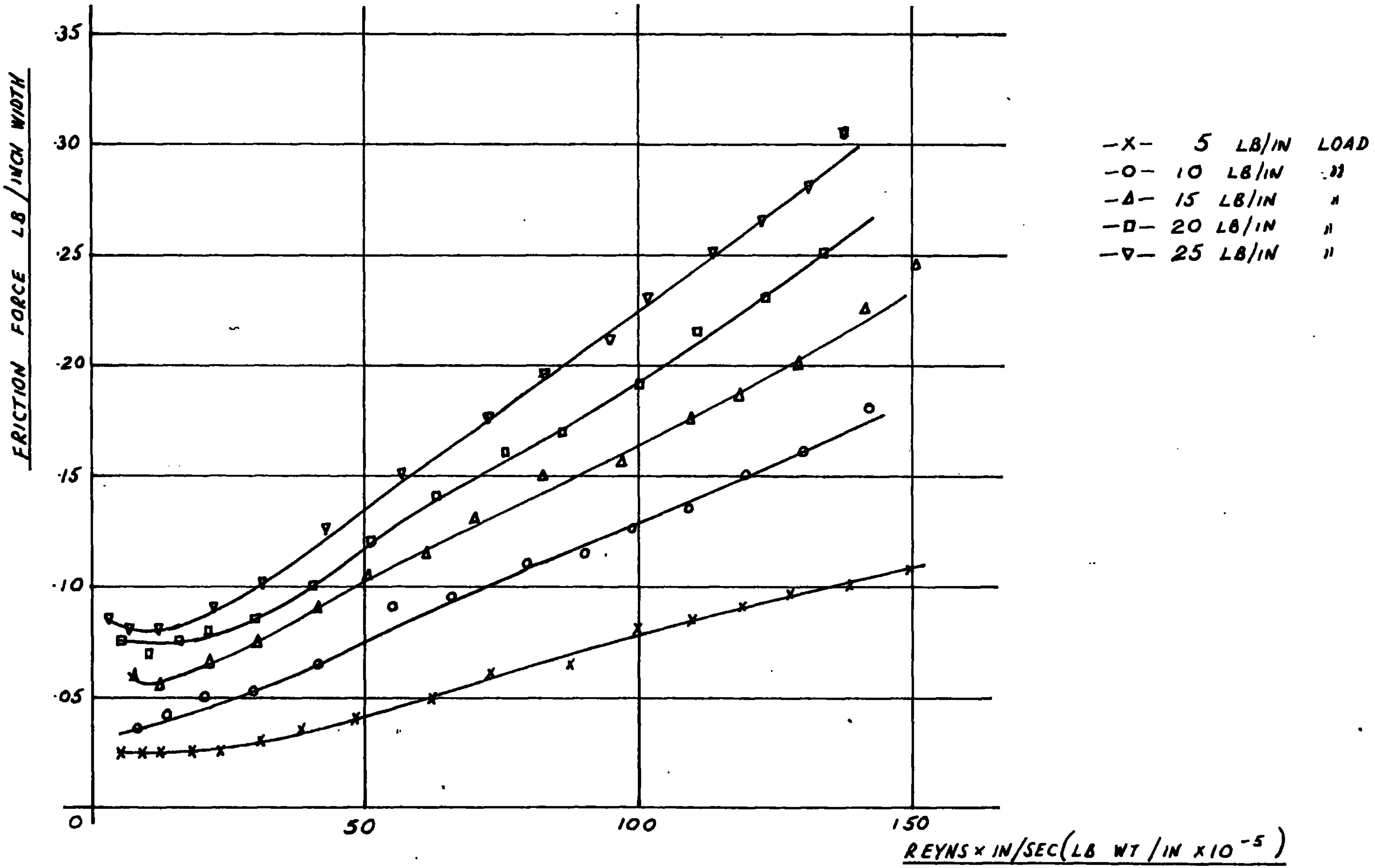

FIG. 3.2. FRICTION FORCE ~ ηu FOR 0·1 INCH SPECIMEN.

The experimental results for the other elastic specimens are shown graphically only. These specimens were .03 inches, .05 inches, .20 inches and .50 inches thick and the corresponding graphs of friction force against ηu are shown in Fig. 3.3., 4., 5., and 6. respectively.

Tests were also carried out on an elastic specimen of .02 inches thickness. This specimen was manufactured by surface grinding a thicker elastic specimen to the required .02 inches.

The .03 inches thick specimen was also prepared in this manner. The resultant surface of the .02 inches specimen was quite rough while that of the .03 inches specimen was reasonably smooth, due mainly to the experience gained in machining the .02 inches specimen.

The graphs of friction force against ηu for the .02 inches thick specimen are shown in Fig. 3.7.

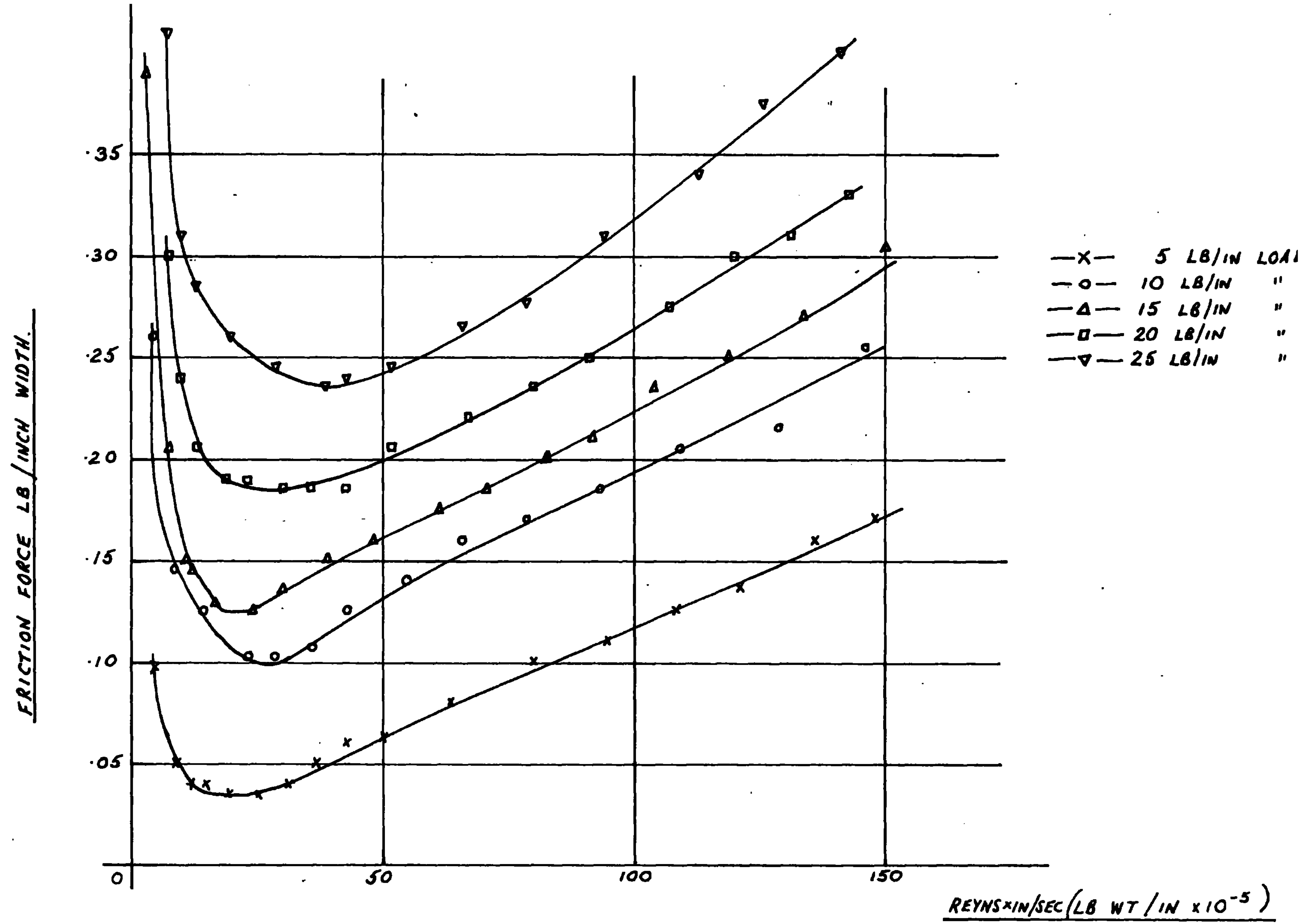

FIG. 3 . 3 . FRICTION FORCE ~ ηU FOR ·03 INCH SPECIMEN.

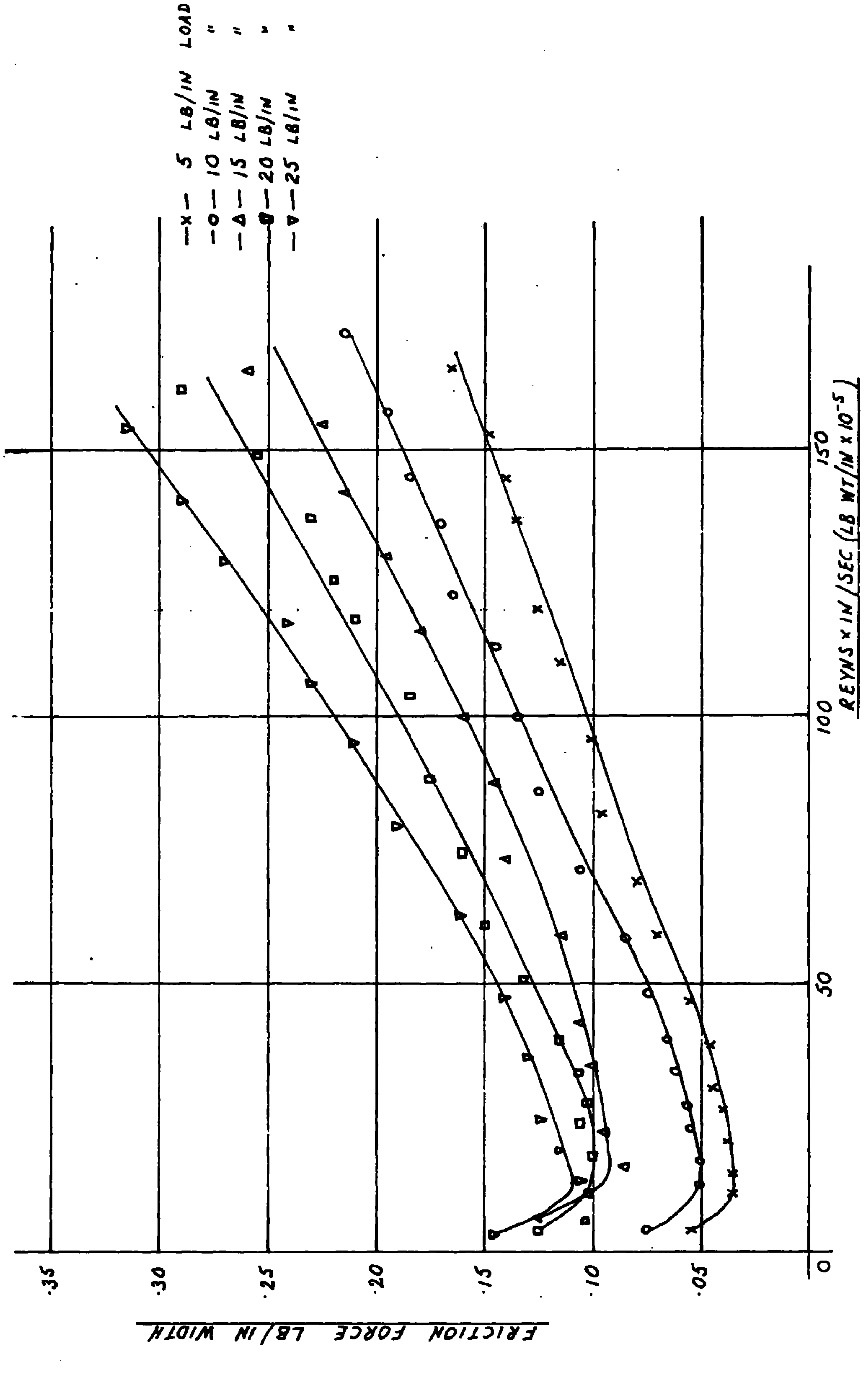

FIG. 3. 4. FRICTION FORCE ~ ηU FOR ·05 INCH SPECIMEN.

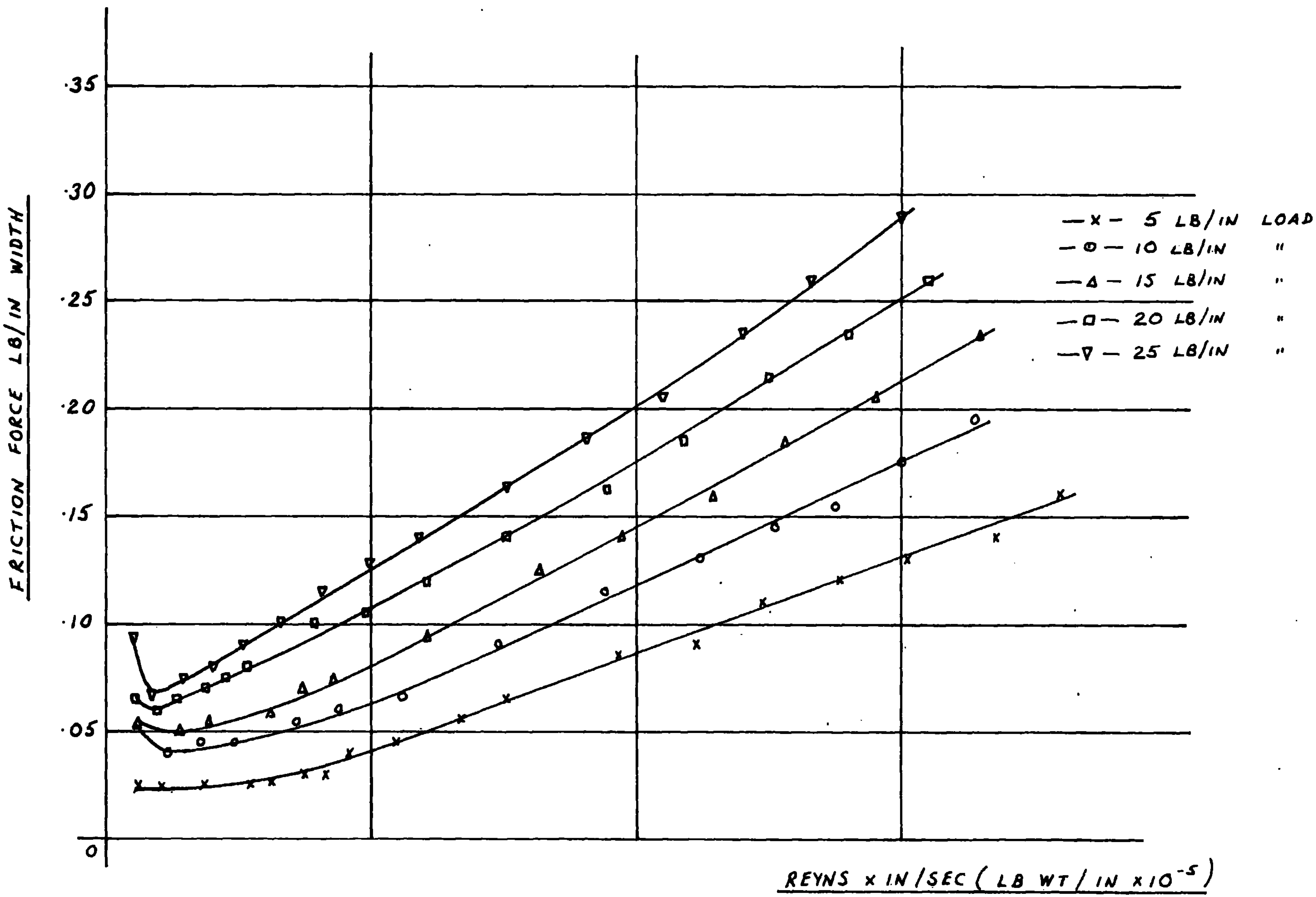

FIG. 3 . 5 . FRICTION FORCE ...

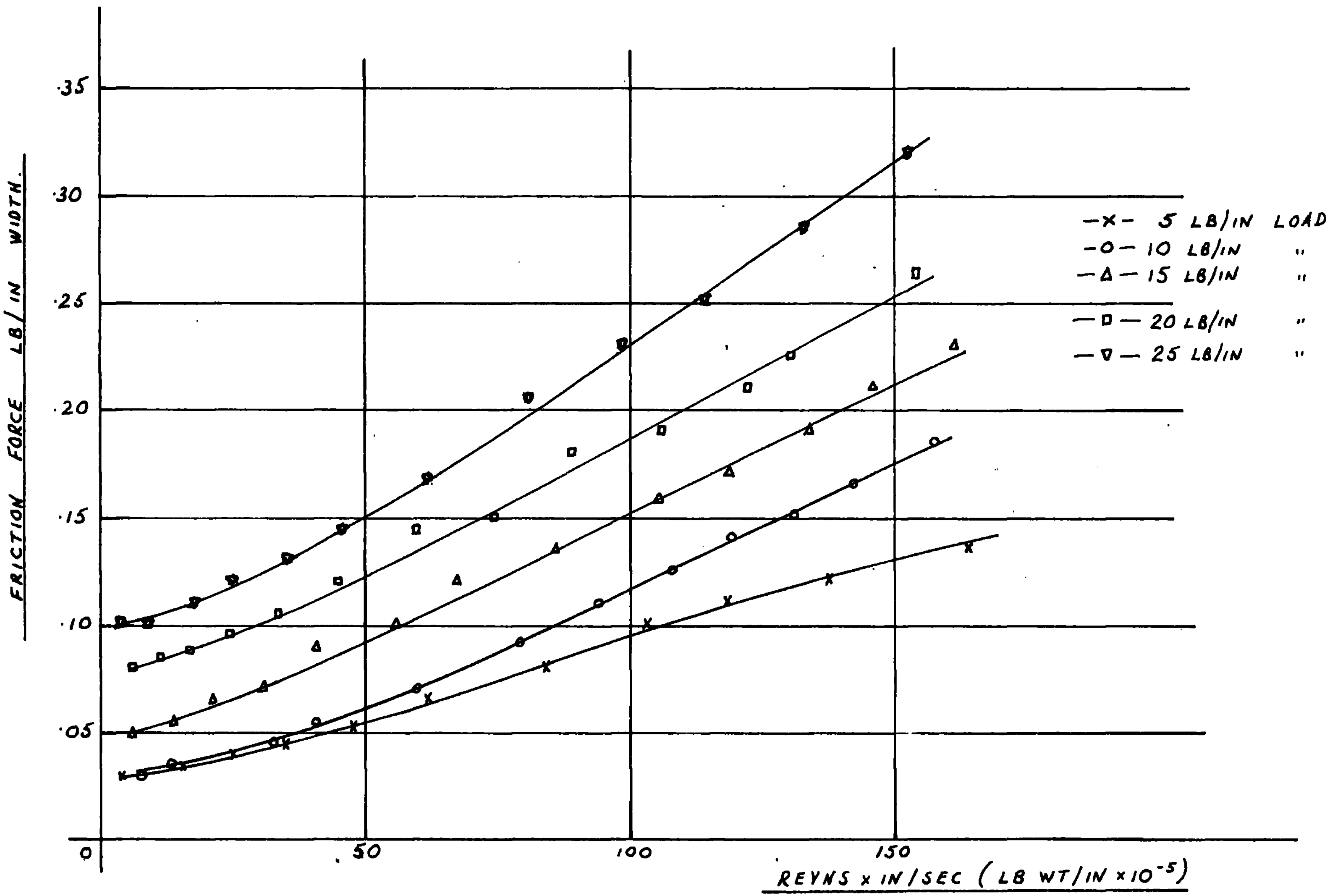

FIG. 3. 6. FRICTION FORCE ~ ηu FOR .5 INCH SPECIMEN.

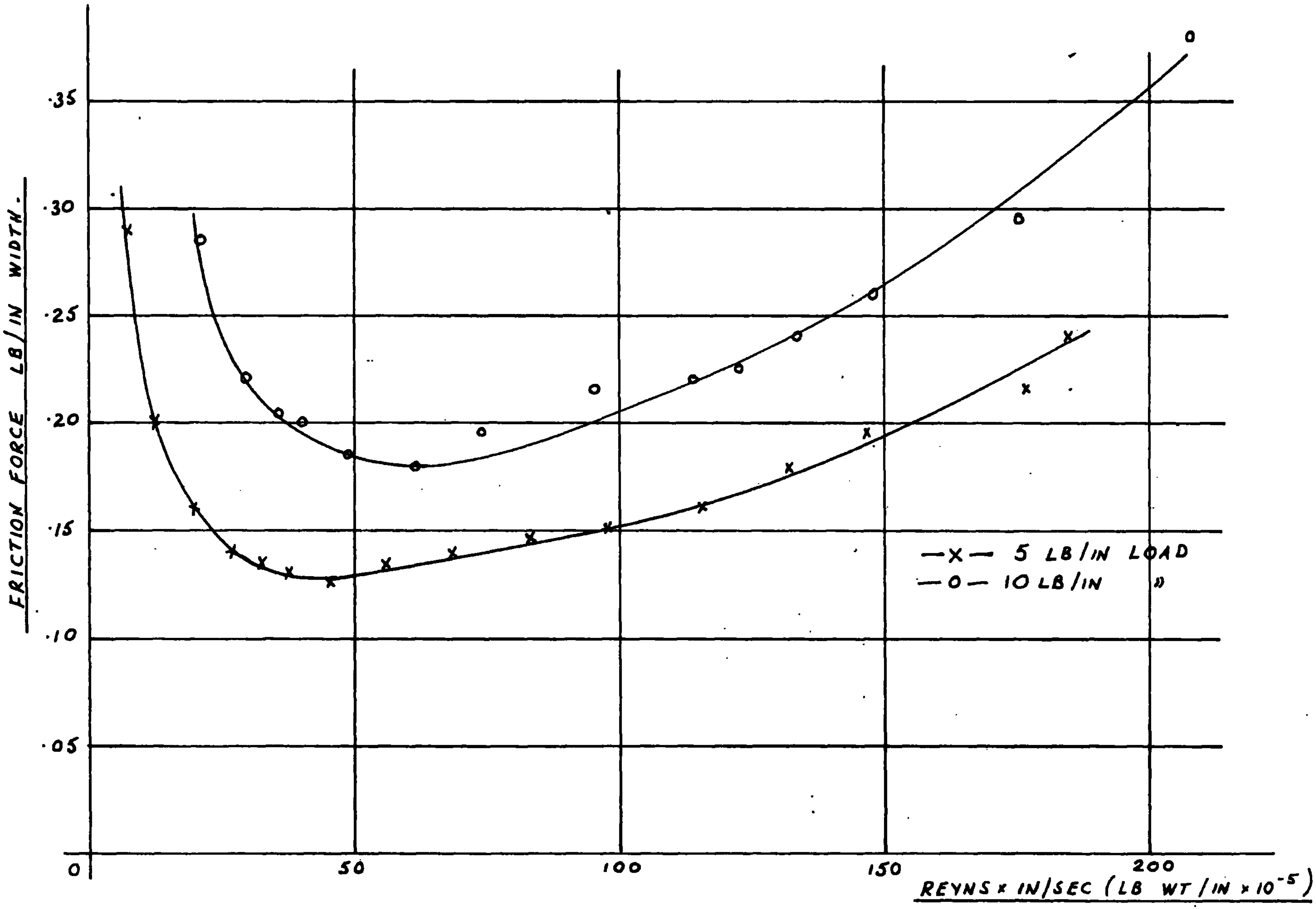

FIG. 3.7. FRICTION FORCE ~ $\mathcal{Z}U$ FOR ·02 INCH SPECIMEN.

CHAPTER 4

Theoretical Calculations and Computing

Section 1. Theoretical Calculations

The relevant integrated form of Reynold's equation as derived in many textbooks is

$$dp/_{dx} = 12 \eta u \left[\frac{h - h_m}{h^3} \right]$$

The system to which the above equation is to be applied is shown diagrammatically in Fig. 4.1.

The separation, h, of a rigid cylinder and plane is given by

$$h \approx h_o + \frac{x^2}{2R}$$

This is a parabolic representation of the cylinder and although the parabolic approximation is not very good at values of $x/_R$ approaching unity, the effect on solutions of the Reynold's equation is small.

Table 4.1. shows the errors between parabolic approximations and the circular cylinder for values of $x/_R$.

TABLE 4.1.

$x/_R$		0	0.1	0.2	0.4	0.6	0.8	1.0	2.0
$\frac{(h - h_o)}{R}$	Circular Cylinder	0	0.00501	0.0202	0.0835	0.20	0.4	1.0	-
	Parabolic Cylinder	0	0.00500	0.0200	0.0800	0.18	0.32	0.5	1.0

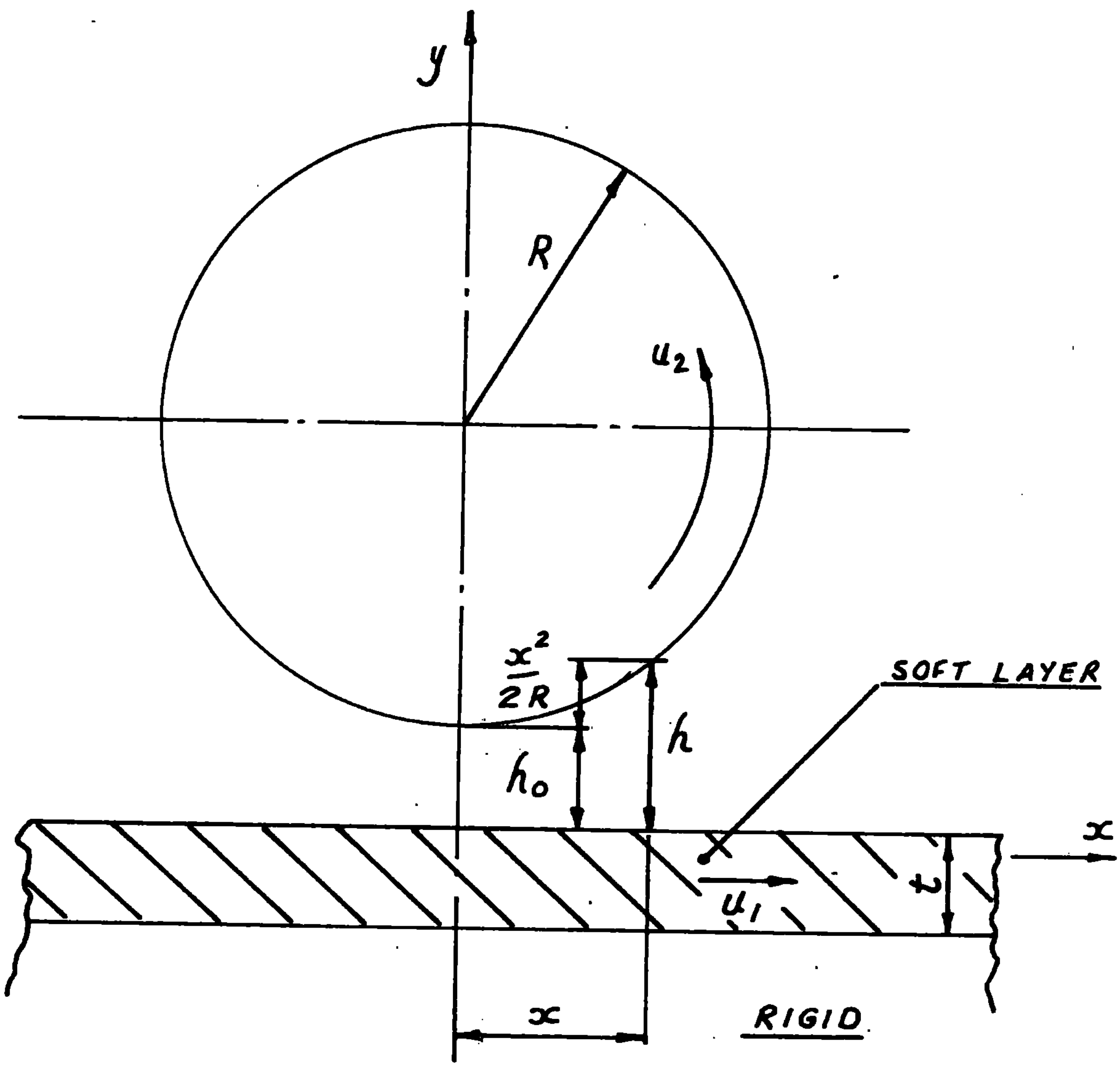

FIG. 4.1. CO-ORDINATES AND VELOCITIES FOR LUBRICATION OF CYLINDER AND PLANE.

In this analysis allowance will be made for the elastic deformation of the soft surface layer. The roller at all times will be treated as rigid as will the material to which the soft elastic layer is attached.

It will be assumed that the soft layer material deforms linearly, according to

$$\delta = {}^{p}/_{\lambda}$$

where δ is deflection and λ is a stiffness. This simple expression neglects both sideways shearing and the distant influence of pressure on deflection.

The expression for film thickness is therefore modified to

$$h = h_o + \frac{x^2}{2R} + {}^{p}/_{\lambda}$$

<u>Lubrication Boundary Conditions</u>

The pressure at the inlet is used as the datum, hence at some value $x = x_i$, the pressure $p = 0$.

The pressure curve ends on the downstream side according to the 'cavitation boundary condition' as described in the following sections.

Thus at some value $x = x_o$, the pressure and the pressure gradient are zero.

It will be worthwhile to point out the other assumptions at this stage before an explanation of the computing procedure is given:-

1. Side leakage is ignored
2. Viscosity is treated as constant

3. The soft layer deflection $\delta = {}^{p}/_{\lambda}$

4. All components other than the surface layer are treated as rigid and geometrically perfect.

Computation

As the integration of Reynold's equation was to be performed numerically it was convenient to express it in dimensionless terms.

The equations to be solved were

$$^{dp}/_{dx} = 12\,\eta u \left[\frac{h - h_m}{h^3}\right]$$

$$\text{and } h = h_o + {}^{x^2}/_{2R} + {}^{p}/_{\lambda}$$

$$\text{and remembering that } u = \frac{u_1 \pm u_2}{2}$$

$$\text{then } {}^{dp}/_{dx} = 12\,\eta\,\frac{u_2}{2}\left[\frac{h - h_m}{h^3}\right]$$

Using dimensionless analysis the following groups were formed:-

$\pi_1 = \dfrac{w}{E_1 R}$ where w is load/unit width of roller and E_1 the elastic modulus of the soft layer.

$\pi_2 = {}^{t}/_{R}$

$\pi_3 = \dfrac{pE_1R^2}{\eta^2}$ where p is fluid density and η is viscosity of fluid.

$\pi_4 = \dfrac{u\eta}{E_1R}$ and again $u = \dfrac{u_1 + u_2}{2}$

$$\therefore \; \pi_4 = \frac{u_2\eta}{2E_1R} = {}^{U}/_{2} \text{ say}$$

$\pi_7 = {}^{f}/_{E_1R}$ where f is the friction force generated/ unit width of roller.

Applying the above dimensionless groups to Reynold's equation and writing

$$X = {}^{x}/_{R} \quad \text{and} \quad P = {}^{p}/_{E}$$

$$\text{gives} \quad \underline{\underline{{}^{dP}/_{dX} = 6\,U \left(\frac{H - H_m}{H^3}\right)}}$$

$$\text{Also} \quad h = h_o + \frac{x^2}{2R} + {}^{p}/_{\lambda}$$

$$\text{becomes} \quad H = H_o + \frac{X^2}{2} + AP$$

$$\text{where} \quad H_o = {}^{h_o}/_{R}$$

A is a dimensionless materials stiffness and is derived as follows:-

As assumed previously the soft layer deflection, δ,

$$= {}^{p}/_{\lambda}$$

Considering an unconfined material in commpression as shown in Fig. 4.2.

$$\text{Stress produced, } \sigma, = {}^{L}/_{A}.$$

$$\text{and strain, } \epsilon, = \frac{\delta l}{l}$$

$$E = \frac{\sigma}{\epsilon}$$

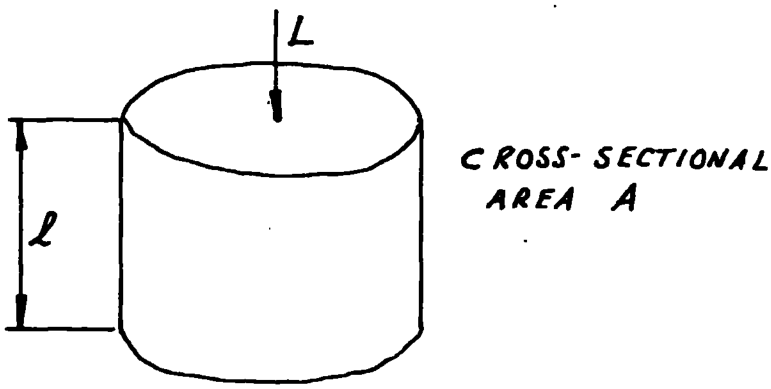

APPLIED LOAD IS L ON A CROSS-SECTIONAL AREA A PRODUCING DEFLECTION $\delta\ell$

FIG. 4.2. COMPRESSION OF UNCONFINED SPECIMEN.

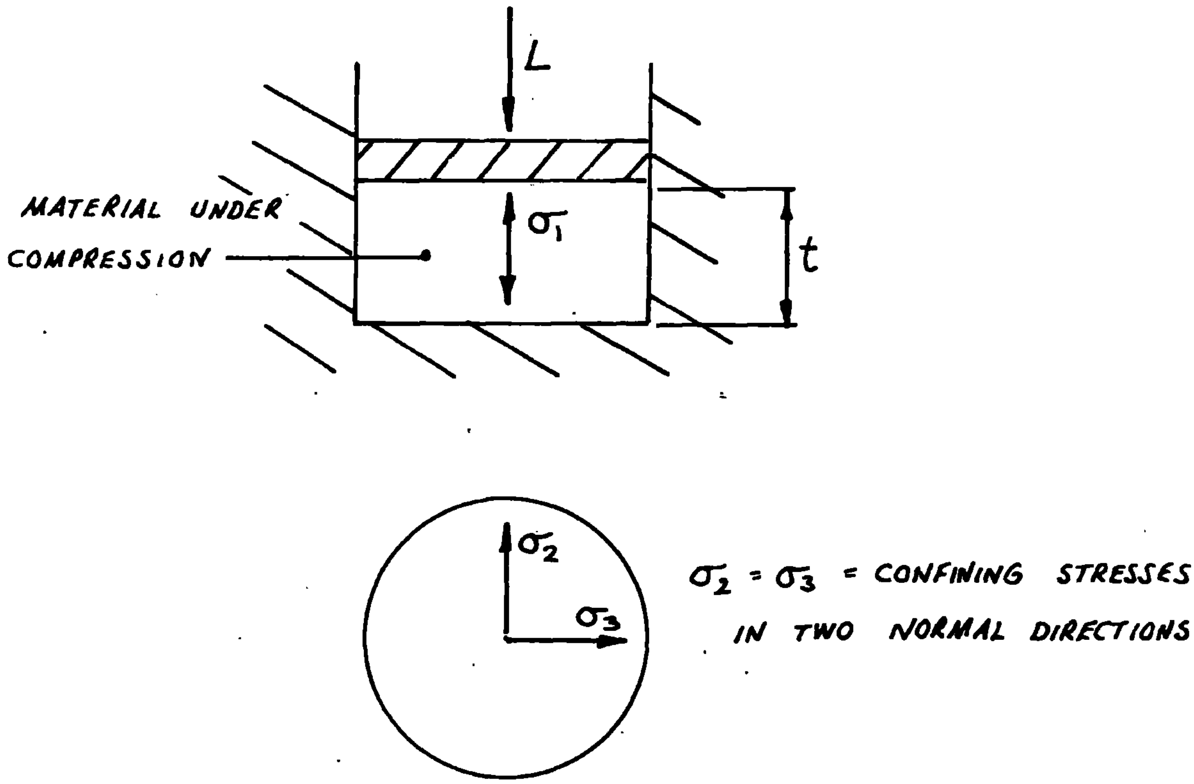

APPLIED LOAD IS L ON A CROSS-SECTIONAL AREA A.

FIG. 4.3. COMPRESSION OF CONFINED SPECIMEN.

Considering a confined material in compression as shown in Fig. 4.3.

The respective strains corresponding to stress σ_1, σ_2 and σ_3 are

$$\epsilon_1 = \frac{1}{E} [\sigma_1 - \upsilon (\sigma_2 + \sigma_3)]$$

where υ is Poisson's ratio for the material

$$\epsilon_2 = \epsilon_3 \text{ as } \sigma_2 = \sigma_3$$

$$\text{and } \epsilon_2 = \epsilon_3 = \frac{1}{E} [\sigma_2 - \upsilon (\sigma_3 + \sigma_1)] = 0$$

$$\text{therefore } \sigma_2 = \sigma_3 = \frac{\upsilon}{1 - \upsilon} \sigma_1$$

$$\epsilon_1 = \frac{1}{E} [\sigma_1 - \frac{2\upsilon^2}{1 - \upsilon} \sigma_1]$$

$$= \frac{\sigma_1}{E} [1 - \frac{2\upsilon^2}{1 - \upsilon}]$$

$$E \text{ confined} = \frac{\sigma_1}{\epsilon_1}$$

$$= \frac{E}{1 - \frac{2\upsilon^2}{1 - \upsilon}}$$

$$\text{and } \frac{1}{\lambda} = \frac{t}{E} [1 - \frac{2\upsilon^2}{1 - \upsilon}]$$

$$\therefore \frac{1}{\lambda} = \frac{t}{E \text{ conf.}}$$

$$\text{Remembering } \delta = {}^{P}/_{\lambda}$$

$$^{\delta}/_{R} = {}^{P}/_{R\lambda}$$

$$= \frac{PE}{R\lambda} \quad \text{as } P = {}^{p}/_{E}$$

and letting $A = \dfrac{E}{R\lambda}$

$$A = {}^{E}/_{R} \quad {}^{t}/_{E \text{ conf.}}$$

$$\therefore A = {}^{t}/_{R} \quad {}^{E}/_{E \text{ conf.}}$$

The equations to be solved are then

$${}^{dP}/_{dX} = 6\,U \left(\frac{H - Hm}{H^3} \right)$$

$$\text{and } H = H_o + {}^{X^2}/_{2} + A.P$$

Determination of the Pressure Distribution

The combination of the equations

$${}^{dP}/_{dX} = 6\,U \left(\frac{H - H_m}{H^3} \right)$$

$$\text{and } H = H_o + {}^{X^2}/_{2} + A.Y$$

is an ordinary differential equation of the first order. The parameter H_m is unknown and must be selected by trial and error so that the boundary conditions are satisfied.

An initial value is selected from H_m and this is successively modified until the location of the downstream boundary is determined. The equation is then solved over the whole range from the inlet boundary to the outlet boundary.

In general the downstream boundary condition will not be satisfied i.e.

$$^{dP}/_{dX} = P = 0$$

and so a limit is set within which the value of the pressure distribution at this point must fall. The details of this will be described in the following sections.

There are many methods available for the step-by-step solution of ordinary differential equations. The one used here is the method of Runge and Kutta which is particularly suitable for solving a first order equation. This was described fully by Higginson (1965) and full details can be found in any textbook of numerical methods.

After the pressure distribution has been determined the load sustained can be found by a simple numerical integration as shown in the following sections. The determination of the friction forces will also be shown in the following sections.

Cavitation Boundary Condition

Before deriving the expressions for friction forces the conditions under which the pressure curve terminates in the divergent clearance will be considered.

Fig. 4.4. shows curves which could represent the pressure distribution at the end of the load carrying film. Dowson and Higginson (1966) have shown that only a pressure distribution of the kind represented by curve (b) in Fig. 4.4. will give flow continuity whilst curve (a) will lead to disruption of the load carrying film, inducing cavitation.

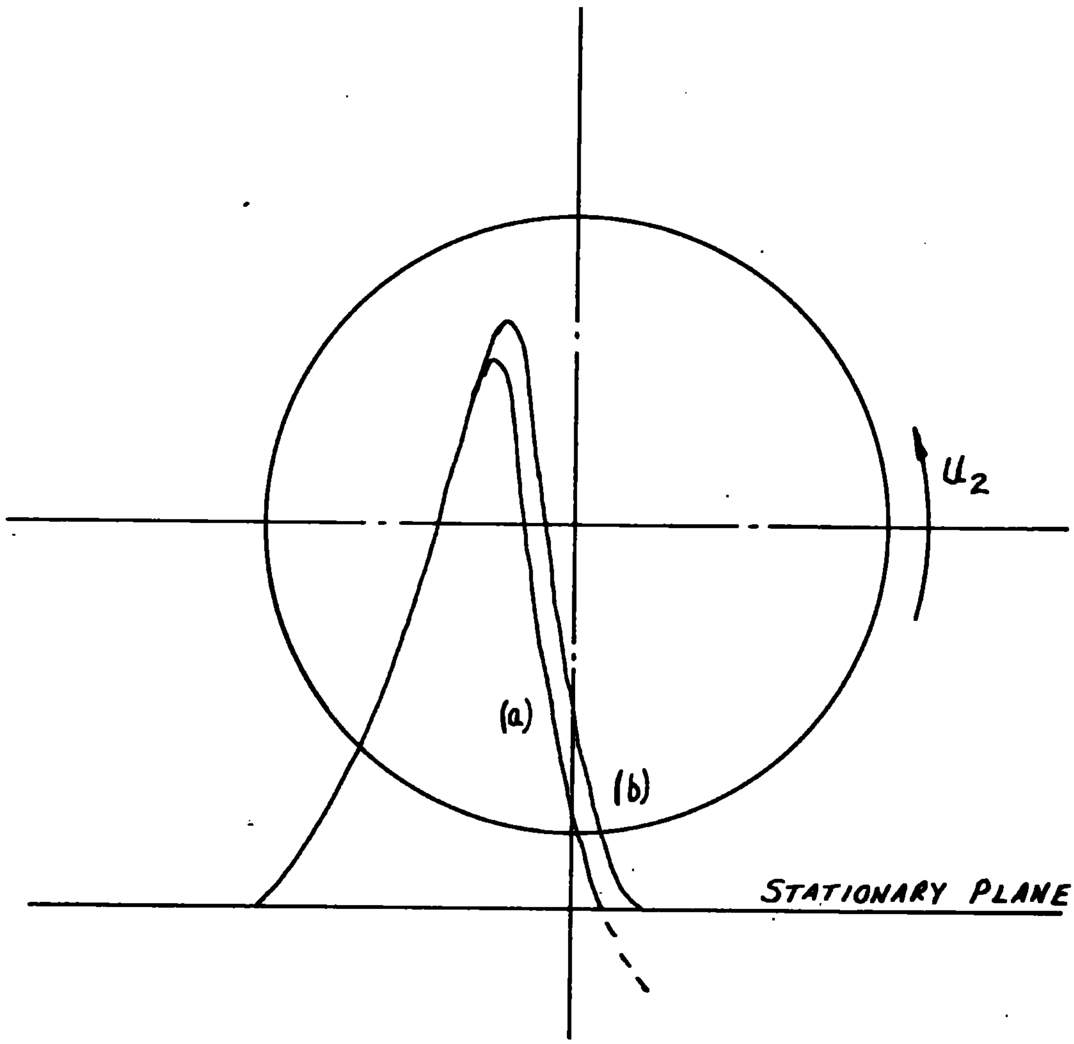

FIG. 4.4. CAVITATION BOUNDARY CONDITION.

Mineral oils contain about 8 to 10 per cent of dissolved air and this air is liberated in the form of bubbles when the lubricant film pressure falls. Observations in the past have revealed that the lubricant traverses the cavitated region of bearings in a series of thin streams. These streams are separated by large spaces of liberated gases resulting from the fall in pressure of the lubricant film.

Referring once more to curve (b) in Fig. 4.4., the cavitation boundary condition to satisfy flow continuity will be,

$$p = {}^{dp}/_{d\theta} = 0, \quad \theta = \theta_2 \text{ (outlet)}$$

where p is the gauge pressure.

The shear stresses in the cavitated region act over a small proportion of the solid surfaces due to the presence of air bubbles and hence different stress equations must be used in the load carrying and cavitated parts of the contact. Referring to the z-direction and allowing $\bar{z}$ to be the fraction of the clearance space width occupied by the lubricant in this direction, then to satisfy flow continuity,

$$\bar{z} = {}^{h_m}/_{h}$$

where h_m is the film thickness at the point of maximum pressure (where ${}^{dp}/_{dx} = 0$).

Determination of Load and Friction Forces

In Fig. 4.5., showing the cylinder and plane with pressure curve the length δr at angle θ^{o} on the cylinder surface can be taken as equal to δx for small angles of θ.

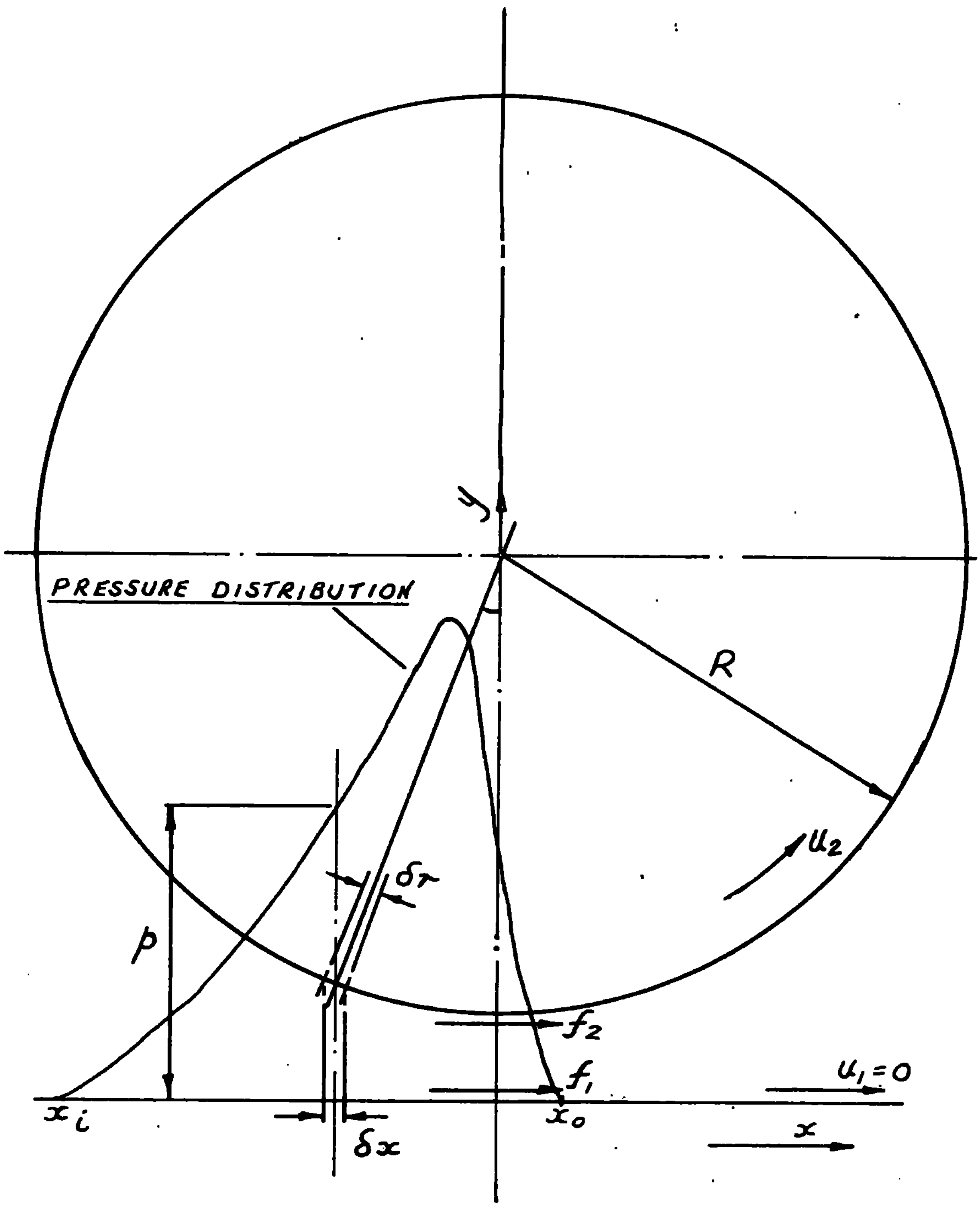

FIG. 4.5. FORCES ON ROLLER AND PLANE.

Therefore over the length x_i to x_o the load w per unit width will be equal to

$$p_x \cdot \delta x$$

$$\therefore \delta w/\text{unit width} = p_x \cdot \delta x$$

$$w = \int_{x_i}^{x_o} p \cdot dx.$$

Thus using Simpson's Rule or some other similar method the above expression can be easily determined.

The general expressions for the tangential (viscous) forces f_1 and f_2 acting on the solids need to be derived not only over the length x_i to x_o but over a length in the cavitated region also, i.e. from x_o to some point downstream. From the section devoted to the cavitation boundary condition it will be seen that flow continuity yields the relationship

$$\bar{z} = {}^{h_m}/_{h}$$

In general the cavitated zone will terminate at some point between x_o and R. Owing to the very small width of the oil streams at large values of x the contribution to the total shear forces from this region is small. For convenience it will be assumed that the cavitated oil film extends to x = R.

The gneral expression for the tangential force f_1

$$= \int_{x_i}^{x_o} \tau \, dx + \int_{x_o}^{R} \bar{z} \, \tau \, dx$$

As only the force acting on the plane is required, f_2 will not be derived.

At the plane, $y = 0$ and as this is the stationary solid $u_1 = 0$.

$$\tau = \eta \, {}^{\partial u}/_{\partial y}$$

$$= {}^{dp}/_{dx} \, (y - {}^{h}/_{2}) + \eta \left(\frac{u_1 - u_2}{2} \right)$$

$$\therefore \tau = - {}^{h}/_{2} \, {}^{dp}/_{dx} + \eta \, {}^{u_2}/_{h}$$

$$\text{and } {}^{dp}/_{dx} = 6 \, \eta \, u_2 \left(\frac{h - h_m}{h^3} \right)$$

$$\therefore \eta \, {}^{u_2}/_{h} - {}^{h}/_{2} \cdot {}^{dp}/_{dx} = {}^{h}/_{2} \cdot 6 \, \eta \, u_2 \left(\frac{h - h_m}{h^3} \right) + \eta \cdot {}^{u_2}/_{h}$$

$$\therefore \underline{\underline{\tau = {}^{\eta u_2}/_{h} \cdot \left[1 - 3 \left(\frac{h - h_m}{h^3} \right) \right]}}$$

The above expression will be valid for τ over the region x_i to x_o. In the cavitated region, however, the pressure term will be absent as the pressure is constant. Hence,

$$\tau = \eta \cdot {}^{u_2}/_{h} \cdot \bar{z}$$

$$= \underline{\underline{\eta \cdot {}^{u_2}/_{h} \cdot {}^{h_m}/_{h}}}$$

The general expression for the tangential force thus becomes

$$f_1 = \int_{x_i}^{x_o} \frac{\eta u_2}{h} \left[1 - 3 \left(\frac{h - h_m}{h} \right) \right] dx + \int_{x_o}^{R} \frac{\eta u_2}{h} \, \frac{h_m}{h} \, dx$$

As with the pressure distribution the numerical calculations for both load and forces will be calculated in dimensionless terms.

$$\text{Load } w = \int_{x_i}^{x_o} p \; dx$$

$$\text{and } P = {}^{p}/_{E} \text{ and } X = {}^{x}/_{R}$$

$$\therefore \quad w = \int_{X_i}^{X_o} P\,E\,R \; dX$$

$$^{w}/_{ER} = W, \text{ say}$$

$$= \int_{X_i}^{X_o} P \; dX$$

$$\therefore \quad W = \int_{X_i}^{X_o} P \; dX$$

Tangential force, f_1,

$$= \int_{x_i}^{x_o} \frac{\eta u_2}{h}\left[1 - 3\left(\frac{h - h_m}{h}\right)\right] dx + \int_{x_o}^{R} \frac{\eta u_2}{h}\,\frac{h_m}{h}\, dx$$

$$\text{and by definition } U = \frac{\eta u_2}{E_1 R}$$

$$\therefore f_1 = \int_{X_i}^{X_o} \frac{UE_1}{H}\left[1 - 3\left(\frac{H - H_m}{H}\right)\right] R \; dX + \int_{X}^{1} \frac{UE_1}{H}\,\frac{H_m}{H}\, R \; dX$$

$$\text{and } f_1/_{E_1 R} = TF, \text{ say,}$$

$$= U \int_{X_i}^{X_o} \left[\left\{ 1 - 3 \left(\frac{H - H_m}{H} \right) \right\} / H \right] dX + U \int_{X_o}^{1} \frac{H_m}{H^2} \, dX$$

$$\therefore TF = U \int_{X_i}^{X_o} \left[\left\{ 1 - 3 \left(\frac{H - H_m}{H} \right) \right\} / H \right] dX + U \int_{X_o}^{1} \frac{H_m}{H} \, dX$$

As the dimensionless radius R = 1 the cavitation friction force will be integrated between X_o and 1.

The terms $\left[\left\{ 1 - 3 \left(\frac{H - H_m}{H} \right) \right\} / H \right]$ and ${}^{H_m}/_{H^2}$ shall be called F and CF respectively for computing purposes, thus,

$$TF = U \int_{X_i}^{X_o} F \, dX + U \int_{X_o}^{1} CF \, dX$$

The terms $U \int_{X_i}^{X_o} F \, dX$ and $U \int_{X_o}^{1} CF \, dX$ shall be called FER and CFER respectively for computing purposes.

Section 2. Computer Notation and Programs

The computer language used to solve the Reynold's equation in section 1 was Fortran IV and the programs used will be more easily understood if reference is made to Fig. 4.6. and the corresponding notation which follows.

UNIT	DIMENSIONLESS FORM	COMPUTER FORM
x_i - pressure inlet	X_i $\left({}^{x_i}/_R\right)$	XI
x_o - pressure outlet	X_o $\left({}^{x_o}/_R\right)$	XO
p - pressure	P $\left({}^{p}/_E\right)$	P
h_o - centre-line film thickness	H_o $\left({}^{h_o}/_R\right)$	HO
h_m - film thickness at ${}^{dp}/_{dx} = p = 0$	H_m $\left({}^{h_m}/_R\right)$	HM
h - total film thickness $= h_o + {}^{x^2}/_{2R} + \delta$	H $\left({}^{h}/_R\right)$	HA
${}^{x^2}/_{2R}$	$\frac{X^2}{2}$	XT
$\delta = {}^{p}/_{\lambda}$ deflection due to pressure p.	AP	Q
η - viscosity u_2 - roller speed	$\frac{\eta u_2}{ER}$	U

UNIT	DIMENSIONLESS FORM	COMPUTER FORM
$x^2/_{2R}$ from AA^1 (i.e. pressure outlet to cavitation exit CE)	$x^2/_2$	S
h - total film thickness in region AA^1 to CE $= h_o + x^2/_{2R}$	$h_x/_R$	HX
w - load carried per unit width of roller	$w/_{ER}$	W
f_1 - friction force per unit width of roller composed of friction force in pressure curve zone and friction force in cavitated zone	$f_1/_{ER}$	TF
f - friction force per unit width of roller in pressure zone	$f/_{ER}$	FER
cf - friction force per unit width of roller in cavitated zone.	$cf/_{ER}$	CFER
Ordinates of term $\left[\left\{1 - 3\left(\frac{H - H_m}{H}\right)\right\}/H\right]$	$\left[\left\{1 - 3\left(\frac{H - HM}{H}\right)\right\}/H\right]$	F
Ordinates of term $H_m/_{H^2}$	$HM/_{H^2}$	CF
A - dimensionless stiffness term of soft layer	$t/_{R.}$ E free$/_{E}$ conf.	A

UNIT	DIMENSIONLESS FORM	COMPUTER FORM
Coefficient of friction over pressure zone only	$\frac{f/ER}{W/ER}$	FER/W (UFER)
Coefficient of friction over zone from pressure inlet to cavitation outlet	$\frac{f_1/ER}{W/ER}$	TF/W (UTF)

Other relevant terms used in the computing procedures are shown overleaf.

FIG.4.6. COMPUTER NOTATION

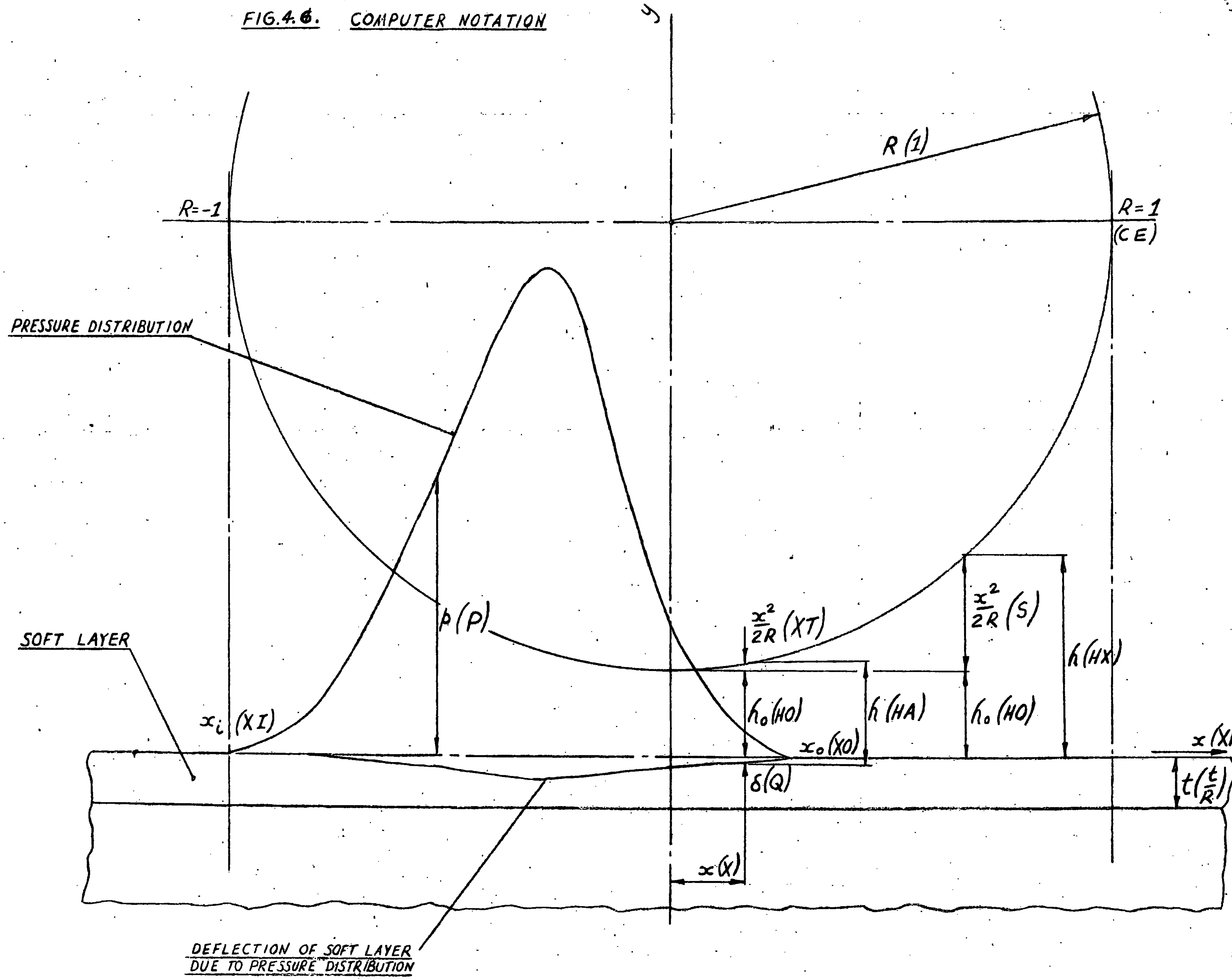

	COMPUTER FORM
Adjustment factor for updating HM	ADJ
Number of spaces distance XI to XO is divided into for computing pressure curve with Runge-Kutta method and friction	Z
Number of points over distance XI to XO	N
Number of spaces distance XO to CE is divided into for computing cavitation friction	C
Number of points over distance XO to CE	M
Area of small strip of pressure curve	QUAD
Area of small strip of friction curve over distance XI to XO	RECT
Area of small strip of cavitation friction over distance XO to CE	OBLO

A number of programs were used, all being programmed for the I.B.M. 360/67 and written in Fortran IV.

The first program to be described will be PROG. ONE which was used for solving rigid cases only. The program is shown under Appendix 1 and the corresponding flow diagram under Fig. 4.7. This program modifies the originally selected value of HM by adding or subtracting a small increment from HM until the downstream boundary is located. It was realised at an early stage that this program was time-consuming and a more efficient program, PROG. TWO, was developed. In PROG. TWO two values of HM are assumed for the first two trials

FIG. 4.2. FLOW CHART FOR PROG. ONE.

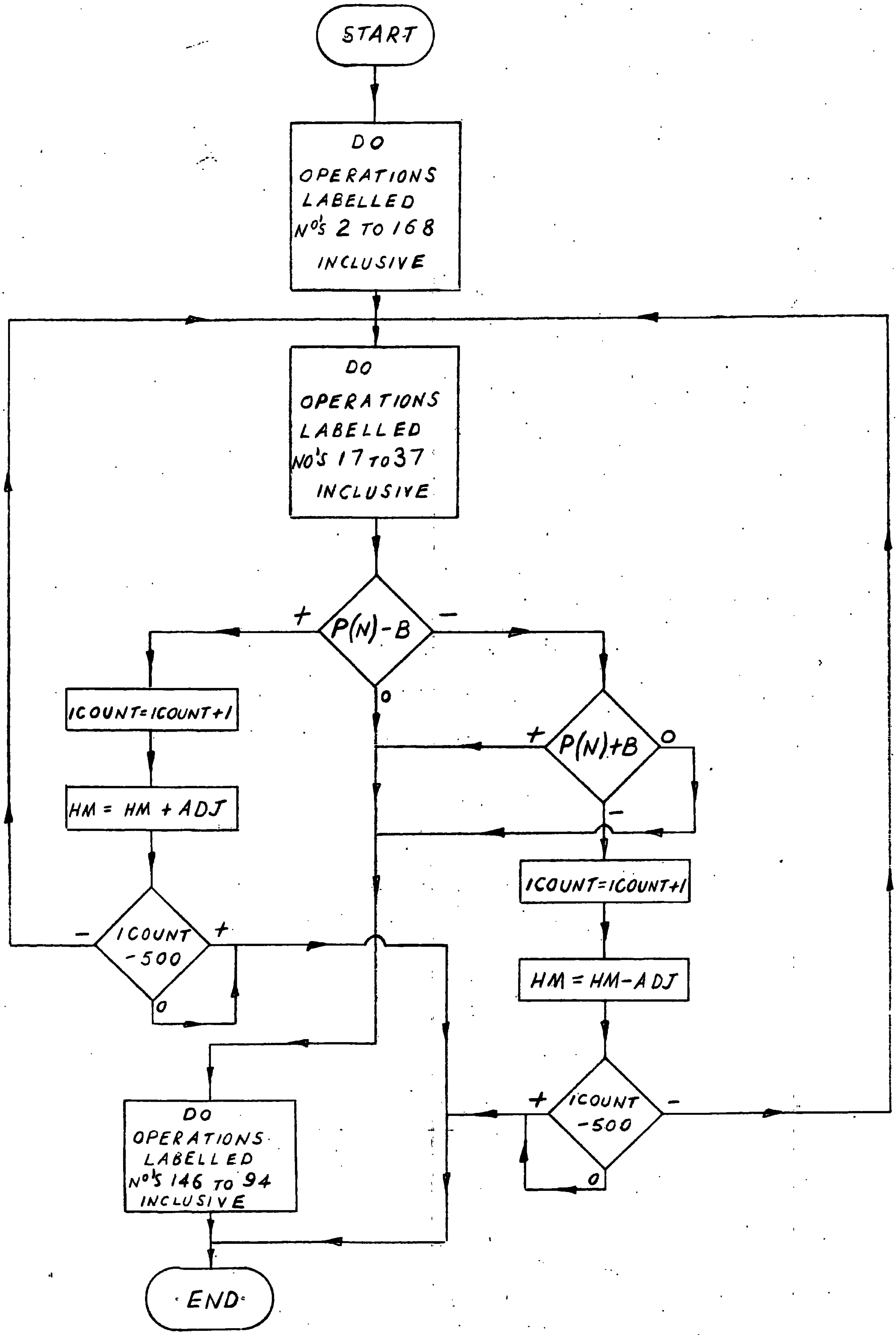

the first value of HM is required to give a positive pressure run-out. The two values of HM are used to interpolate a third value of HM to give a pressure run-out nearer to zero. The process is continued until the pressure run-out is within an acceptably small value. The program and its corresponding flow chart are shown under Appendix 2 and Fig. 4.8. respectively.

PROG. TWO worked very well for the rigid cases for all the selected values of centre-line film thickness, HO, and all dimensionless speeds, U. The program also worked well for the elastic cases for values of HO which were not less than 10^{-3} and worked over the entire selected speed range for elastic cases where A, the dimensionless stiffness term, did not exceed 15.40×10^{-3} i.e. the 0.05 inch and 0.1 inch thick specimens. However, with values of HO less than 10^{-3} with the 0.05 inch and 0.1 inch thick specimens, some difficulty was met in obtaining a satisfactory pressure run-out. This also applied for values of HO less than 10^{-2} with the 0.2 inch and 0.5 inch thick specimens i.e. the sensitivity of the pressure run-out increases with a decrease in centre-line film thickness and increases as the dimensionless stiffness term, A, increases.

Many methods have been adopted in the past to obtain satisfactory pressure curves such as those developed by Dowson and Higginson (1959) and Dowson and Whitaker (1964). None of the methods used in the past was adopted however as it was found that a suitable pressure curve could be obtained quite easily by a simple modification to the program PROG. TWO previously described. The modified PROG. TWO is shown under Appendix 3 as PROG. THREE, and its corresponding flow chart, which varies little from that of PROG. TWO, under Fig. 4.9.

FIG. 4.8 FLOW CHART FOR PROG. TWO.

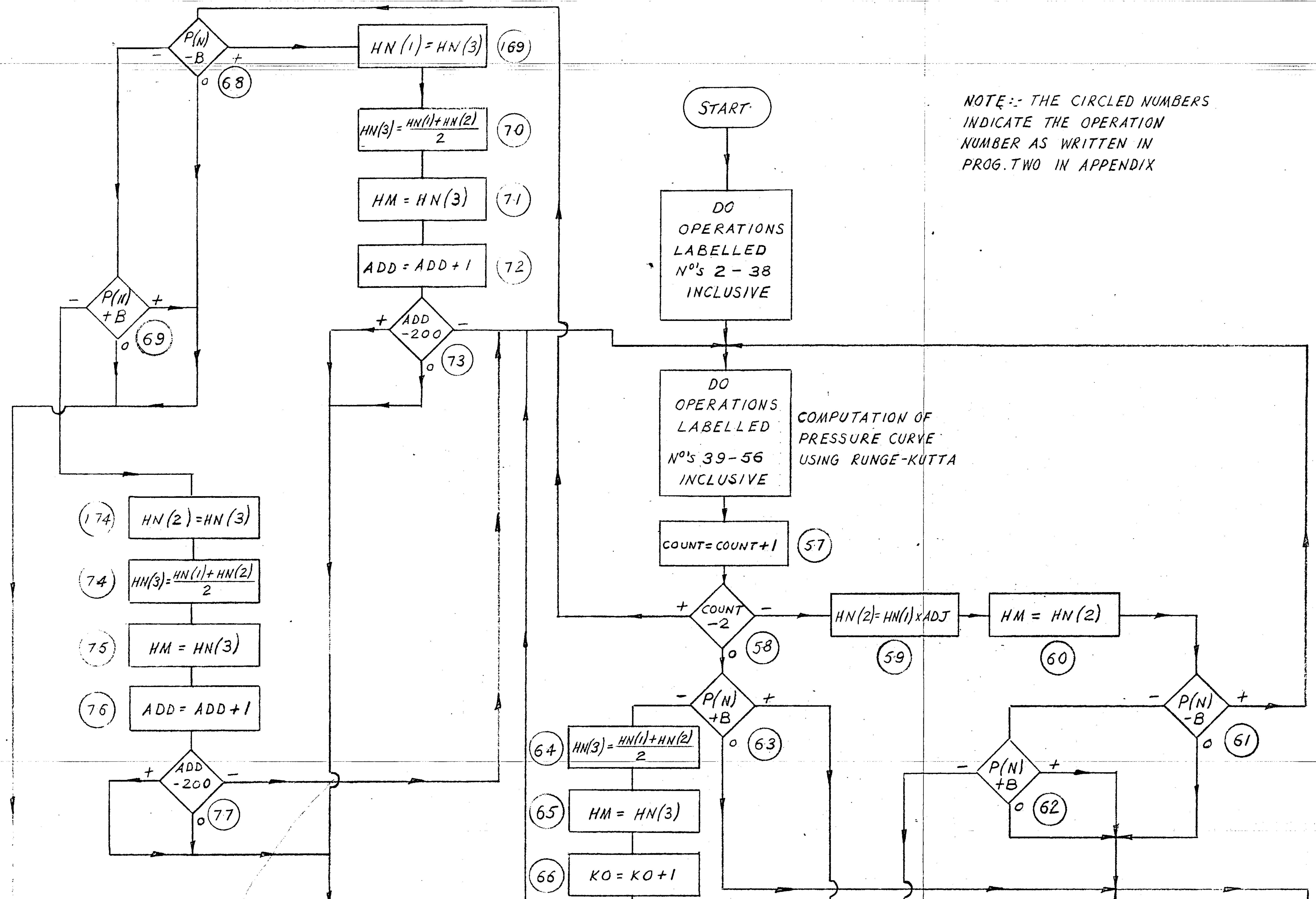

FIG. 4.9. FLOW CHART FOR PROG. THREE.

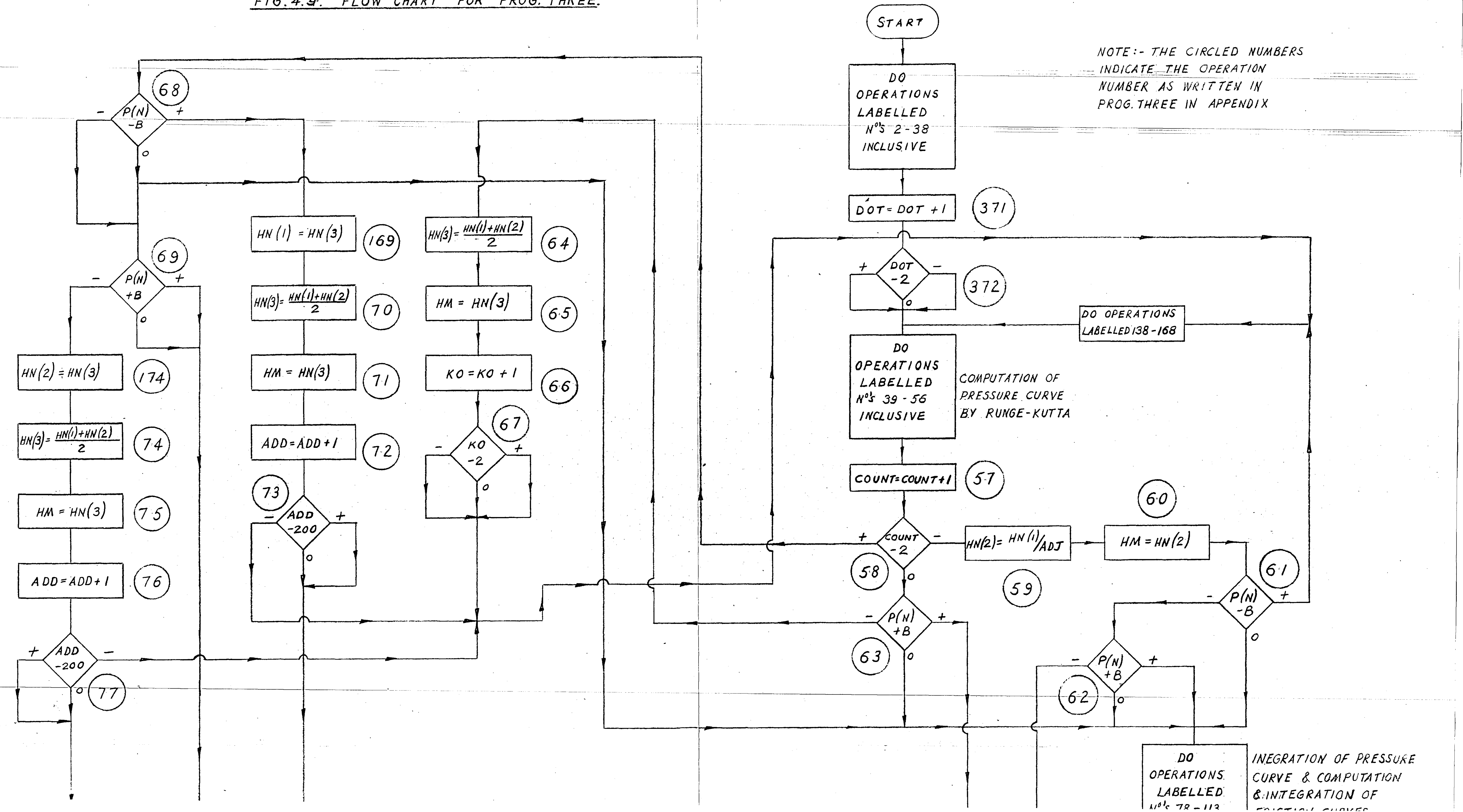

As with PROG. TWO two values of HM are assumed for the first two trial pressure curves. However, instead of working forward from the pressure inlet, XI, towards the pressure outlet, XO, the program works backwards from the normal pressure outlet, XO, to the pressure inlet, XI. This drastically reduces the sensitivity of the calculation to the position of the end of the pressure curve (which is of course the inlet point physically) and whereas with the forward calculation it is difficult to obtain a satisfactory pressure curve, this reverse solution gives a perfectly acceptable curve in a few cycles. If reference is made to Fig. 4.10 and Fig. 4.11 a comparison can be made of the respective pressure curves obtained using PROG. TWO and PROG. THREE respectively. As with PROG. TWO once the pressure curve has been found the friction forces and load are calculated in the same manner as in PROG. TWO.

FIG. 4.10. DEVELOPMENT OF PRESSURE CURVES USING PROG. TWO.

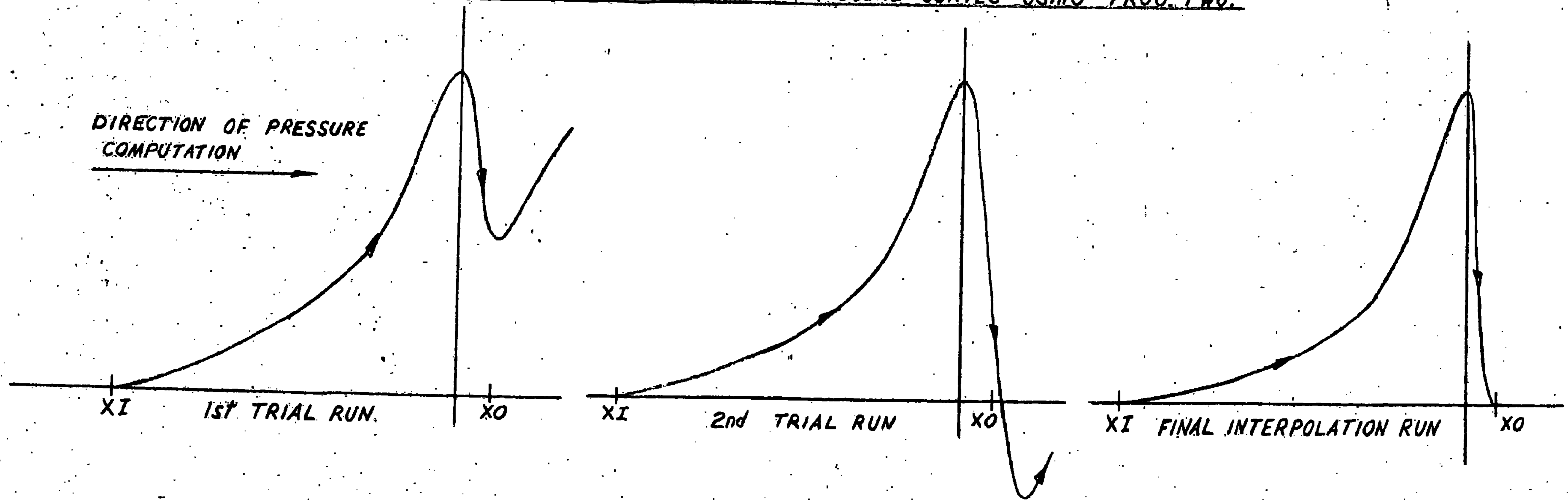

FIG. 4.11. DEVELOPMENT OF PRESSURE CURVE USING PROG. THREE.

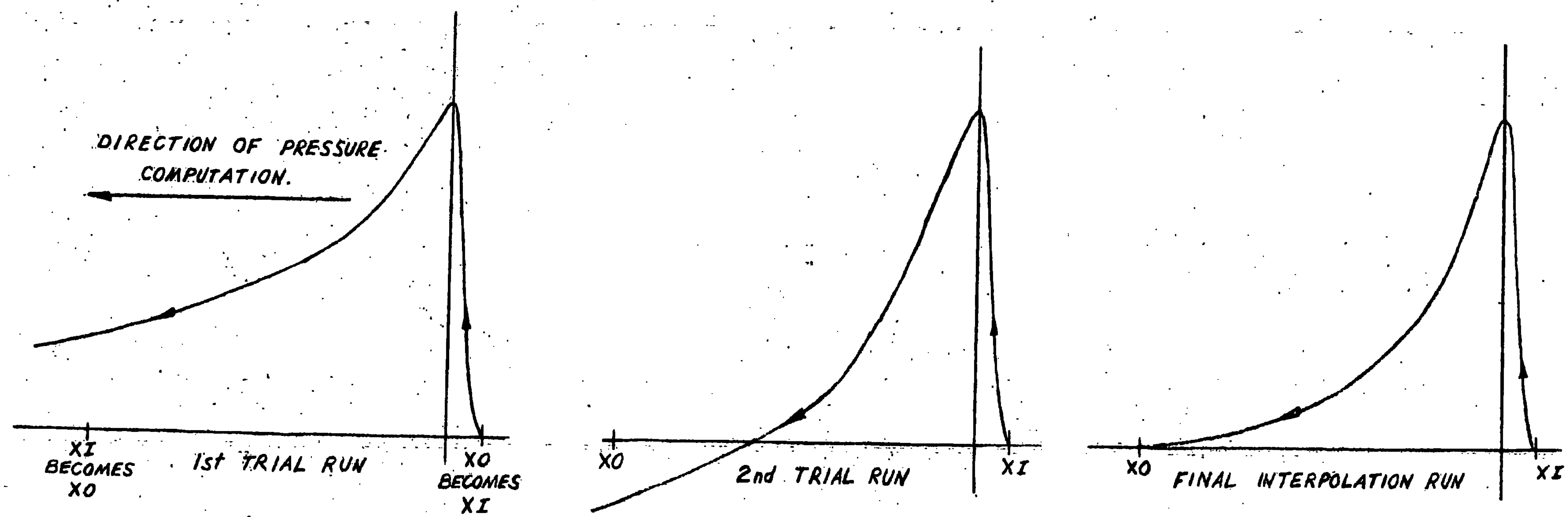

FIG. 4. 10. & 11.

CHAPTER 5

Discussion of Results

Section 1. Experimental Results

Graphs to show the comparisons of friction force against viscosity and speed for loads of 10 and 20 lb/in are shown in Figs. 5.1. and 5.2. respectively. The graphs show comparisons for the rigid and elastic specimens excluding the .03 inch thick specimen.

It will be seen that the values of friction force for each given load and speed are very much the same for all the elastic specimens. The values of friction force, in fact, fall within a band approximately .025 lb/in wide. The upper limit of this band belongs clearly to the .05 and .1 inch thick specimens and the lower limit to the thicker .2 and .5 inch thick specimens. The rigid specimen friction forces are only slightly higher than those of the elastic specimens, this being more apparent in Fig. 5.1. where hydrodynamic lubrication persists to a lower speed with the rigid specimen than it does in Fig. 5.2.

The most striking feature about the elastic specimens is the extreme persistance of hydrodynamic lubrication down to very low speeds. For example, the coefficient of friction is only .003 for 10 lb/in load at 2.5 in/sec sliding speed and .004 for 20 lb/in load at the same speed. In comparison, Dowson, Longfield, Walker and Wright (1968) state that friction forces in healthy human joints are extremely low, even at high load and low speed, and friction co-efficients as low as .002 have been recorded.

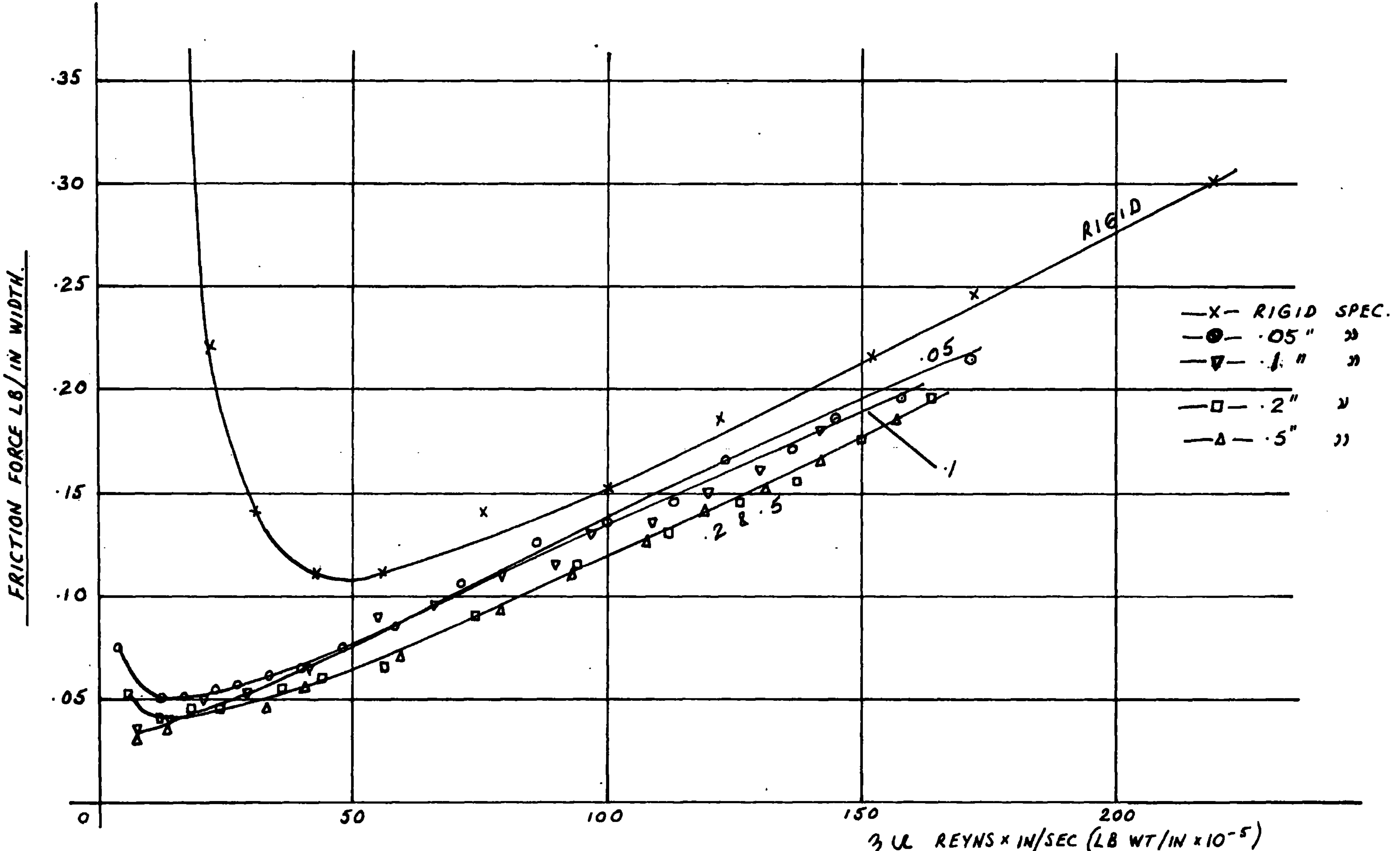

FIG. 5 . 1 . COMPARISON OF EXPT. RESULTS FOR RIGID, ·05, ·1, ·2 & ·5 SPECS. FOR 10LB/IN LOAD.

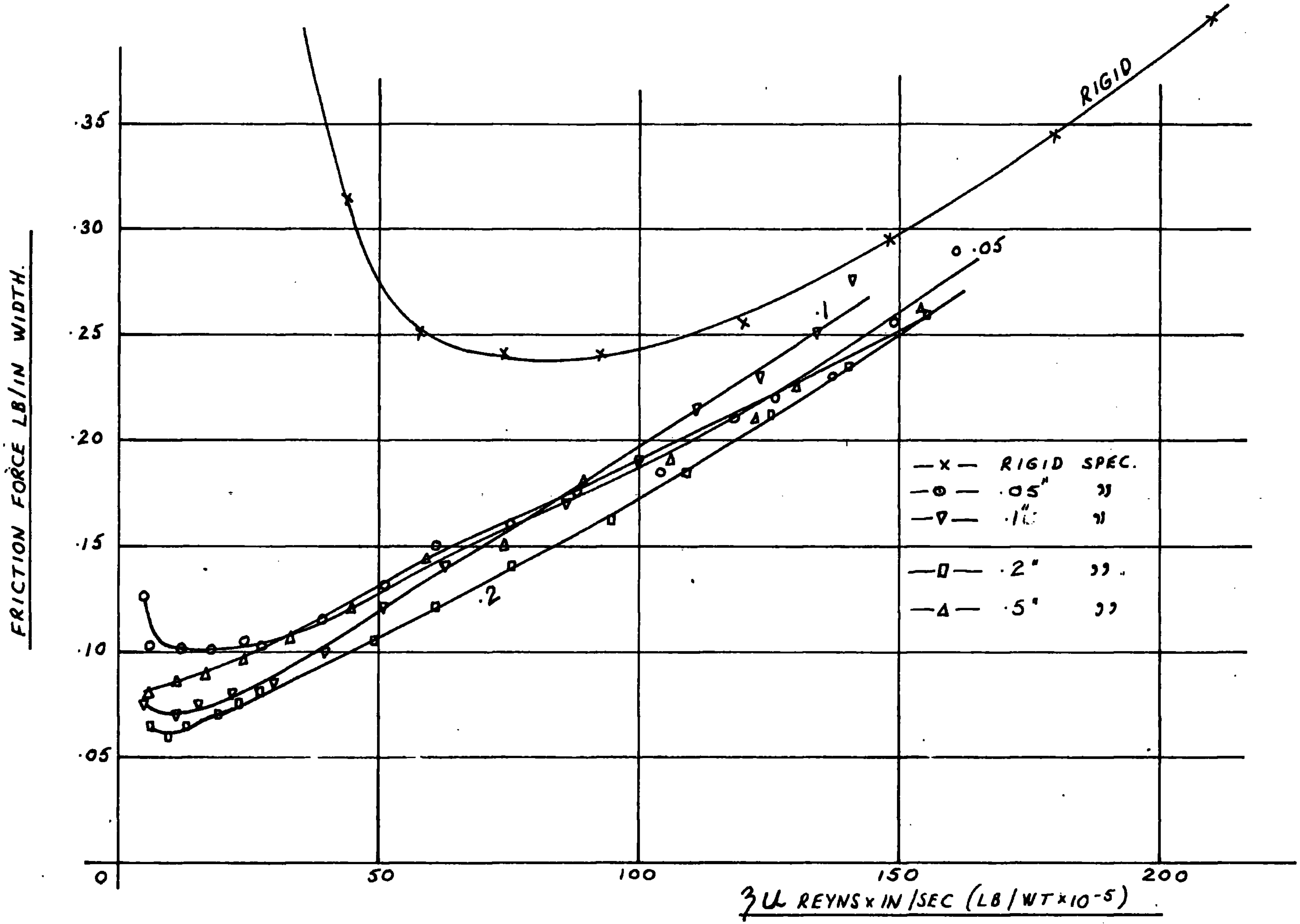

FIG. 5.2. COMPARISON OF EXPT. RESULTS FOR RIGID, ·05, ·1, ·2 & ·5 SPECS. FOR 20 LB/IN LOAD.

The rigid specimen friction forces show the characteristic sharp increase as sliding speed falls below that at which hydrodynamic lubrication predominates and boundary lubrication starts to take effect. The measured surface roughness figures for the roller and Tufnol were 20 and 30 μ-inches C.L.A. respectively. These figures would give peak-to-valley heights of approximately 80 and 120 μ-inches. The sum of the peak-to-valley heights is then in the region of 200 μ-inches. It is worth noting at this point the theoretical minimum film thickness for the rigid specimen (as shown for example in Figs. 5.15. and 5.16.). The minimum film thicknesses for a load of 10 lb/in at 100 rev/min are approximately 200 and 300 μ-inches respectively. The above speeds correspond to the speeds in Figs. 5.1. and 5.2. where the "rigid" curves start to depart significantly from the hydrodynamic regime. It will be seen that the sum of peak-to-valley heights of 200 μ-inches corresponds closely to the theoretical minimum film thickness.

The thinner elastic specimens, in particular the .05 inch thick specimen, show the same tendency as the rigid specimen of an increase in friction force as speed falls. However, the speed at which this occurs is greatly reduced as compared to the rigid specimen for the same loads. For example, at 20 lb/in load, hydrodynamic lubrication persists down to approximately 50 in/sec with the rigid specimen whilst it continues to approximately 5 in/sec with the .05 inch thick elastic specimen.

Examination of the results obtained from tests on the .03 inch thick elastic specimen differ significantly from results obtained from the elastic specimens mentioned above. Figs. 5.3. and 5.4. show comparisons of friction force against viscosity and speed for the

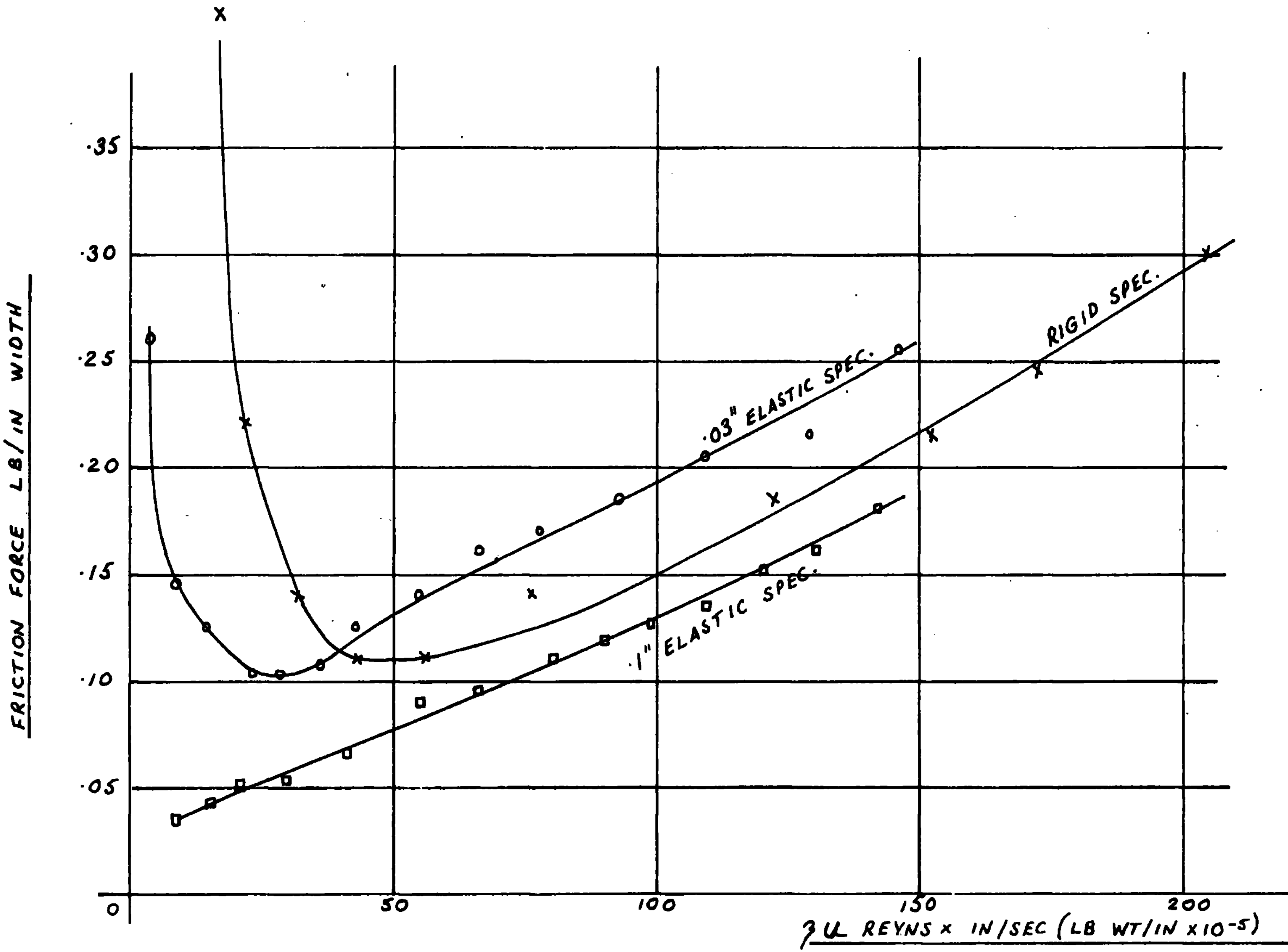

FIG. 5.3. COMPARISON OF EXPT. RESULTS FOR RIGID, ·03 & ·1 SPECS. FOR 10 LB/IN LOAD.

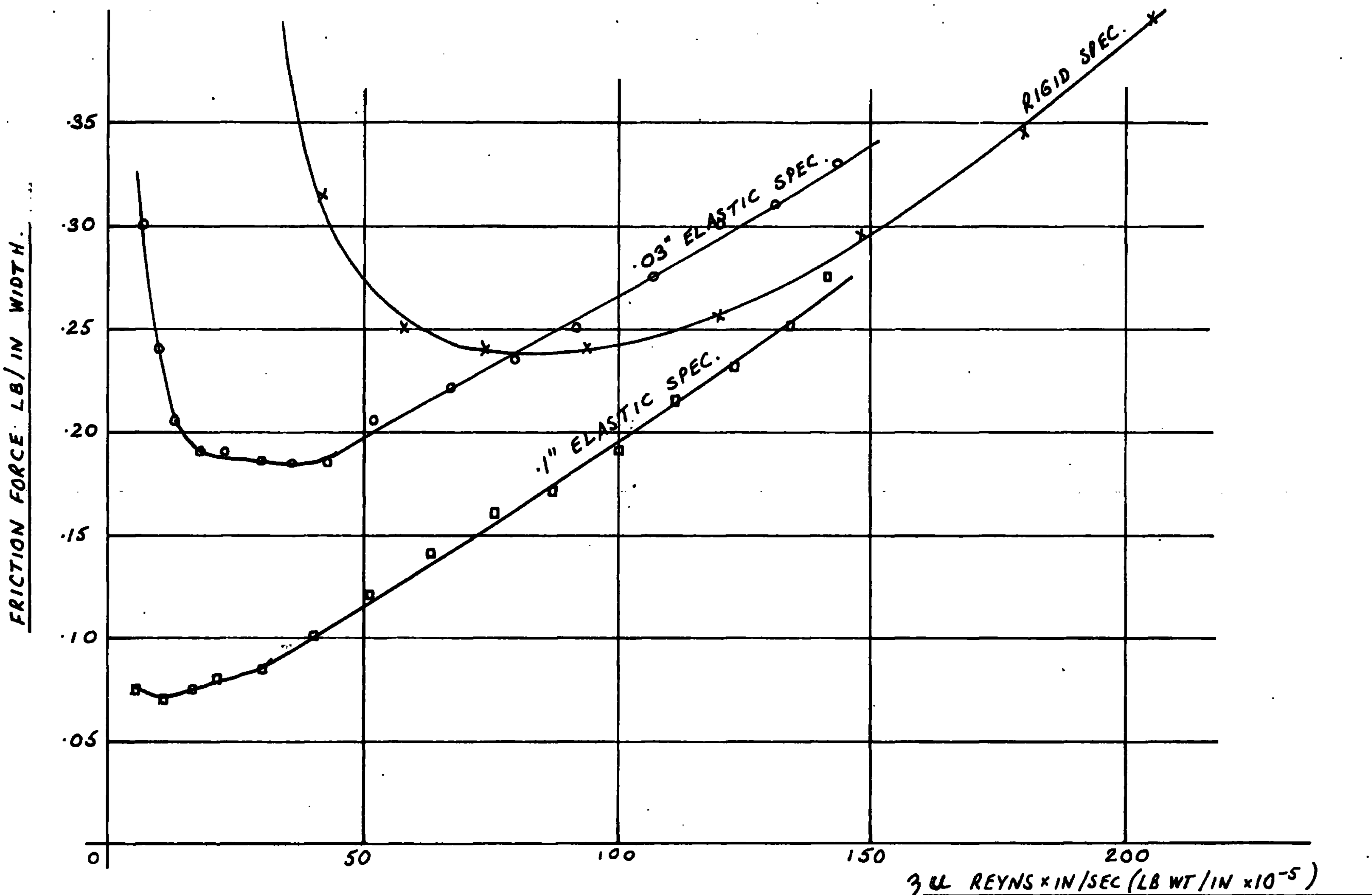

FIG. 5.4. COMPARISON OF EXPT. RESULTS FOR RIGID, ·03 & ·1 SPEC. FOR 20 LB/IN LOAD.

rigid, .03 inch thick and .1 inch thick elastic specimens for 10 and 20 lb/in loads respectively. It will be remembered at this stage that the .03 inch thick specimen had been ground to this thickness.

It can be clearly seen that the .03 inch thick specimen provides the beneficial effect of hydrodynamic lubrication to speeds lower than those for the rigid specimen at both loads. This is not as pronounced as the other elastic specimens however and the marked differences in comparison to the .1 inch thick specimen can be clearly seen in Figs. 5.3. and 5.4. As speed falls there is an increase of friction force which is typical of the rigid specimen. The notable difference between the .03 inch thick specimen and the other elastic specimens is the presence in the former of higher friction forces in the hydrodynamic region than those of the rigid specimen. This is presumably due to roughness effects and if reference is made to Fig. 3.7. the friction forces in the hydrodynamic region of the .02 inch thick specimen will be seen to be even higher than those of the .03 inch thick specimen. Although the .02 and .03 inch thick specimens were produced by grinding, the comparable surface roughness figures are 156 μ-inches C.L.A. and 62 μ-inches C.L.A. respectively. This furthers the above presumption that as surface roughness increases, there is a corresponding increase of friction force in the hydrodynamic region.

Section 2. Theoretical Results

The theoretical results are not tabulated but shown graphically only.

Fig. 5.5. shows the results for the rigid specimen as they were obtained from the computer. The dimensionless load, W, was plotted against the dimensionless friction force on the flat plate, TF, for various values of dimensionless speed, U. The horizontal lines a, b, c, d and e represent dimensionless loads equivalent to 5, 10, 15, 20 and 25 lb/in respectively. From Fig. 5.5. the graphs as shown in Fig. 5.6. were interpolated. Fig. 5.6. shows graphs of friction force (dimensionless) plotted against speed (dimensionless) for various loads, these loads being the dimensionless equivalents of 5, 10, 15, 20 and 25 lb/in.

Graphs similar to those in Fig. 5.6. were obtained for all the elastic specimens and are shown under Figs. 5.10., 11, 12, 13 and 14.

A plot was also made of μ, coefficient of friction $^{TF}/_{W}$, against $^{U}/_{W}$ for all loads for the rigid specimen. It was found, as expected, that one line satisfied all the points obtained and the graph is shown in Fig. 5.7.

Graphs of $^{TF}/_{W}$ against $^{U}/_{W}$ were also plotted for the elastic specimens. Two of these graphs are shown under Fig. 5.8. and Fig. 5.9. corresponding to the .03 inch thick specimen and the .1 inch thick specimen respectively.

Referring to Fig. 5.8., some small divergence of the points corresponding to different loads can be seen, but one line can be drawn to satisfy all the points fairly well. However, referring

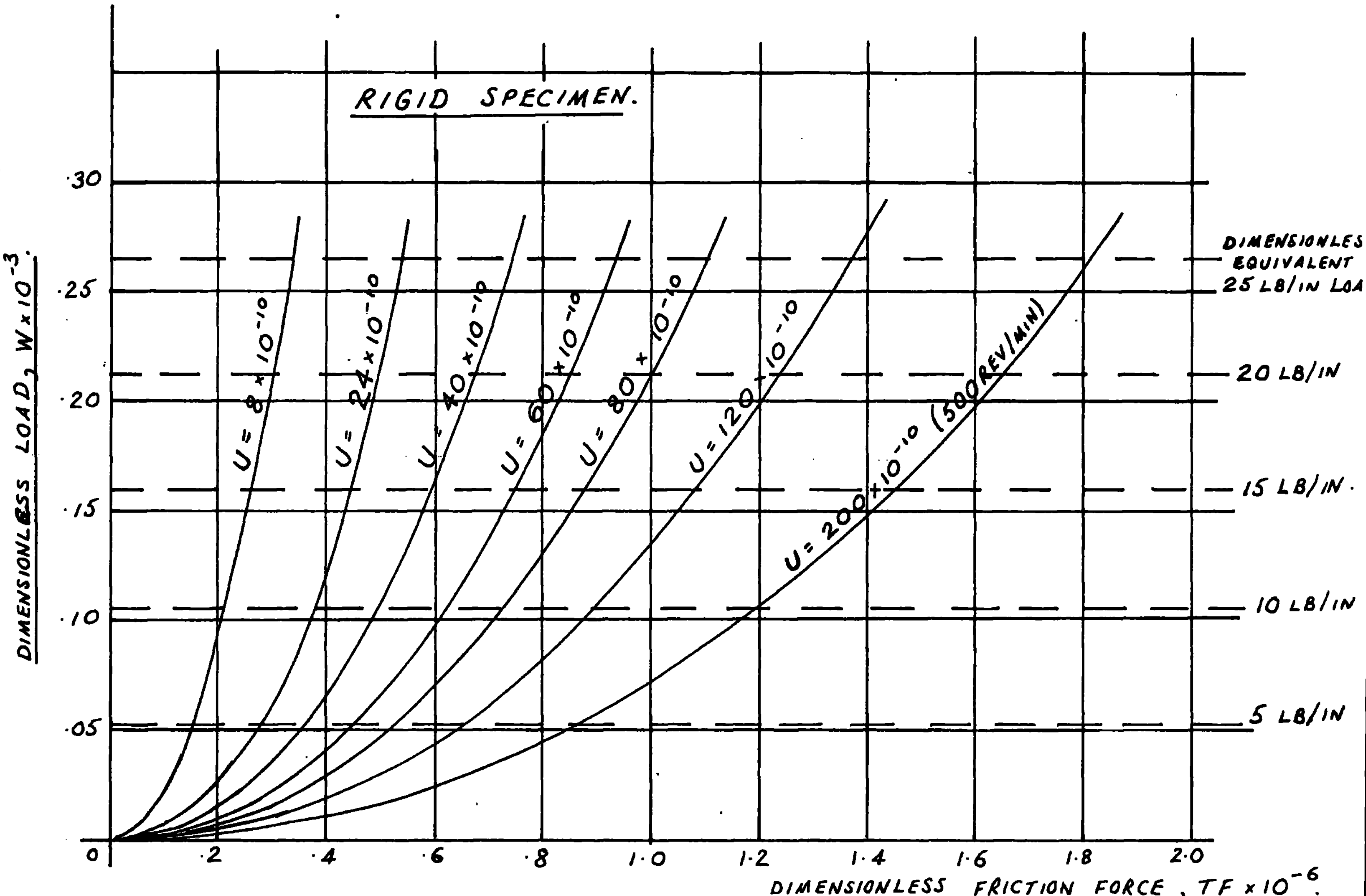

FIG. 5.5. THEORETICAL CURVES FOR LOAD~FRICTION FORCE FOR VARIOUS SPEEDS.

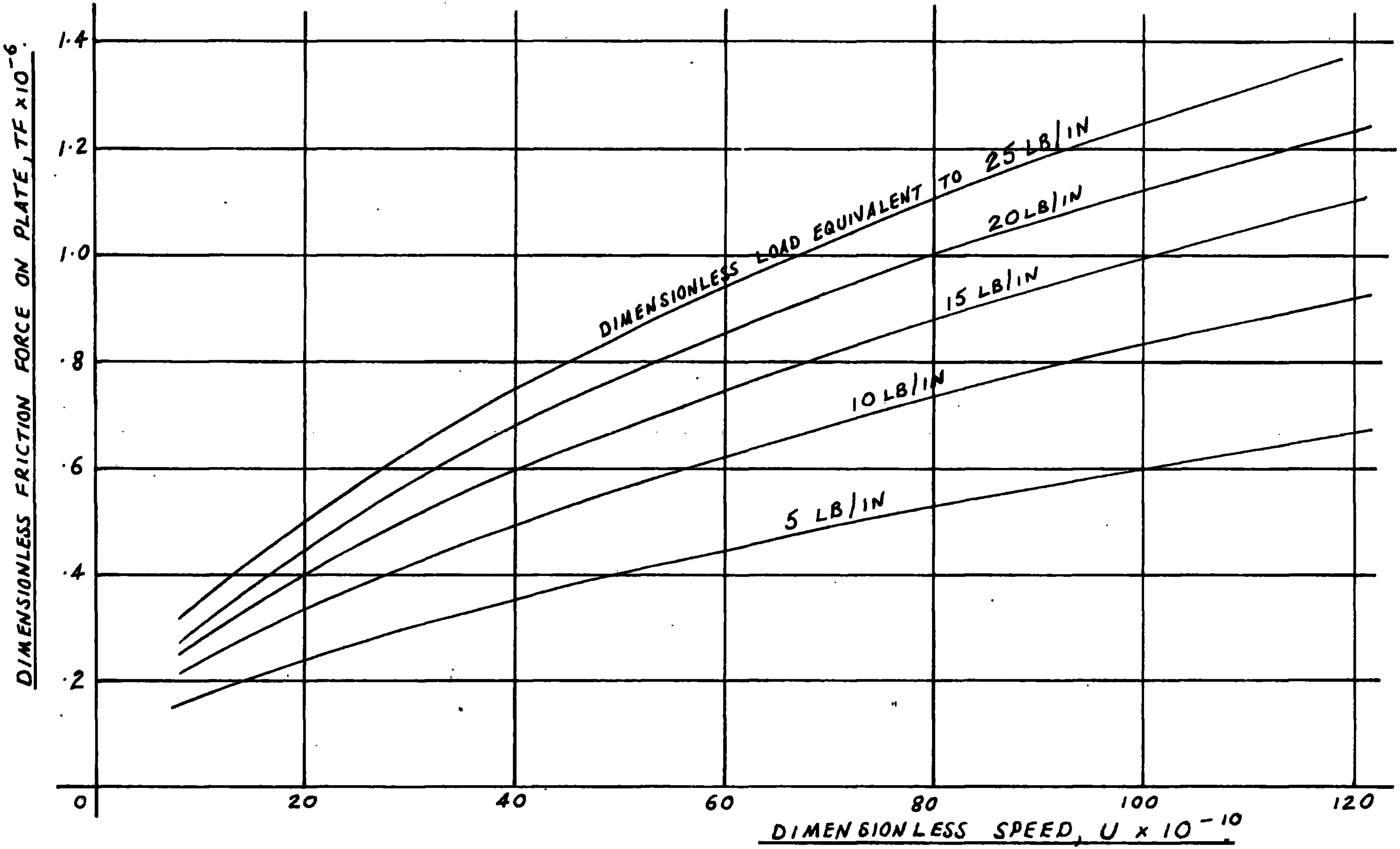

FIG. 5.6. THEORETICAL CURVES FOR FRICTION FORCE ~ SPEED FOR RIGID SPECIMEN.

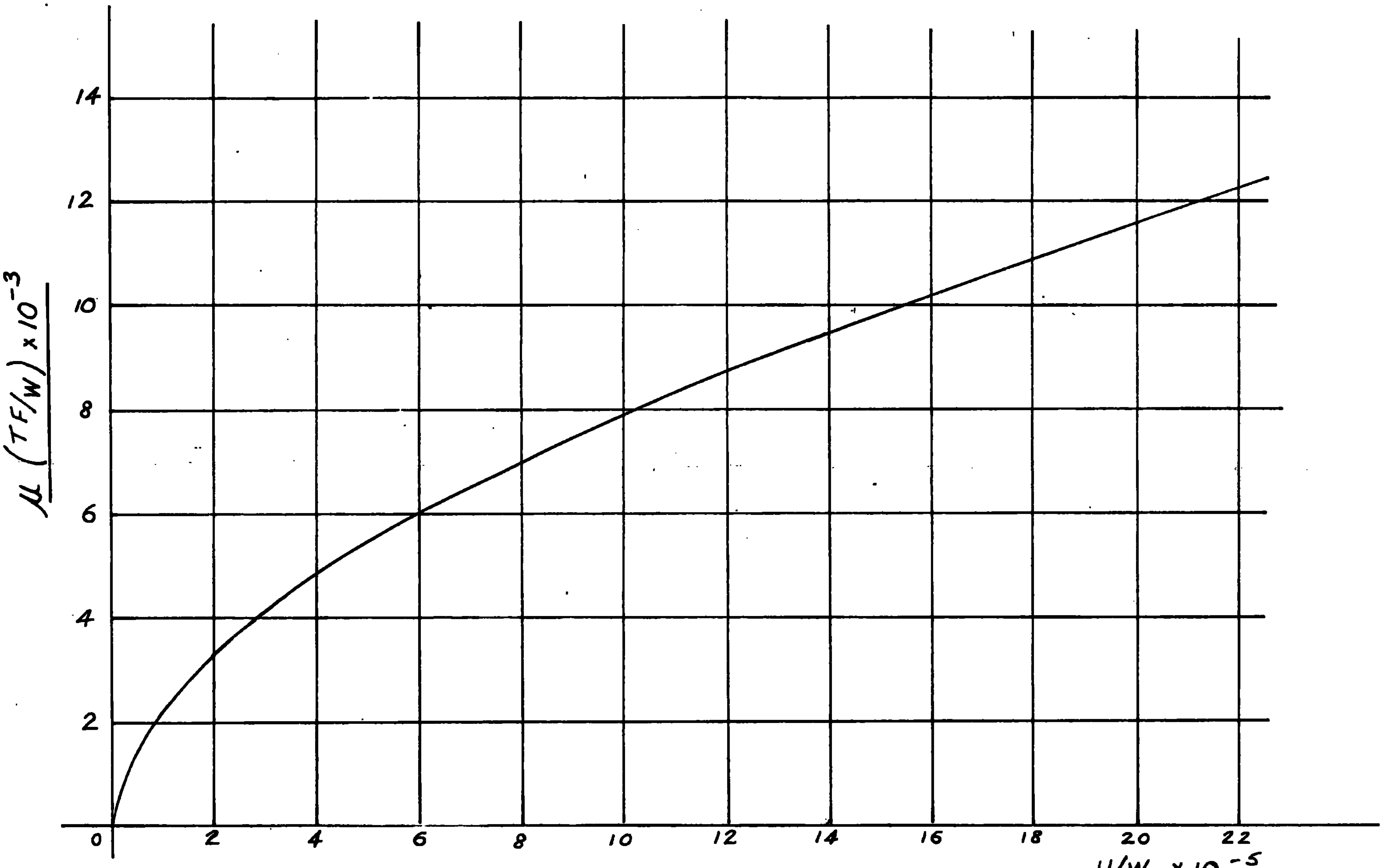

FIG. 5.7. GRAPH OF $\mu\,(TF/W) \sim U/W$ FOR RIGID SPEC.

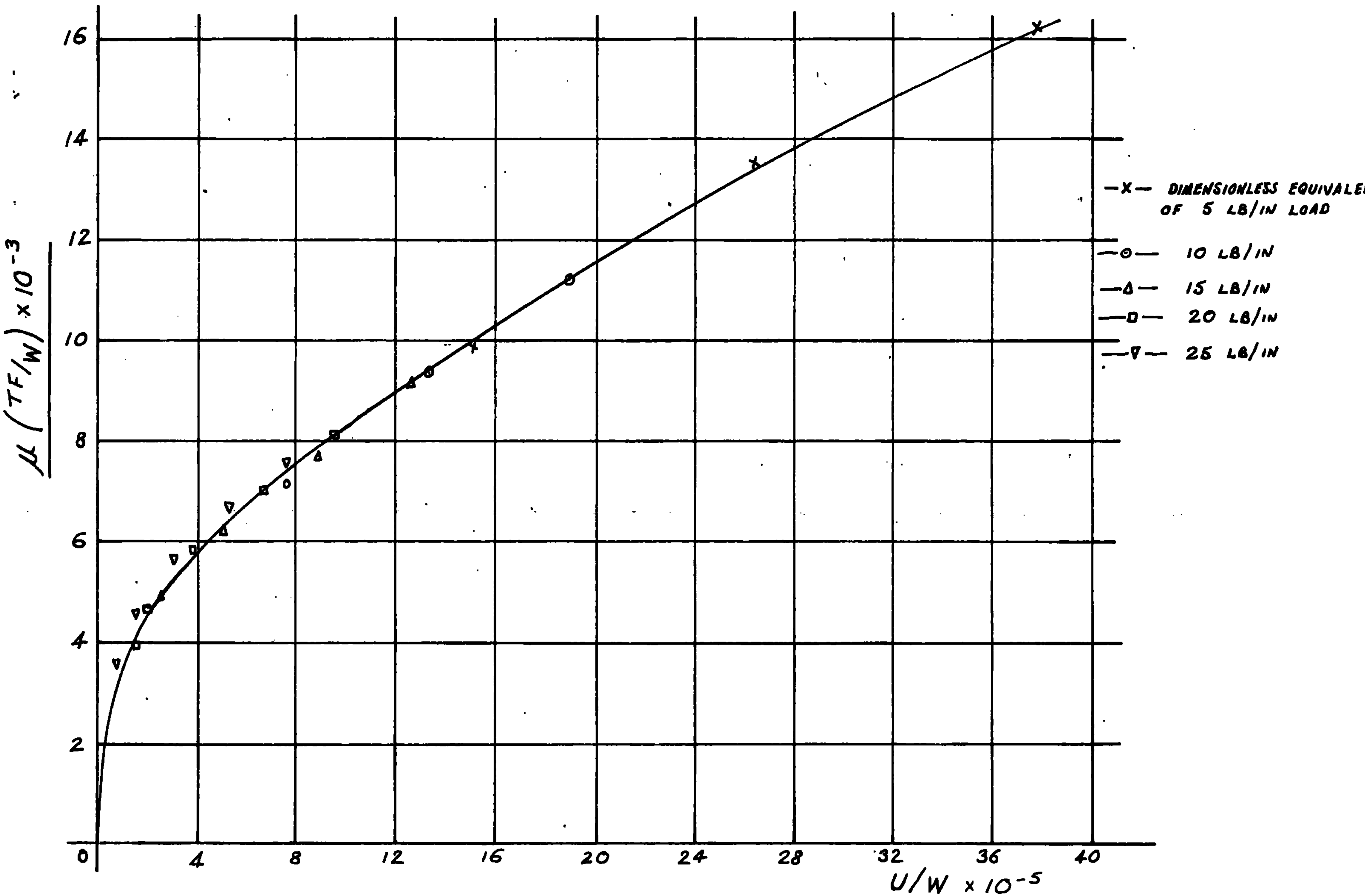

FIG. 5.8. GRAPH OF $\mu\ (TF/W) \sim U/W$ FOR ·03" SPECIMEN.

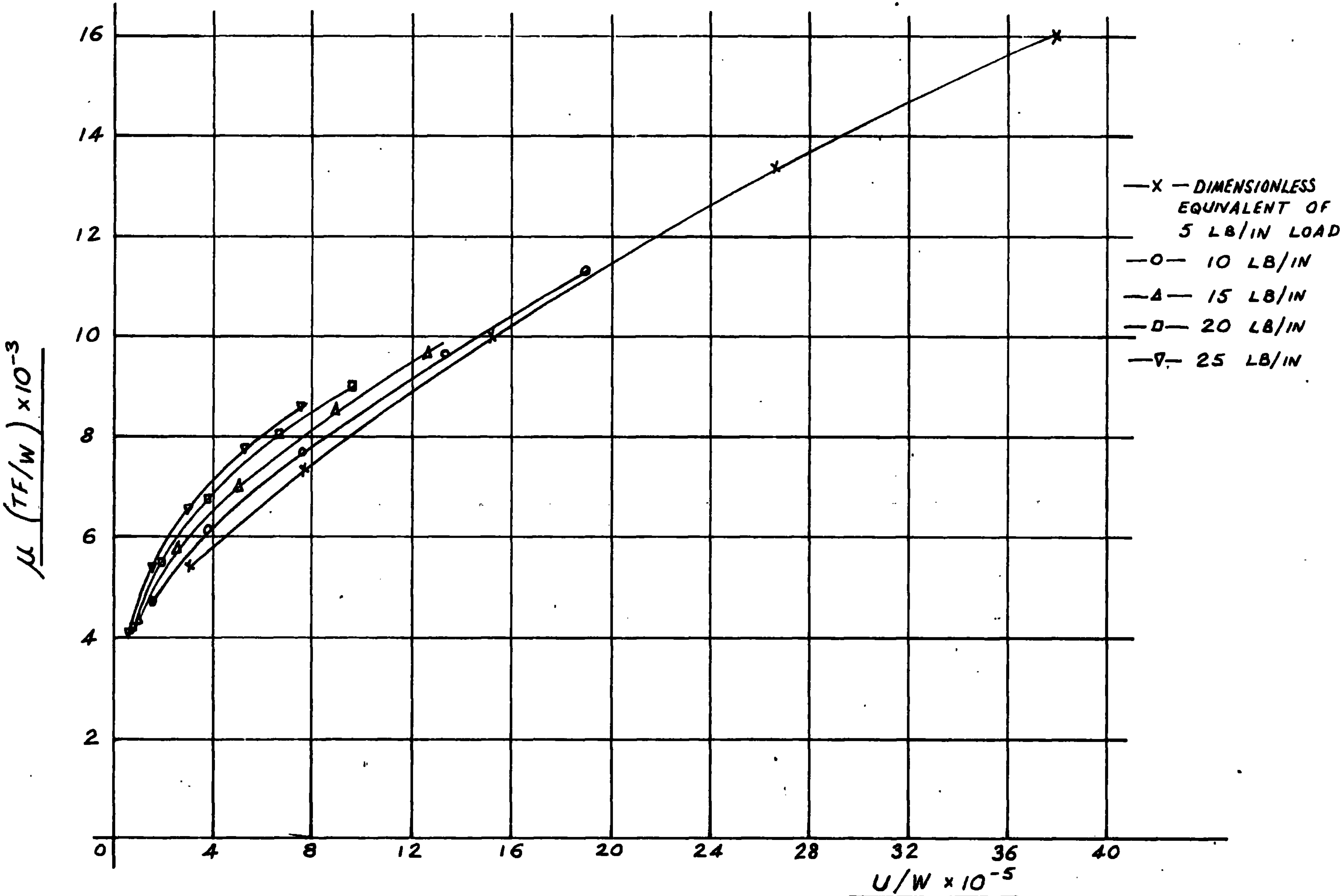

FIG. 5.9. GRAPH OF $\mu\,(TF/W) \sim U/W$ FOR ·1" SPECIMEN.

to Fig. 5.9. the divergence of the different loads is even more pronounced and no one curve can be drawn to satisfy all the points. As the specimen thickness increases the divergence became even greater than that shown in Fig. 5.9.

Plots of pressure curves and film thicknesses for two different conditions of load and speed for the rigid, .05 inch thick and .2 inch thick specimens are shown under Figs. 5.15. and 16. The pressures are in real terms (lb/in^2) to enable comparisons to be made while the film thicknesses are in dimensionless form.

Both sets of curves show similar results. Higginson (1965) showed graphs of pressure distribution and film shapes for a journal bearing with rigid and soft liners. Unlike Higginson's results for the soft journal bearing, the curves in Fig. 5.15. and 5.16. show much larger film thicknesses for the elastic specimens than for the rigid specimen. The graphs also show an increase in film thickness as the thickness of the elastic specimen is increased. The rigid specimens in both sets of results show high peak pressures while the elastic specimens' pressure distributions are less sharp and their peak pressures are much lower. The exit points of the pressure distributions have also moved much further out from the roller centre-line with increases in elastic specimen thickness.

Similar conclusions to those made by Hooke, Brighton and O'Donoghue (1966) for thin shell bearings can be drawn up as follows:-

as the thickness of the elastic layer is increased:

(a) the minimum film thickness is increased.

(b) the peak pressure is reduced.

(c) the outlet point is increased.

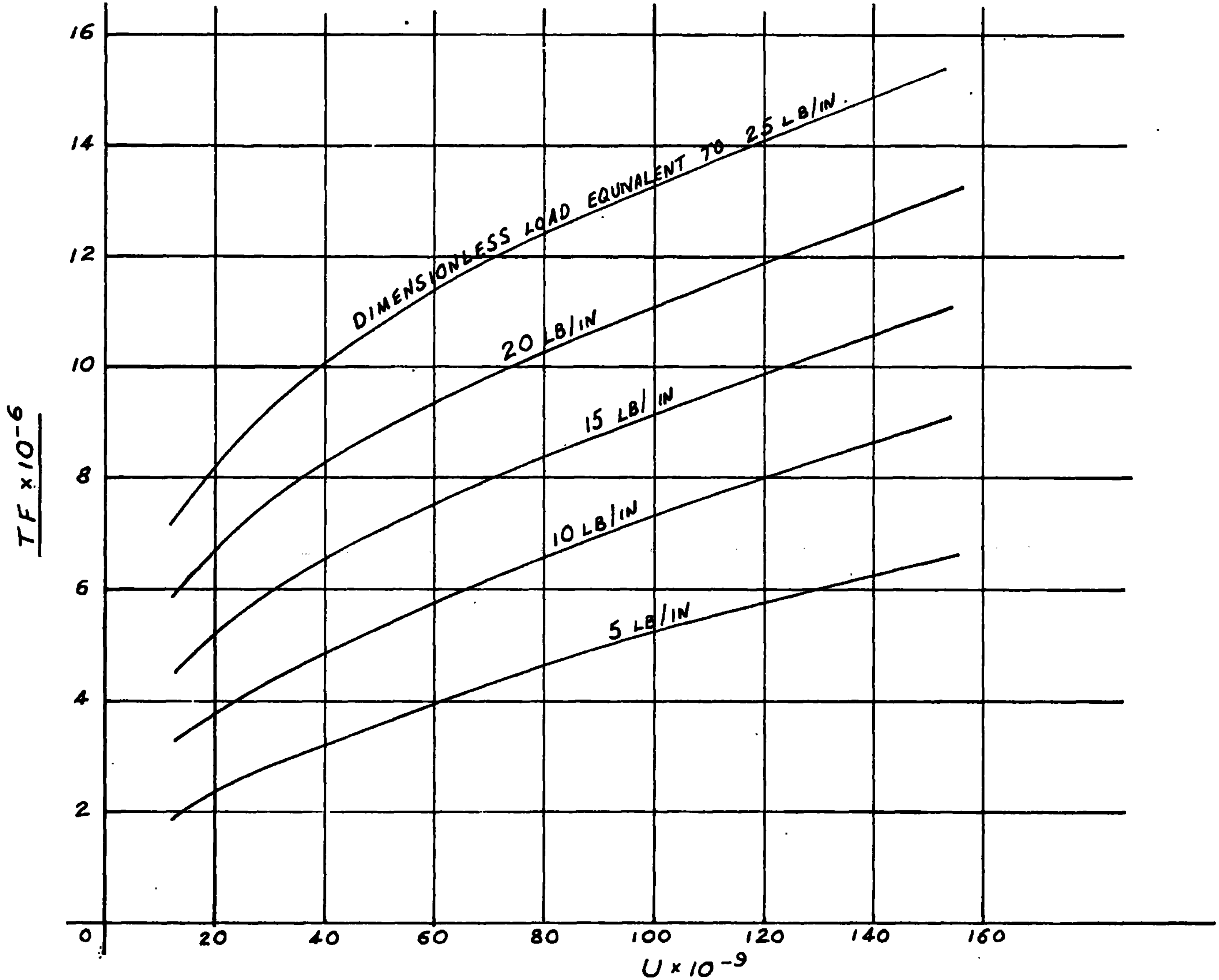

FIG. 5.10. THEORETICAL CURVES FOR FRICTION FORCE ~ SPEED FOR .03" SPECIMEN.

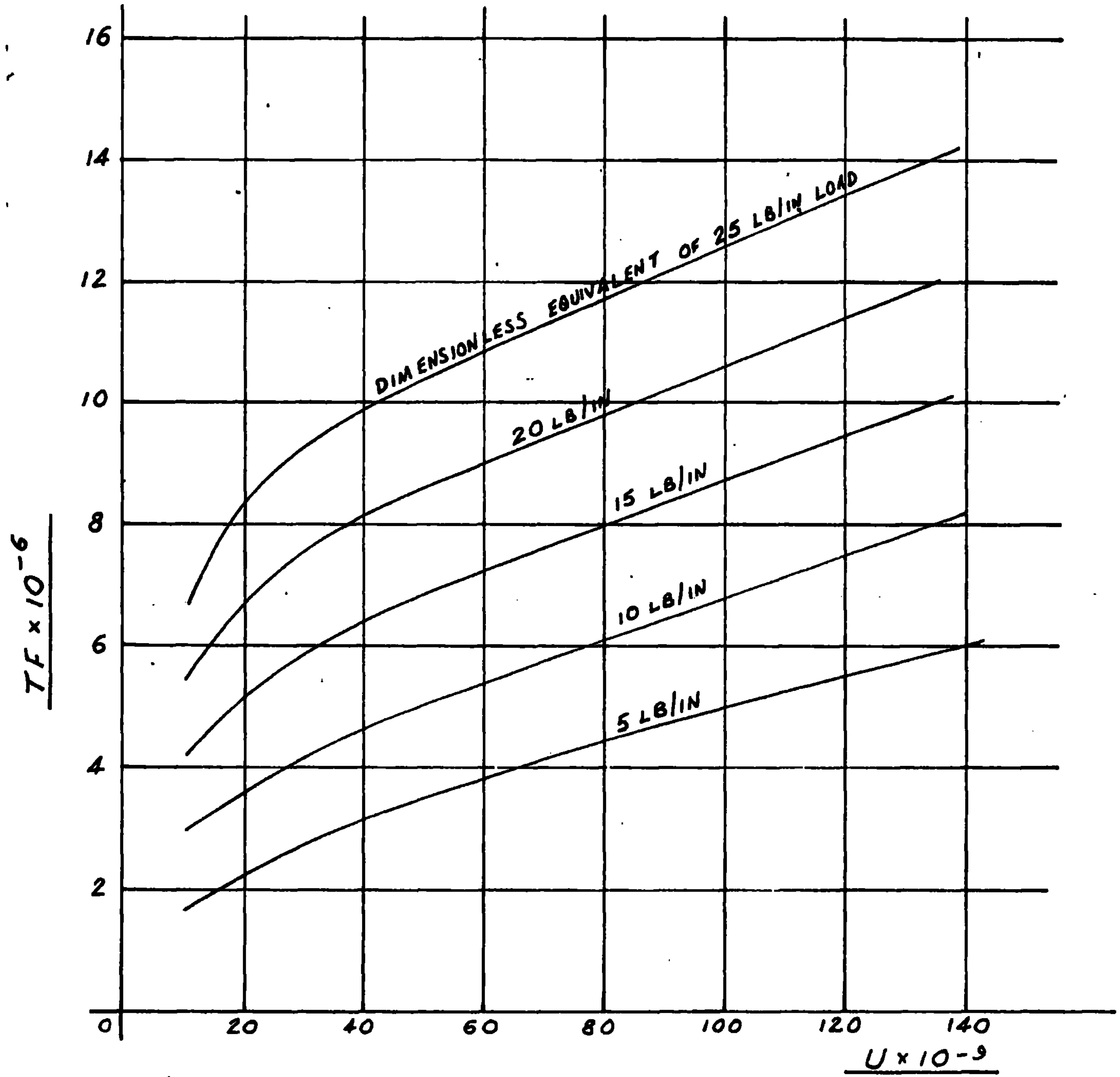

FIG. 5. 11. THEORETICAL CURVES FOR FRICTION FORCE ~ SPEED FOR ·05" SPECIMEN.

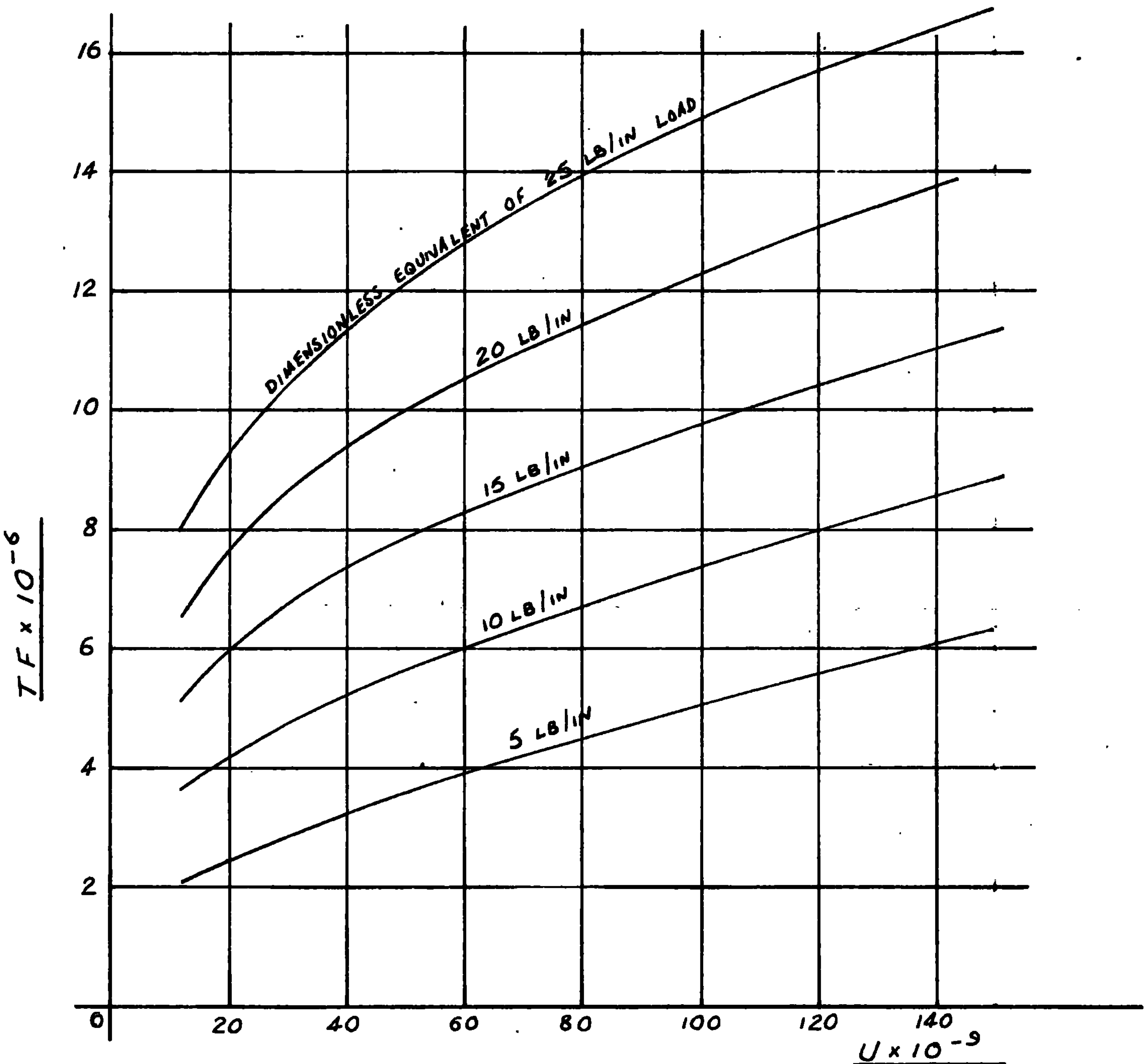

FIG. 5.12. THEORETICAL CURVES FOR FRICTION FORCE ~ SPEED FOR ·1" SPECIMEN.

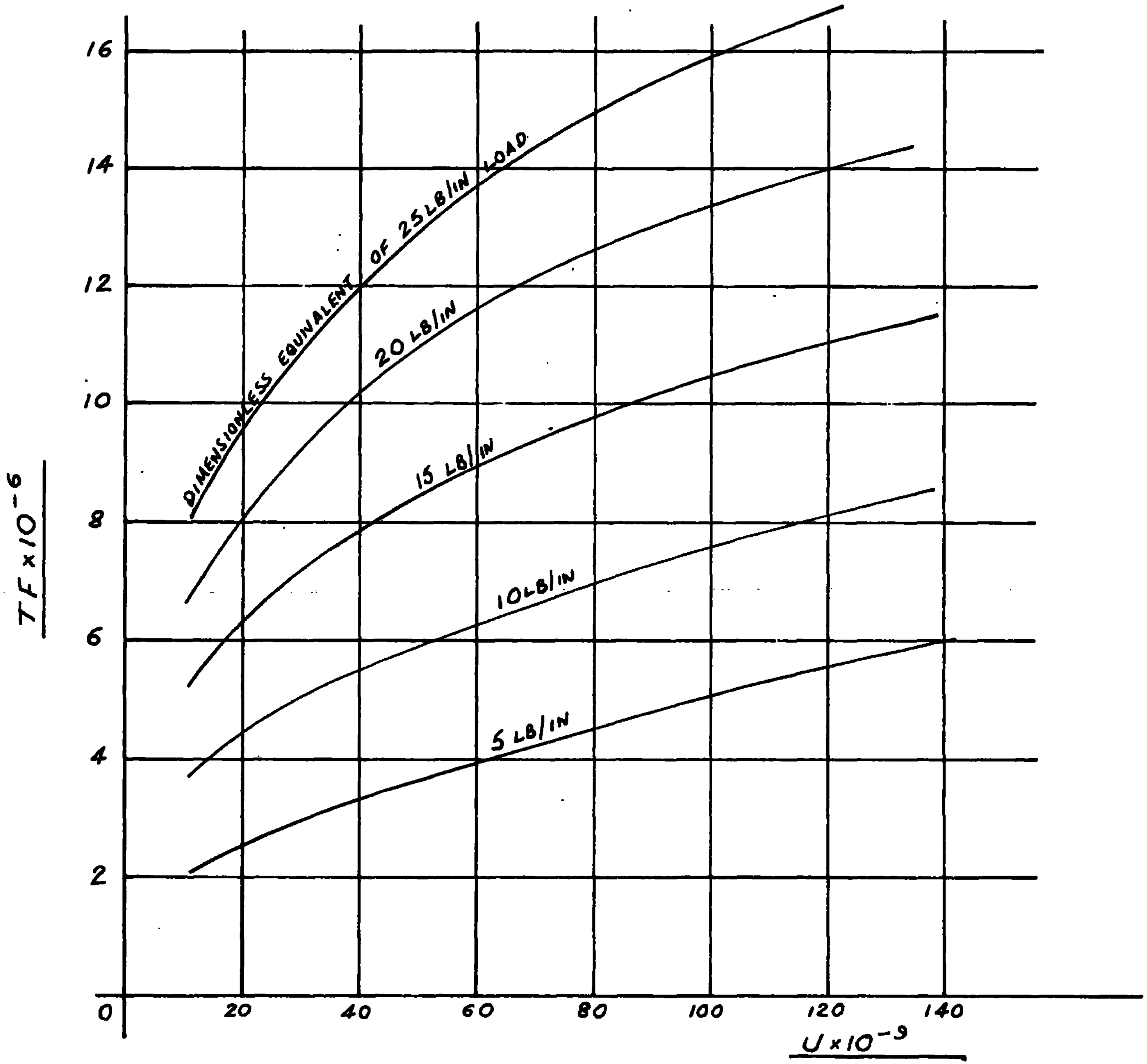

FIG. 5. 13. THEORETICAL CURVES FOR FRICTION FORCE ~ SPEED FOR ·2" SPECIMEN.

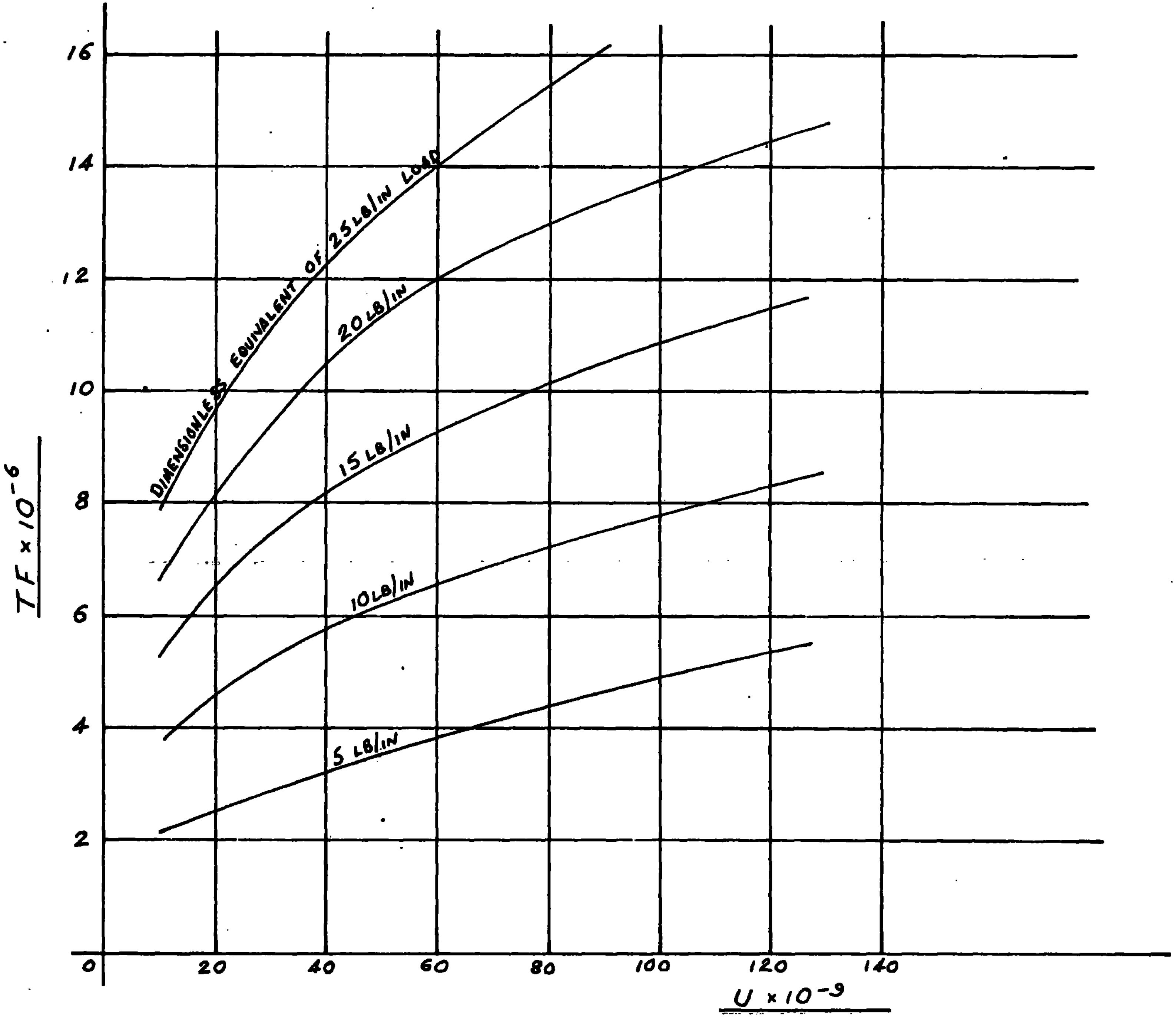

FIG. 5. 14. THEORETICAL CURVES FOR FRICTION FORCE ~ SPEED FOR .5" SPECIMEN

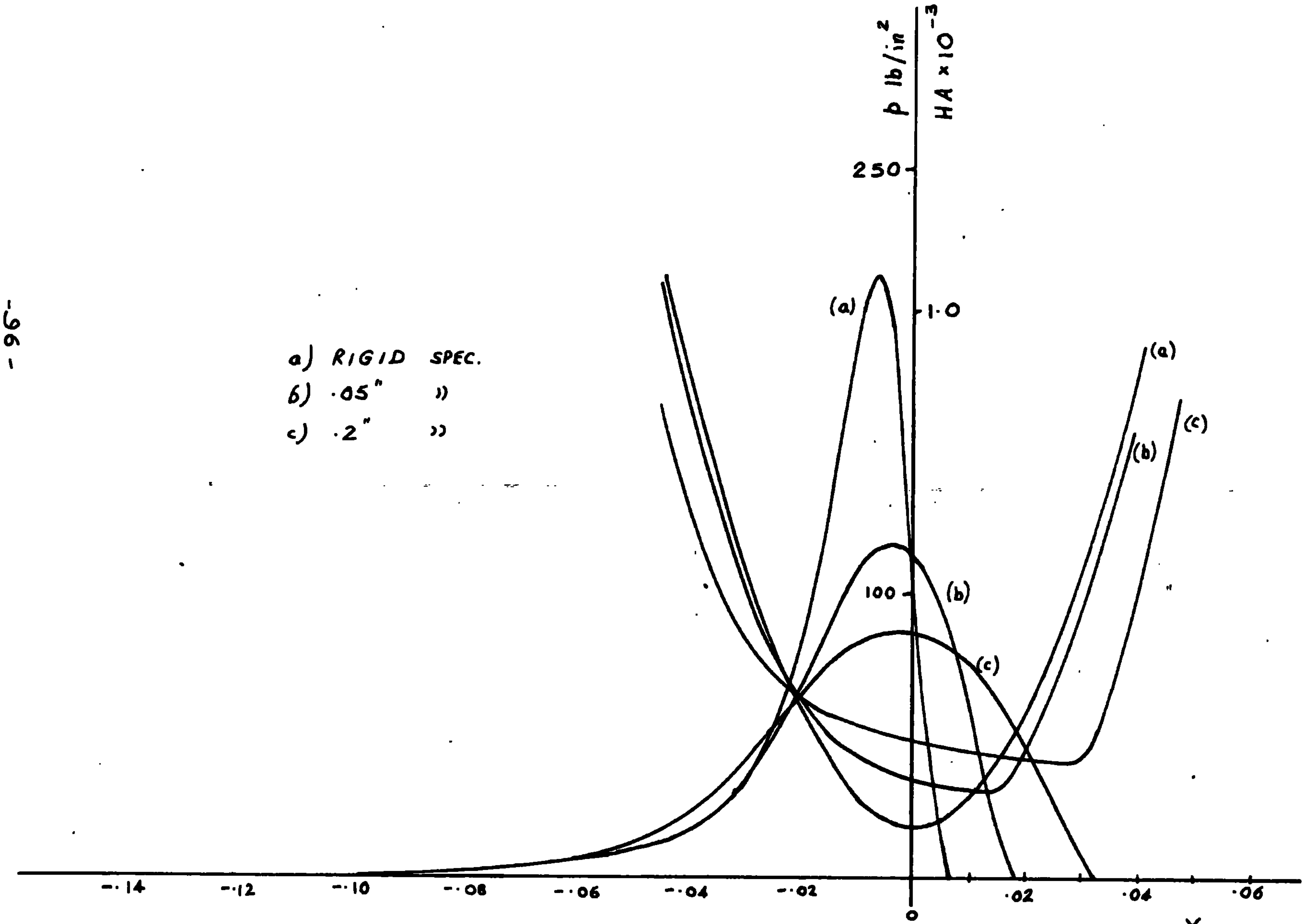

FIG. 5.15. COMPARISON OF PRESSURE CURVES & FILM THICKNESSES FOR 10 LB LOAD AT 100 REV/MIN.

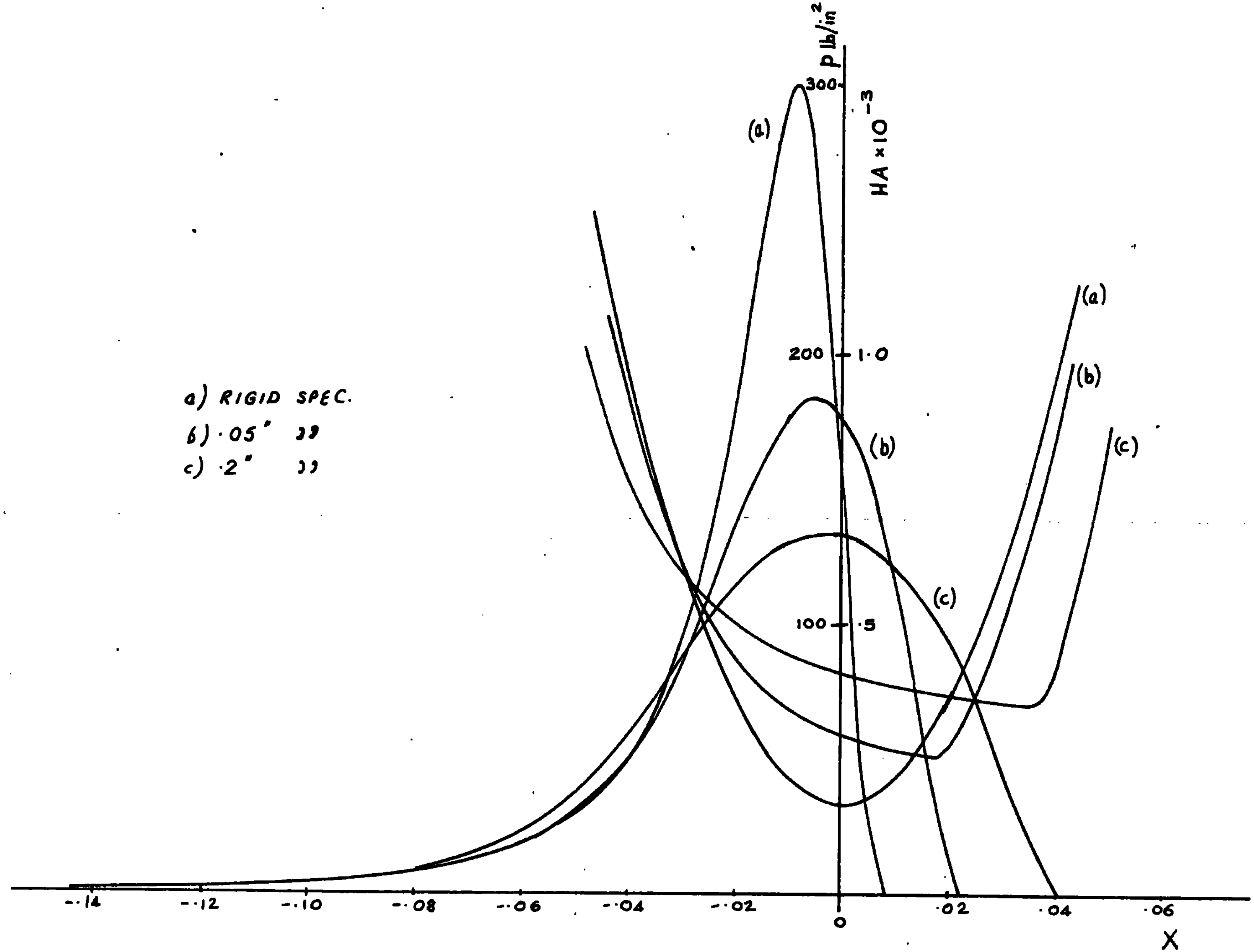

FIG. 5.16. COMPARISON OF PRESSURE CURVES & FILM THICKNESSES FOR 20 LB/IN LOAD AT 350 REV/MIN.

Comparisons in real terms are made of friction force (lb/in) against viscosity and speed (Reyns x in/sec) in Figs. 5.17. and 5.18. for the rigid, .05, .1 and .5 inch thick specimens for 10 and 20 lb/in loads respectively.

Both sets of graphs show similar results with increased friction forces for each specimen as the load is increased. The notable point about the graphs is that friction forces are greatest for the thickest elastic specimen (.5 inch thick) and fall as the elastic thickness is reduced. The lowest values of friction forces computed are for the rigid specimens in each case.

The values of friction force in Fig. 5.17. fall within an almost parallel band approximately .025 lb/in wide, the .5 inch thick elastic specimen forming the upper limit of the band and the rigid specimen forming the lower limit. Referring to Fig. 5.18., the values of friction force again fall within an almost parallel band but the width of the band is greatly increased and is of the order of .075 lb/in wide. The .5 inch thick specimen and the rigid specimen again form the upper and lower limits of the band as in the case of the 10 lb/in load graphs in Fig. 5.17.

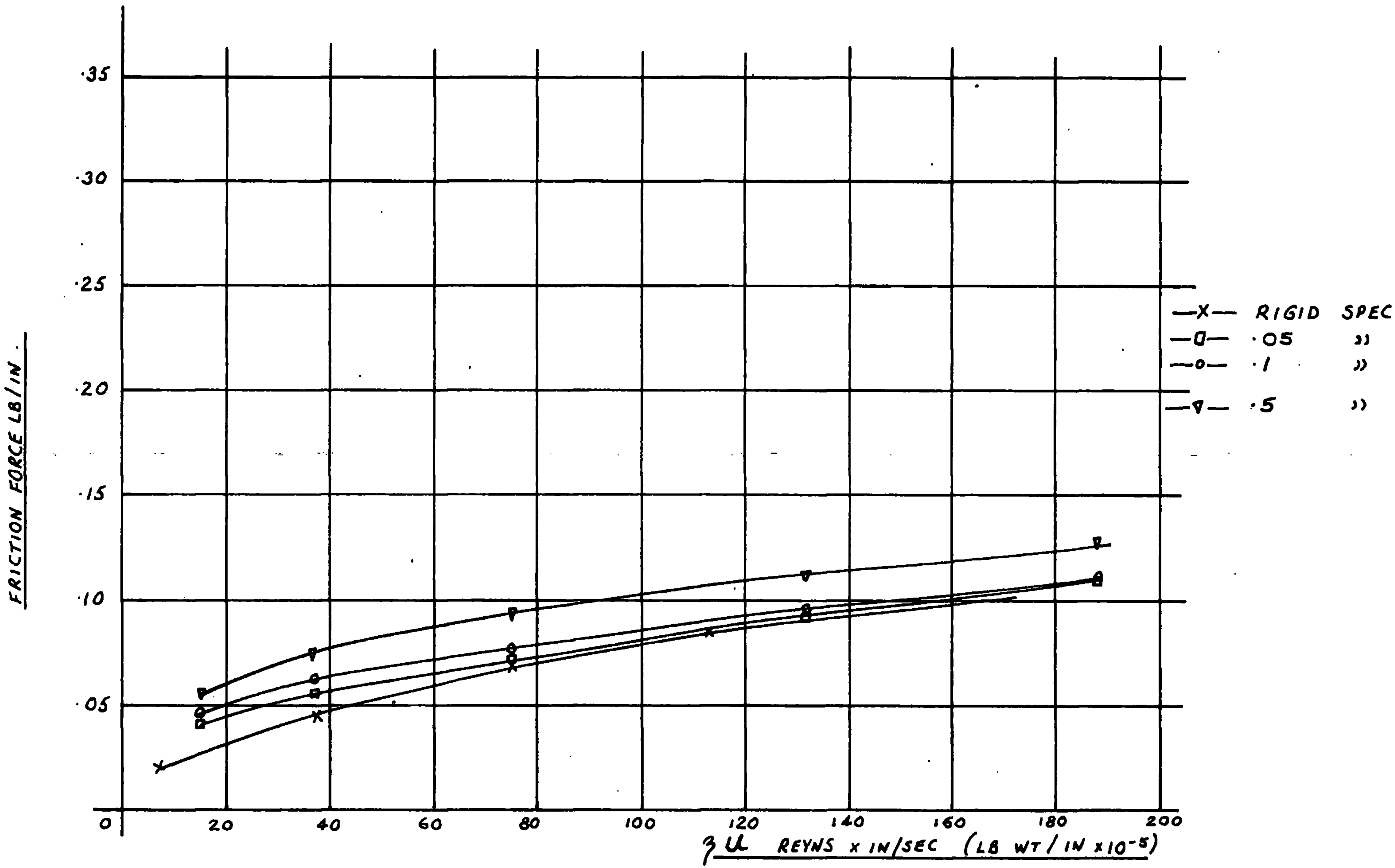

FIG. 5.17. COMPARISONS OF THEORETICAL RESULTS FOR RIGID, ·05, ·1 & ·5 SPECS. AT 10LB/IN LOAD.

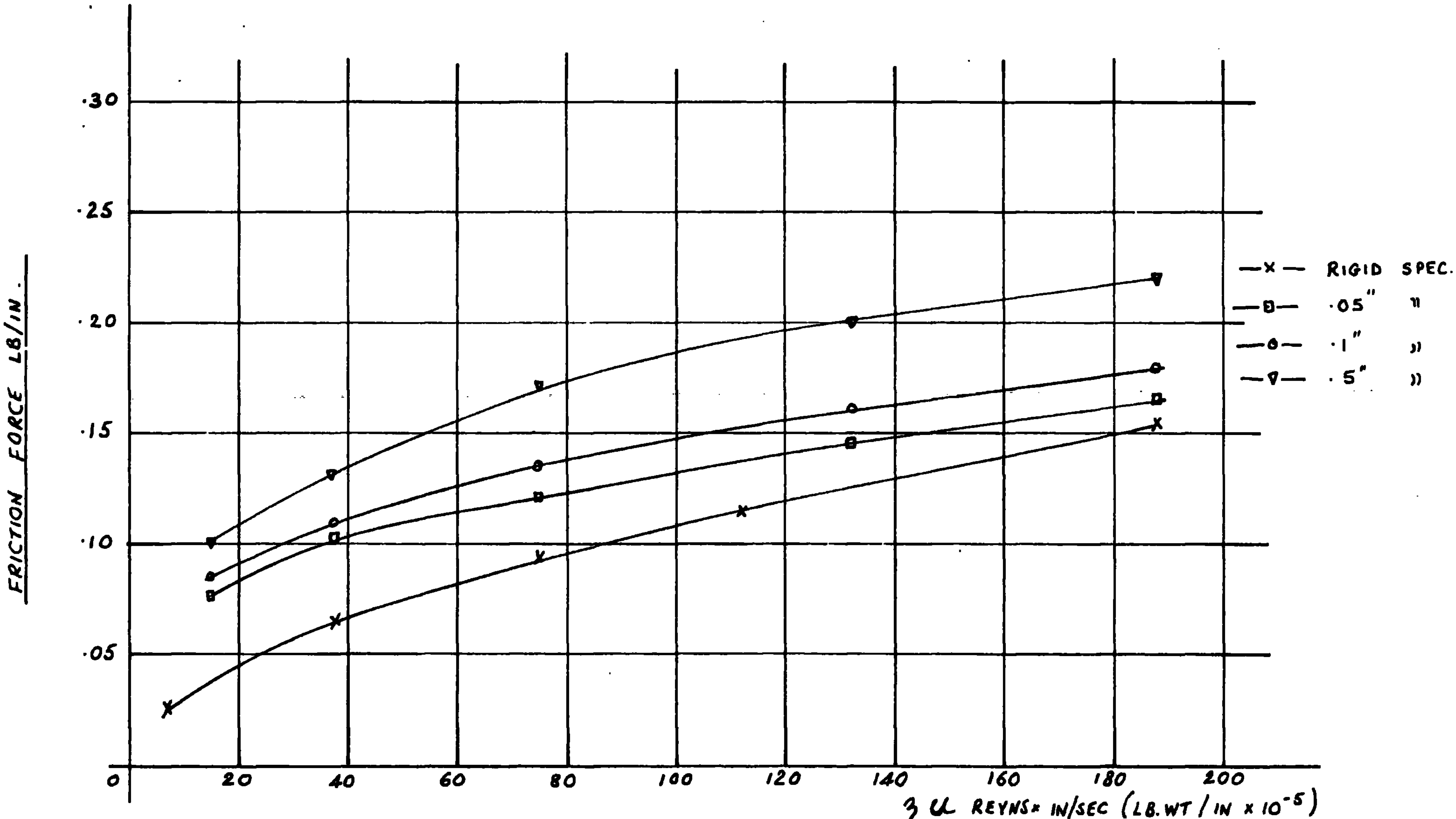

FIG. 5.18. COMPARISON OF THEORETICAL RESULTS FOR RIGID, ·05, ·1 & ·5 SPECS. AT 20 LB/IN LOAD.

Section 3. Comparison of Experimental and Theoretical Results

The theoretical results shown in Section 2 of this chapter for rigid solids agree very closely with those tabulated in other references, for example, Dowson and Higginson (1965). However, as will be seen in Figs. 5.19. and 20, large discrepencies exist between the experimental and theoretical results.

Fig. 5.19. shows theoretical and experimental results for the rigid specimen at 10 and 20 lb/in loads. The differences between the sets of curves are seen to increase greatly as speed increases. Fig. 5.20., showing comparisons for the .1 inch thick elastic specimen, also illustrates a divergence between corresponding curves for 10 and 20 lb/in loads. At speeds below 120 rev/min ($\eta u = 45 \times 10^{-5}$) the friction forces for corresponding curves are very much the same but diverge quite sharply as speed increases above 120 rev/min.

The experimental arrangement was examined in an attempt to account for the large discrepancies.

First, an examination of the experimental rig was made to discover if any major faults existed. The rollers and planes were checked for size, parallelism and straightness. No variation from the original specification for the rollers and planes could be found. The rig self-aligning system was checked to see if uniformity of loading was achieved across the face of the roller, and this was found to be functioning very well. This was verified by tests made with the modified rig for viewing the contact and cavitation zones. (See Appendix 4). With dry stationary contact under load, a parallel zone of compression could be seen for all the elastic specimens.

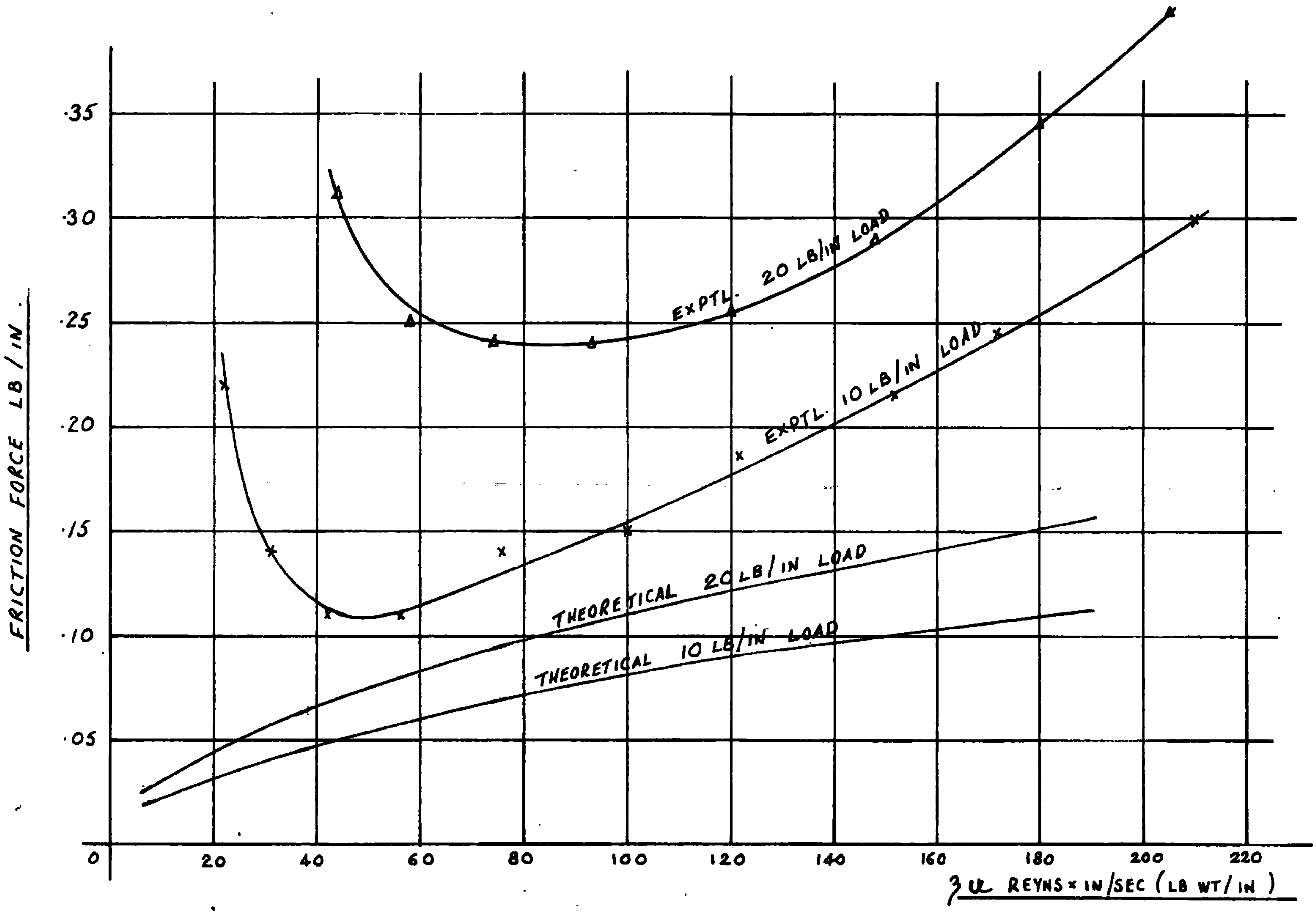

FIG. 5. 19. COMPARISON OF THEORETICAL & EXPERIMENTAL RESULTS FOR RIGID SPEC.

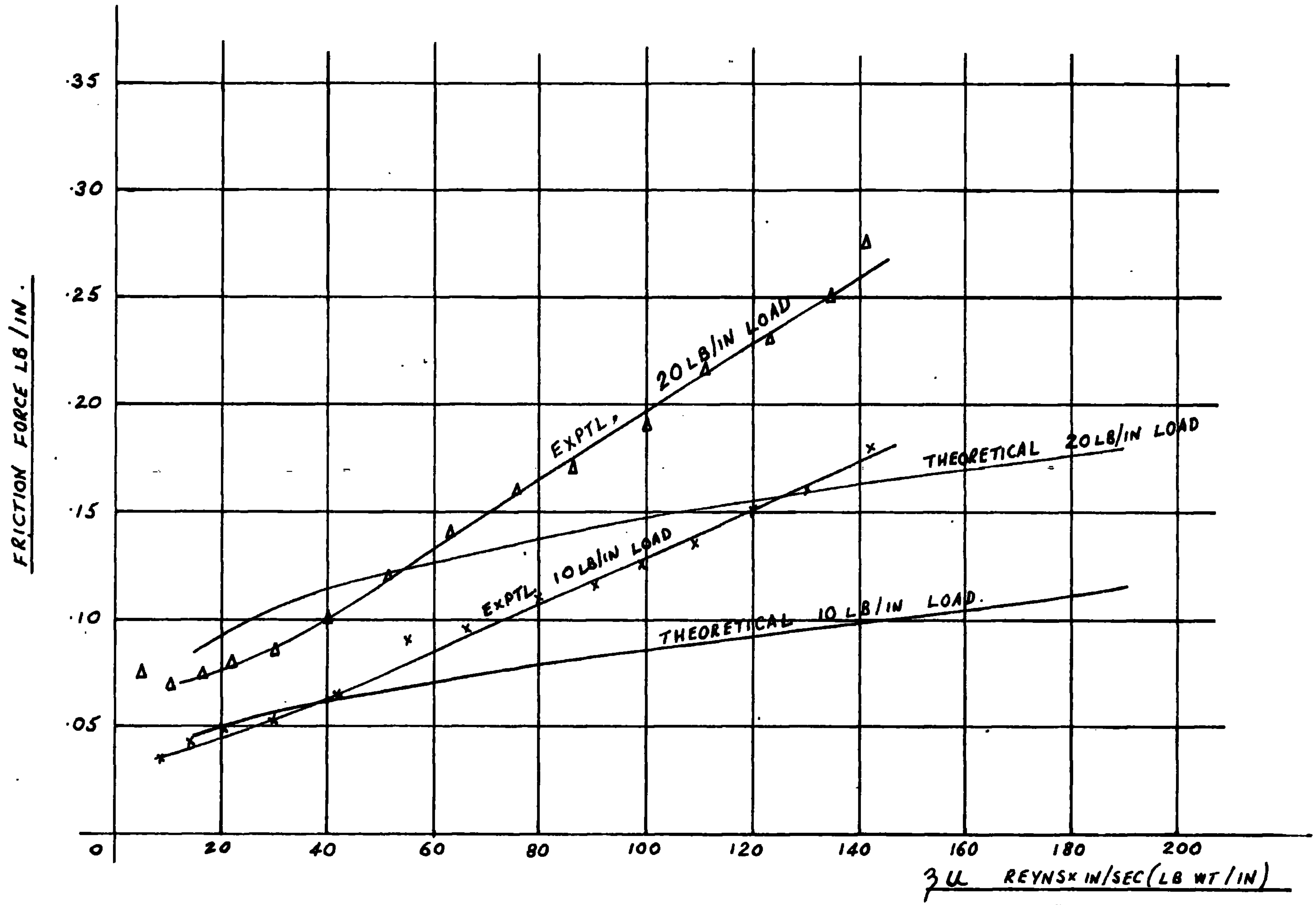

FIG. 5.20 COMPARISON OF THEORETICAL & EXPTL. RESULTS FOR ·1" SPEC.

A large load was also applied to the rollers while the rig was in the static condition to see if any deflection of the friction measuring beam was taking place. No strain reading was recorded.

It was concluded from the examination of the rig that the force being measured was indeed the friction force, to a good approximation.

Detailed examination of the theory then became necessary to establish whether any fundamental errors existed.

The numerical results for the rigid specimen appear to be correct within the assumptions made because they are confirmed by results tabulated elsewhere, as mentioned above. The assumptions included:-

(a) constant viscosity

(b) no side-leakage effects

and (c) perfect geometry and surface finish.

For high loads with the rigid specimen the viscosity may be increased by a few per cent due to pressure effects on the lubricant. This would not be enough to alter the friction forces significantly.

The effect of temperature rise of the lubricant was also considered. Calculations for the rigid specimen showed that in the most extreme condition where all the energy dissipation is absorbed by the lubricant, then a temperature rise in the region of 20°C may occur. This temperature rise would drastically reduce the viscosity but calculations made on this basis for a constant load predicted that thermal effects could only reduce the friction force.

A paper by Dowson and Whomes (1967) also confirms the assumption that there would be no significant side leakage effects in the present experiment.

The effect of poor surface finish has been discussed earlier, but this effect would be expected to diminish with increase in speed and corresponding increase in film thickness, whereas the discrepancy under examination increases with speed. In any case, the surface finishes on the steel cylinders and Tufnol plates were good in the context of the experiment.

Finally, a brief examination of the inlet boundary condition was made (necessarily brief because the author's leave of absence from employment was drawing to an end). It was always the author's belief that there was an ample supply of oil to the lubrication zone, but the possibility of oil starvation was the only remaining idea to explain the discrepancy. Mr. R. J. Boness, of the Royal Military College of Science, has made a detailed theoretical study of the effect of oil starvation on the lubrication of a rigid cylinder and plane, and has very generously placed his results (as yet unpublished) at the disposal of the author.

Boness has shown that flow rate is practically unaltered by variation of the inlet point for given speed and film thickness. For a fixed flow rate, the film thickness would decrease with increasing speed. However it is known that much of the lubricant remains on the roller and is carried round again to the zone, so it may be that the film thickness will remain essentially constant as the speed increases. If this is assumed to be so, Boness's results can be used to calculate the friction force with a starved oil film.

Fig. 5.21. shows the curve for a 10 lb/in load resulting from this calculation, based on the assumption that the oil supply was "ample" at a value of ηu of 20×10^{-5} reyns x in/s. If in fact the flow rate were constant and h decreased with increasing u, the effect on friction force would be even greater. It must be confessed, however, that this is as yet far from being a satisfactory explanation.

To conclude this section, above the disappointment of the lack of agreement between theory and experiment, must be remembered the very impressive experimental demonstration of the effectiveness of the soft surface layer in extending the range of full-film lubrication.

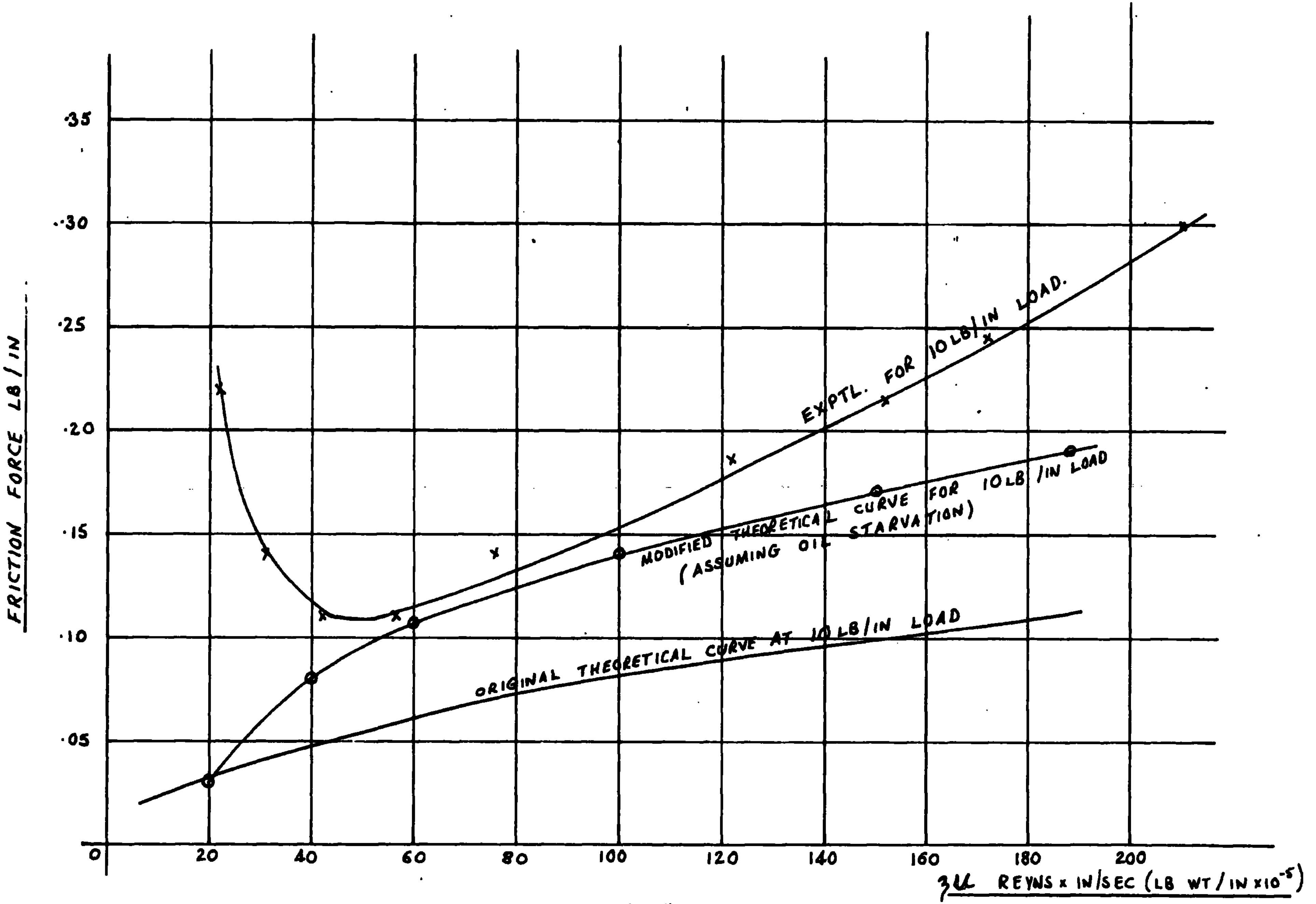

FIG. 5. 21. COMPARISON OF THEORETICAL (ACCORDING TO BONESS) & EXPTL FOR RIGID SPECIMEN

Section 4. Conclusions and suggestions for further work

The principal conclusion is a clear achievement of the original aim to find out whether Charnley's remarks about a human joint applied to soft bearings generally. Certainly for the geometry used in this work the answer is a firm Yes.

The other main outcome of the work is the major discrepancy between theory and experiment, which has still not been satisfactorily explained. Plainly the explanation must have the highest priority under the heading of further work.

The first step in the future must be to run the apparatus with the rollers and plane fully immersed in lubricant, to ensure "flooded" conditions. If this does not close the gap between theory and experiment, detective work in the form of pressure and film thickness measurements will be needed.

In the longer term it would be valuable to extend the kinematics to include a normal approach velocity, to find out whether comparable improvements to those in pure sliding are to be obtained, particularly in "squeeze-film times".

A possible improvement to the theory would be to incorporate a more accurate determination of elastic deformations, but this is not worth considering until the large discrepancy is sorted out.

```
      C       PROG.ONE     PROG.ONE     PROG.ONE     PROG.ONE
      C       SOLUTION FOR REYNOLDS EQUATION FOR RIGID ROLLER AND PLANE
              DIMENSION X(210),P(210),HA(210),XT(210),Q(210),F(210),
            1 S(410),HX(410),CF(410)
            2 FORMAT(1HO,10X,E12.4,5X,E14.6,5X,E13.5,5X,E13.5,5X,E13.5,
            2 5X,E14.6)
          202 FORMAT(1HO,13X,E12.4,10X,E13.5,10X,E14.6)
          203 FORMAT(1HO,10X,E14.6,5X,E14.6,5X,E14.6,5X,E14.6)
          204 FORMAT(1HO,13X,E12.4,5X,E12.4)
            3 FORMAT(I3,4X,E10.2,4X,E7.1)
            4 READ(5,3)N,XI,B
            5 FORMAT(1HO,10X,I3,4X,E10.2,4X,E7.1)
            6 WRITE(6,5)N,XI,B
              ICOUNT=0
            8 PI=0
            9 FORMAT(3E10.2,E13.5)
           10 READ(5,9)HO,A,U,HM
          110 FORMAT(E10.2)
          111 READ(5,110)ADJ
          112 FORMAT(1HO,E10.2)
          113 WRITE(6,112)ADJ
           11 FORMAT(E10.1)
           12 READ(5,11)Z
           13 FORMAT(1HO,10X,E10.1)
           14 WRITE(6,13)Z
           15 FORMAT(I3,4X,E10.1,4X,E10.2)
           16 READ(5,15)M,C,CE
          161 FORMAT(1HO,10X,I3,4X,E10.1,4X,E10.2)
          162 WRITE(6,161)M,C,CE
          163 I=1
          164 P(I)=PI
          165 X(I)=XI
          166 XT(I)=X(I)**2/2.
          167 HA(I)=HO+XT(I)
          168 Q(I)=A*P(I)
           17 H=(SQRT(2.*(HM-HO))-(XI))/Z
          182 H2=H/2.
           20 FORMAT(1HO,10X,3E10.2,E17.9)
           21 WRITE(6,20)HO,A,U,HM
           22 DO 37 I=1,N
           23 HB=HO+(X(I)**2/2.)+(A*P(I))
           24 T1=6.*U*((HB-HM)/(HB**3))
           25 HC=HO+((X(I)+H2)**2/2.)+(A*(P(I)+(T1*H2)))
           26 T2=6.*U*((HC-HM)/(HC**3))
           27 HD=HO+((X(I)+H2)**2/2.)+(A*(P(I)+(T2*H2)))
           28 T3=6.*U*((HD-HM)/(HD**3))
           29 HE=HO+((X(I)+H)**2/2.)+(A*(P(I)+(T3*H)))
           30 T4=6.*U*((HE-HM)/(HE**3))
           31 P(I+1)=P(I)+H*(T1+2.*T2+2.*T3+T4)/6.
           32 X(I+1)=X(I)+H
           34 XT(I+1)=X(I+1)**2/2.
           35 Q(I+1)=A*P(I+1)
           37 HA(I+1)=HO+XT(I+1)+Q(I+1)
           39 IF(P(N)-B)40,146,41
           40 IF(P(N)+B)44,146,146
           41 ICOUNT=ICOUNT+1
           42 HM=HM+ADJ
[illegible]
[illegible] IF(ICOUNT-500)17,95,95
          146 D=(CE-X(N))/C
         1146 J=1
          246 S(J)=X(N)
           47 HX(J)=HA(N)
           48 DO 50 J=1,M
           49 S(J+1)=S(J)+D
           50 HX(J+1)=HO+S(J+1)**2/2.
           52 DO 54 I=1,N
           54 F(I)=((1.-((3.*(HA(I)-HM))/HA(I)))/HA(I))
           56 MO=N-1
           57 W=0
           58 DO 60 I=2,MO
           59 QUAD=2.*P(I)
           60 W=W+QUAD
           61 W=((P(1)+P(N)+W)*(-(H)))/2.
           62 SUMF=0
           63 DO 65 I=2,MO
           64 RECT=2.*F(I)
           65 SUMF=SUMF+RECT
           66 SUMF=((F(1)+F(N)+SUMF)*(-(H)))/2.
           67 FER=U*SUMF
           69 DO 70 J=1,M
           70 CF(J)=(HM/HX(J)**2)
           72 JO=M-1
           73 SUMC=0
           74 DO 76 J=2,JO
           75 OBLO=2.*CF(I)
           76 SUMC=SUMC+OBLO
           77 SUMC=((CF(1)+CF(M)+SUMC)*D)/2.
           78 CFER=U*SUMC
           80 TF=FER+CFER
           82 UFER=FER/W
           84 UTF=TF/W
           86 DO 87 I=1,N
           87 WRITE(6,2)X(I),P(I),HA(I),XT(I),F(I)
           89 DO 90 J=1,M
           90 WRITE(6,202)S(J),HX(J),CF(J)
           92 WRITE(6,203)W,FER,CFER,TF
           94 WRITE(6,204)UFER,UTF
           95 STOP
              END
```

```
      C        PROG.TWO      PROG.TWC       PROG.TWC       PROG.TWC
      C        SOLUTION TO REYNOLDS EQUAT. FOR RIGID ROLLER AND SOFT PLANE
               DIMENSION X(210),P(210),HA(210),XT(210),Q(210),F(210),
            1  S(410),HX(410),CF(410),HN(5)
         2     FORMAT(1H0,10X,E12.4,5X,E14.6,5X,E13.5,5X,E13.5,5X,E13.5,
            2  5X,E14.6)
      1115     FORMAT(1H0,20X,E12.4,10X,E14.6)
         3     FORMAT(1H0,13X,E12.4,10X,E13.5,10X,E14.6)
         4     FORMAT(1H0,10X,E14.6,5X,E14.6,5X,E14.6,5X,E14.6)
         5     FORMAT(1H0,13X,E12.4,5X,E12.4)
         6     FORMAT(E10.2)
         7     READ(5,6)ADJ
         8     FORMAT(1H0,E10.2)
         9     WRITE(6,8)ADJ
        10     FORMAT(I3,4X,E10.2,4X,E7.1)
        11     READ(5,10)N,XI,B
        12     FORMAT(1H0,10X,I3,4X,E10.2,4X,E7.1)
        13     WRITE(6,12)N,XI,B
        14     COUNT=0
        15     KO=1
        16     ADD=0
        17     PI=0.
        18     FORMAT(3E10.2,E13.5)
        19     READ(5,18)H0,A,U,HM
        24     FORMAT(E10.1)
        25     READ(5,24)Z
        26     FORMAT(1H0,10X,E10.1)
        27     WRITE(6,26)Z
        28     FORMAT(I3,4X,E10.1,4X,E10.2)
        29     READ(5,28)M,C,CE
        30     FORMAT(1H0,10X,I3,4X,E10.1,4X,E10.2)
        31     WRITE(6,30)M,C,CE
        32     I=1
        33     P(I)=PI
        34     X(I)=XI
        35     XT(I)=X(I)**2/2.
        36     HA(I)=H0+XT(I)
        37     Q(I)=A*P(I)
        38     HN(1)=HM
        39     H=(SQRT(2.*(HM-H0))-(XI))/Z
        40     H2=H/2.
        41     FORMAT(1H0,10X,3E10.2,E17.9,10X,E14.6)
        42     WRITE(6,41)H0,A,U,HM,P(N)
        43     DO 56 I=1,N
        44     HB=H0+(X(I)**2/2.)+(A*P(I))
        45     T1=6.*U*((HB-HM)/(HB**3))
        46     HC=H0+((X(I)+H2)**2/2.)+(A*(P(I)+(T1*H2)))
        47     T2=6.*U*((HC-HM)/(HC**3))
        48     HD=H0+((X(I)+H2)**2/2.)+(A*(P(I)+(T2*H2)))
        49     T3=6.*U*((HD-HM)/(HD**3))
        50     HE=H0+((X(I)+H)**2/2.)+(A*(P(I)+(T3*H)))
        51     T4=6.*U*((HE-HM)/(HE**3))
        52     P(I+1)=P(I)+H*(T1+2.*T2+2.*T3+T4)/6.
        53     X(I+1)=X(I)+H
        54     XT(I+1)=X(I+1)**2/2.
        55     Q(I+1)=A*P(I+1)
        56     HA(I+1)=H0+XT(I+1)+Q(I+1)
        57     COUNT=COUNT+1
        58     IF(COUNT-2)59,63,68
        59     HN(2)=HA(1)*ADJ
        60     HM=HN(2)
        61     IF(P(N)-B)62,78,39
        62     IF(P(N)+B)114,78,78
        63     IF(P(N)+B)64,78,1114
        64     HN(3)=(HN(1)+HN(2))/2.
        65     HM=HN(3)
        66     KO=KO+1
        67     IF(KO-2)39,39,39
        68     IF(P(N)-B)69,78,169
        69     IF(P(N)+B)174,78,78
       169     HN(1)=HN(3)
        70     HN(3)=(HN(1)+HN(2))/2.
        71     HM=HN(3)
        72     ADD=ADD+1
        73     IF(ADD-200)39,114,114
       174     HN(2)=HN(3)
        74     HN(3)=(HN(1)+HN(2))/2.
        75     HM=HN(3)
        76     ADD=ADD+1
        77     IF(ADD-200)39,114,114
        78     D=(CE-X(N))/C
        79     J=1
        80     S(J)=X(N)
        81     HX(J)=HA(N)
        82     DO 84 J=1,M
        83     S(J+1)=S(J)+D
        84     HX(J+1)=H0+S(J+1)**2/2.
        85     DO 86 I=1,N
        86     F(I)=((1.-((3.*(HA(I)-HM))/HA(I))))/HA(I))
        87     MO=N-1
        88     W=0
        89     DO 91 I=2,MO
        90     QUAD=2.*P(I)
        91     W=W+QUAD
        92     W=(P(1)+P(N)+W)*H2
       192     SUMF=0
        93     DO 95 I=2,MO
        94     RECT=2.*F(I)
        95     SUMF=SUMF+RECT
       196     SUMF=(F(1)+F(N)+SUMF)*H2
        96     FER=U*SUMF
        97     DO 98 J=1,M
        98     CF(J)=(HM/HX(J)**2)
        99     JO=M-1
       100     SUMC=0
       101     DO 103 J=2,JO
       102     OBLO=2.*CF(I)
       103     SUMC=SUMC+OBLO
      1104     SUMC=((CF(1)+CF(M)+SUMC)*D)/2.
       104     CFER=U*SUMC
       105     TF=FER+CFER
       106     UFER=FER/W
       107     UTF=TF/W
       108     DO 109 I=1,N
       109     WRITE(6,2)X(I),P(I),HA(I),XT(I),Q(I),F(I)
       110     DO 111 J=1,M
       111     WRITE(6,3)S(J),HX(J),CF(J)
       112     WRITE(6,4)W,FER,CFER,TF
       113     WRITE(6,5)UFER,UTF
      1114     WRITE(6,1115)X(N),P(N)
       114     STOP
               END
```

```
C         PROG.THREE     PROG.THREE     PROG.THREE     PROG.THREE
C         SOLUTION TO REYNOLDS EQUAT. FOR RIGID ROLLER AND SOFT PLANE
C         **********(SOLVING BACKWARDS FROM NORMAL OUTLET)***********
          DIMENSION X(210),P(210),HA(210),XT(210),Q(210),F(210),
     1    S(410),HX(410),CF(410),HN(5)
    2     FORMAT(1H0,10X,E12.4,5X,E14.6,5X,E13.5,5X,E13.5,5X,E13.5,
     2    5X,E14.6)
 1115     FORMAT(1H0,20X,E12.4,10X,E14.6)
    3     FORMAT(1H0,13X,E12.4,10X,E13.5,10X,E14.6)
    4     FORMAT(1H0,10X,E14.6,5X,E14.6,5X,E14.6,5X,E14.6)
    5     FORMAT(1H0,13X,E12.4,5X,E12.4)
    6     FORMAT(E10.2)
    7     READ(5,6)ADJ
    8     FORMAT(1H0,E10.2)
    9     WRITE(6,8)ADJ
   10     FORMAT(I3,4X,E10.2,4X,E7.1)
   11     READ(5,10)N,XO,B
   12     FORMAT(1H0,10X,I3,4X,E10.2,4X,E7.1)
   13     WRITE(6,12)N,XO,B
   14     COUNT=0
  214     COT=0
   15     KO=0
   16     ADD=0
   17     PI=0
   18     FORMAT(3E10.2,E13.5)
   19     READ(5,18)HO,A,U,HM
   24     FORMAT(E10.1)
   25     READ(5,24)Z
   26     FORMAT(1H0,10X,E10.1)
   27     WRITE(6,26)Z
   28     FORMAT(I3,4X,E10.1,4X,E10.2)
   29     READ(5,28)M,C,CE
   30     FORMAT(1H0,10X,I3,4X,E10.1,4X,E10.2)
   31     WRITE(6,30)M,C,CE
   32     I=1
  132     X(1)=SQRT(2.*(HM-HO))
   33     P(1)=PI
   35     XT(1)=X(1)**2/2.
   36     Q(1)=A*P(1)
   37     HA(1)=HO+XT(1)+Q(1)
   38     HN(1)=HM
  371     COT=COT+1
  372     IF(COT-2)39,39,39
  138     I=1
  238     X(1)=SQRT(2.*(HM-HO))
  338     P(1)=PI
  438     XT(1)=X(1)**2/2.
  538     HA(1)=HO+XT(1)
  638     Q(1)=A*P(1)
   39     H=-(SQRT(2.*(HM-HO))-(XO))/Z
   40     H2=H/2.
   41     FORMAT(1H0,10X,3E10.2,E17.9,10X,E14.6)
   42     WRITE(6,41)HO,A,U,HM,P(N)
   43     DO 56 I=1,N
   44     HB=HO+(X(I)**2/2.)+(A*P(I))
   45     T1=6.*U*((HB-HM)/(HB**3))
   46     HC=HO+((X(I)+H2)**2/2.)+(A*(P(I)+(T1*H2)))
   47     T2=6.*U*((HC-HM)/(HC**3))
   48     HD=HO+((X(I)+H2)**2/2.)+(A*(P(I)+(T2*H2)))
   49     T3=6.*U*((HD-HM)/(HD**3))
   50     HE=HO+((X(I)+H)**2/2.)+(A*(P(I)+(T3*H)))
   51     T4=6.*U*((HE-HM)/(HE**3))
   52     P(I+1)=P(I)+H*(T1+2.*T2+2.*T3+T4)/6.
   53     X(I+1)=X(I)+H
   54     XT(I+1)=X(I+1)**2/2.
   55     Q(I+1)=A*P(I+1)
   56     HA(I+1)=HO+XT(I+1)+Q(I+1)
   57     COUNT=COUNT+1
   58     IF(COUNT-2)59,63,68
   59     HN(2)=HN(1)/ADJ
   60     HM=HN(2)
   61     IF(P(N)-B)62,78,138
   62     IF(P(N)+B)114,78,78
   63     IF(P(N)+B)64,78,1114
   64     HN(3)=(HN(1)+HN(2))/2.
   65     HM=HN(3)
   66     KO=KO+1
   67     IF(KO-2)138,138,138
   68     IF(P(N)-B)69,78,169
   69     IF(P(N)+B)174,78,78
  169     HN(1)=HN(3)
   70     HN(3)=(HN(1)+HN(2))/2.
   71     HM=HN(3)
   72     ADD=ADD+1
   73     IF(ADD-200)138,114,114
  174     HN(2)=HN(3)
   74     HN(3)=(HN(1)+HN(2))/2.
   75     HM=HN(3)
   76     ADD=ADD+1
   77     IF(ADD-200)138,114,114
   78     D=(CE-X(1))/C
   79     J=1
   80     S(J)=X(1)
   81     HX(J)=HA(1)
   82     DO 84 J=1,M
   83     S(J+1)=S(J)+C
   84     HX(J+1)=HO+S(J+1)**2/2.
   85     DO 86 I=1,N
   86     F(I)=((1.-((3.*(HA(I)-HM))/HA(I))))/HA(I))
   87     MO=N-1
   88     W=0
   89     DO 91 I=2,MO
   90     QUAD=2.*P(I)
   91     W=W+QUAD
   92     W=(P(1)+P(N)+W)*(-(H2))
  192     SUMF=0
   93     DO 95 I=2,MO
   94     RECT=2.*F(I)
   95     SUMF=SUMF+RECT
  196     SUMF=(F(1)+F(N)+SUMF)*(-(H2))
   96     FER=U*SUMF
   97     DO 98 J=1,M
   98     CF(J)=(HM/(X(J)**2))
   99     JO=M-1
  100     SUMC=0
  101     DO 103 J=2,JO
  102     DBLC=2.*CF(I)
  103     SUMC=SUMC+DBLC
 1104     SUMC=((CF(1)+CF(M)+SUMC)*C)/2.
  104     CFER=U*SUMC
  105     TF=FER+CFER
  106     UFER=FER/W
  107     UTF=TF/W
  108     DO 109 I=1,N
  109     WRITE(6,2)X(I),P(I),HA(I),XT(I),Q(I),F(I)
  110     DO 111 J=1,M
  111     WRITE(6,3)S(J),HX(J),CF(J)
  112     WRITE(6,4)W,FER,CFER,TF
  113     WRITE(6,5)UFER,UTF
 1114     WRITE(6,1115)X(N),P(N)
  114     STOP
          END
```

APPENDIX 4

Determination of Elastic Constants for the Soft Layers

The E.V.A. Polythene Copolymer, from which the elastic specimens were made, was said by I.C.I. to have a modulus of elasticity in tension in the region of 1500 lb/in^2.

The important elastic constants for computing purposes were the moduli in compression of the copolymer in the free and confined conditions. It will be remembered at this point from Chapter 4 that the dimensionless stiffness term,

$$A = {}^{t}/_{R} \cdot {}^{E}/_{E\ conf.}$$

where t = elastic specimen thickness

R = radius of roller

E = Modulus of compression in free state

E conf. = Modulus of compression in confined state.

Two methods were used to determine the values of E and E conf. and these are described in the following text.

Method 1. Compression Chamber

Fig. A.1 (a) and (b) shows drawings of the compression chamber which was designed to test the copolymer in the free and confined condition. The compression chamber basically consisted of a bottom plate and removable cylinder into which fitted a piston. Fig. A.2. shows a photograph of the exploded compression chamber.

A typical result of load against deflection obtained is shown in Fig. A.3. The non-linear shape of the curve for the confined test indicated that the specimen was not a perfect fit in the cylinder

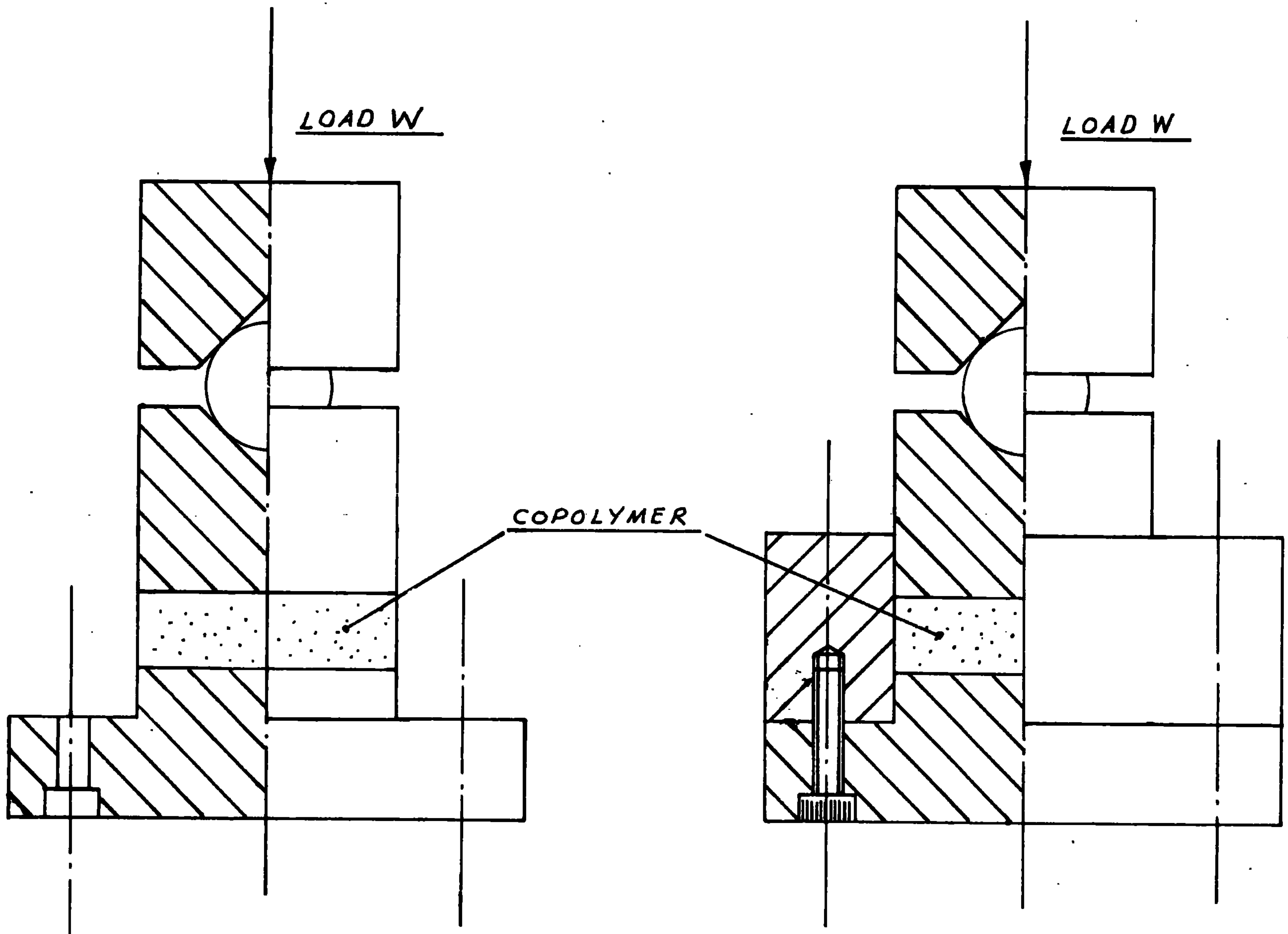

FIG. A.1(a) FREE COMPRESSION

FIG. A.1(b) CONSTRAINED COMPRESSION

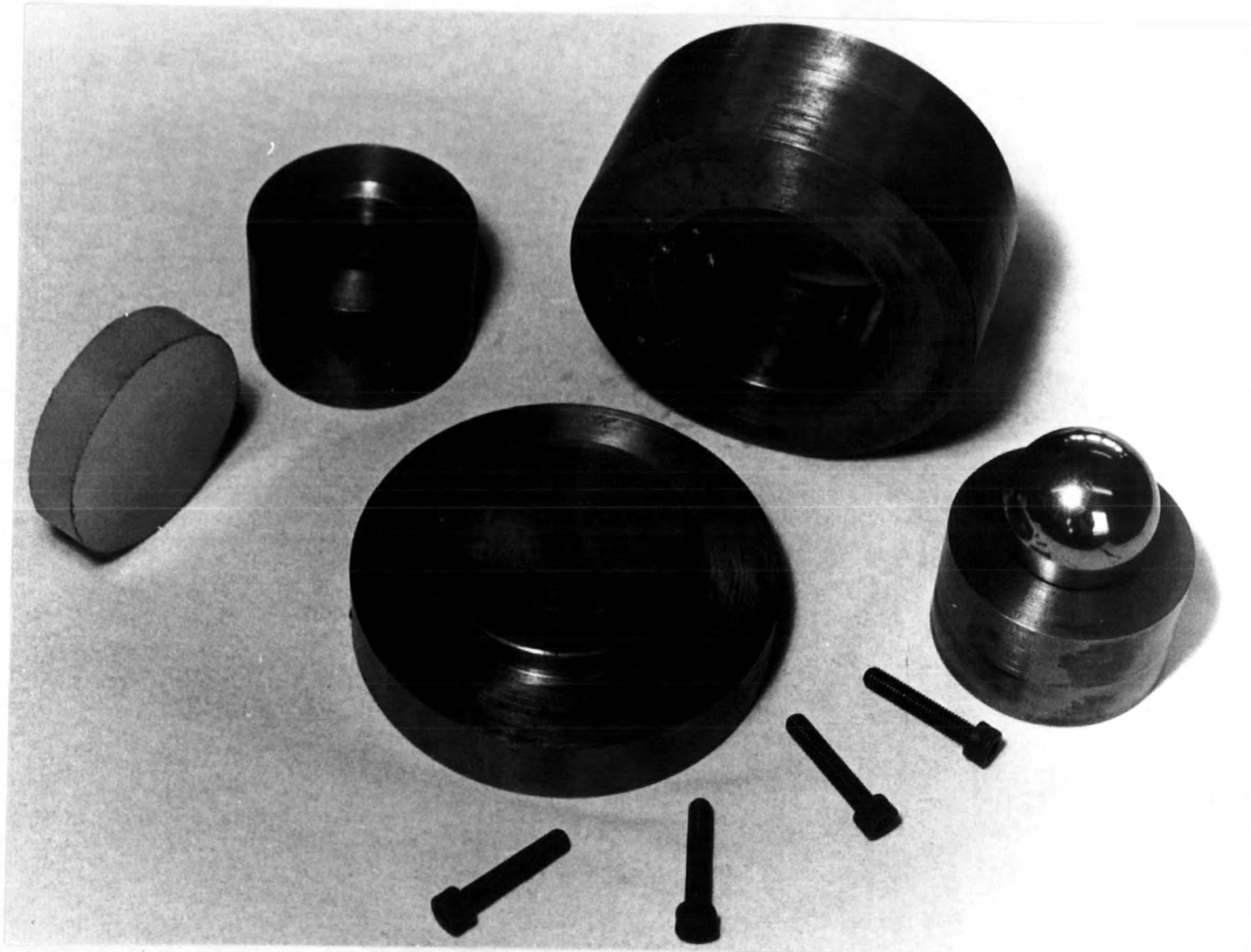

Fig. A.2. EXPLODED VIEW OF COMPRESSION CHAMBER

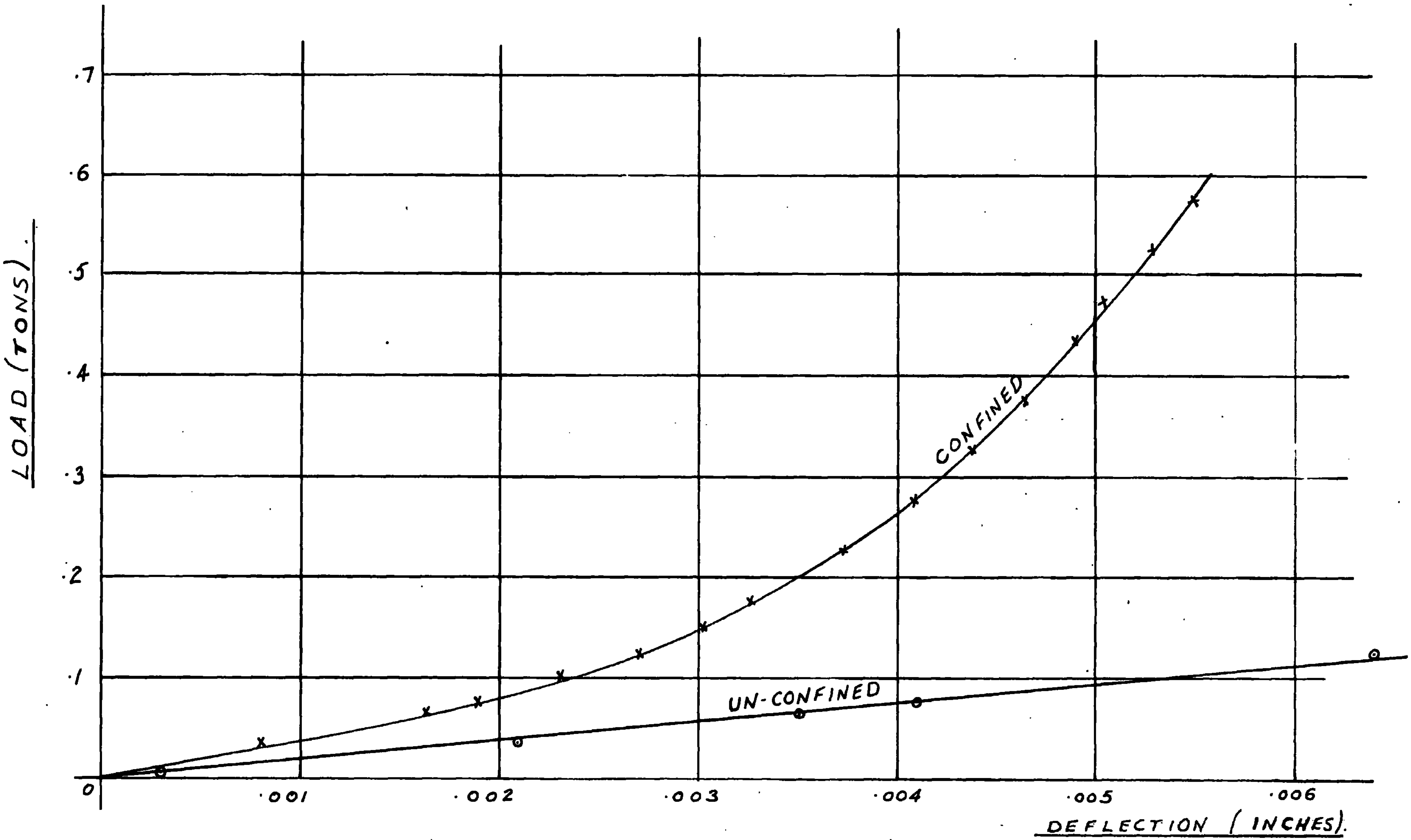

FIG. A.3. GRAPHS OF LOAD ~ EXTENSION FOR ·5" THICK SPECIMEN.

and so it was decided that some other means of determining E conf. must be used.

<u>Method 2. Use of Modified Friction Measuring Rig</u>

The roller rig was modified to press one roller on to an elastic specimen secured to a thick (and effectively rigid) Perspex backing plate.

Loads were applied to the roller while the rig was in the static condition. The width of the field of compression for each load was measured using a travelling microscope. The results obtained were compared to theoretical results obtained from a simple theory as follows.

With the roller pressed against the polymer the resulting contact zone will be of width 2b.

Then referring to Fig. A.4.

$$\delta o \times 2R = b^2$$

assuming δo to be small compared to R

$$\delta o = b^2/2R$$

and $$\delta = \delta o - \frac{x^2}{2R} = \frac{1}{2R}(b^2 - x^2)$$

$$p = \frac{\lambda}{2R}(b^2 - x^2)$$

as $\delta = {}^{p}/_{\lambda}$ where λ is the stiffness of the plymer

$\therefore$ w, the load/unit length of the roller will be

$$w = \int_{-b}^{b} p \, dx$$

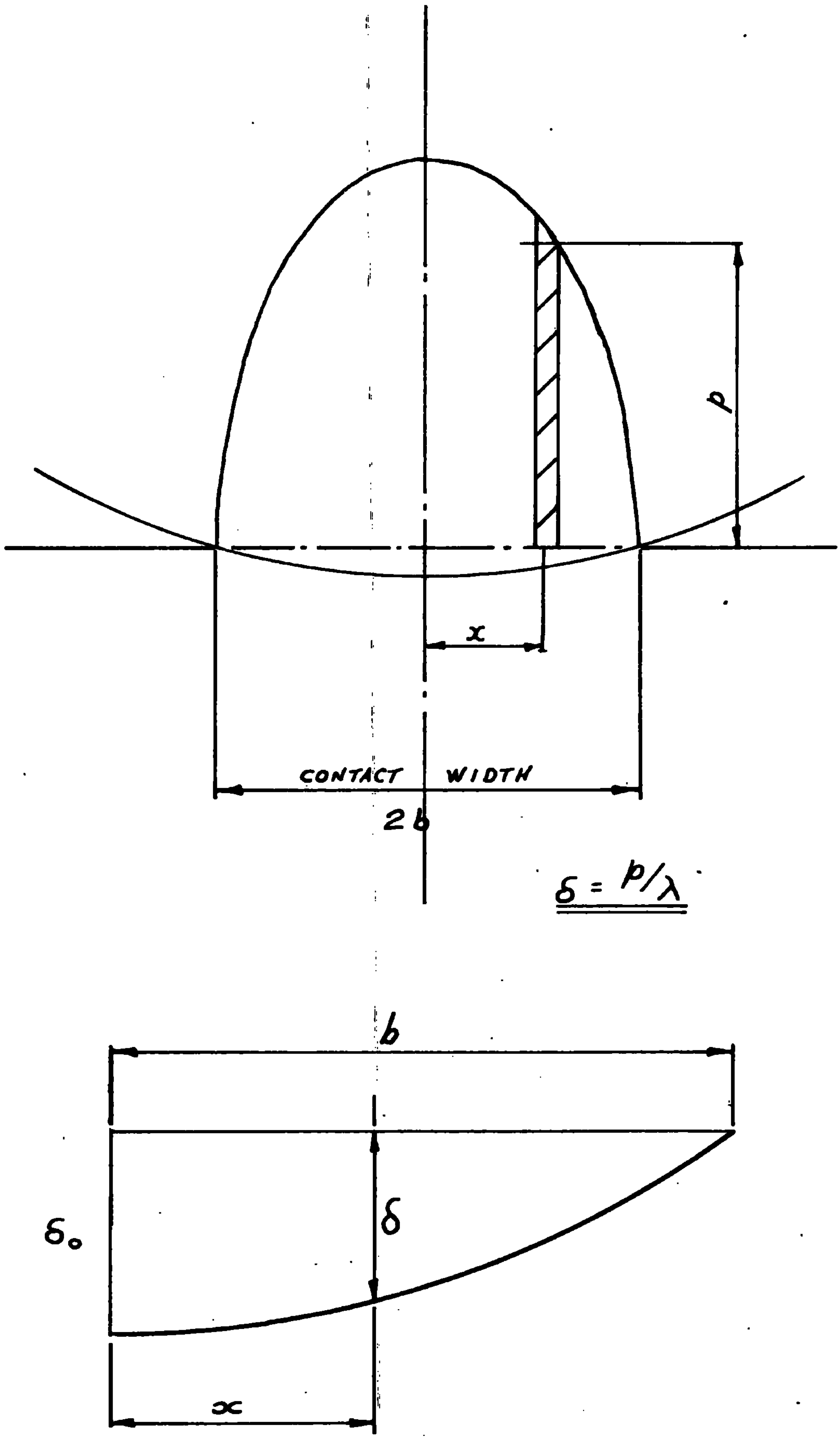

FIG. A.4. DEFORMATION OF POLYMER IN STATIC CONDITION.

$$= \frac{\lambda}{2R} \left[b^2 x - x^3/3 \right]_{-b}^{b}$$

$$\therefore w = {}^2/_3 \cdot \frac{\lambda b^3}{R}$$

Figs. A.5., 6 and 7 show the experimental and theoretical curves of field width, 2b, against load for the .05, .1 and .2 inch thick specimens. The curves corresponded fairly well and the results from the tests were used to determine the dimensionless stiffness term, A, for computing purposes. The values were:

Thickness (in)	E con (lb/in^2)	A
.05	16372	8.42×10^{-3}
.10	16500	15.40×10^{-3}
.20	14800	36.55×10^{-3}

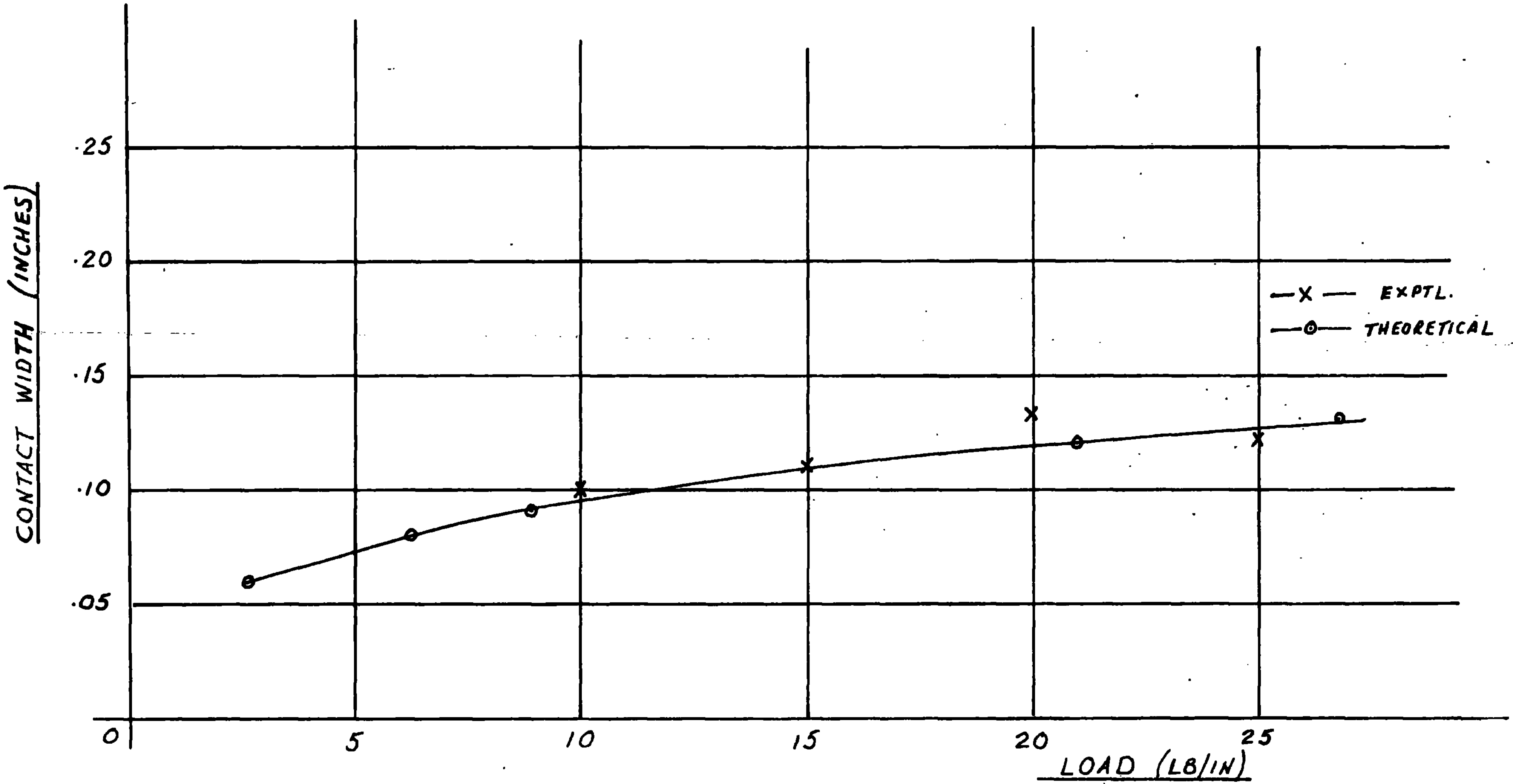

FIG. A.5. COMPARISON OF CONTACT WIDTHS ~ LOAD (THEORETICAL & EXPTL.) FOR ·05" SPEC.

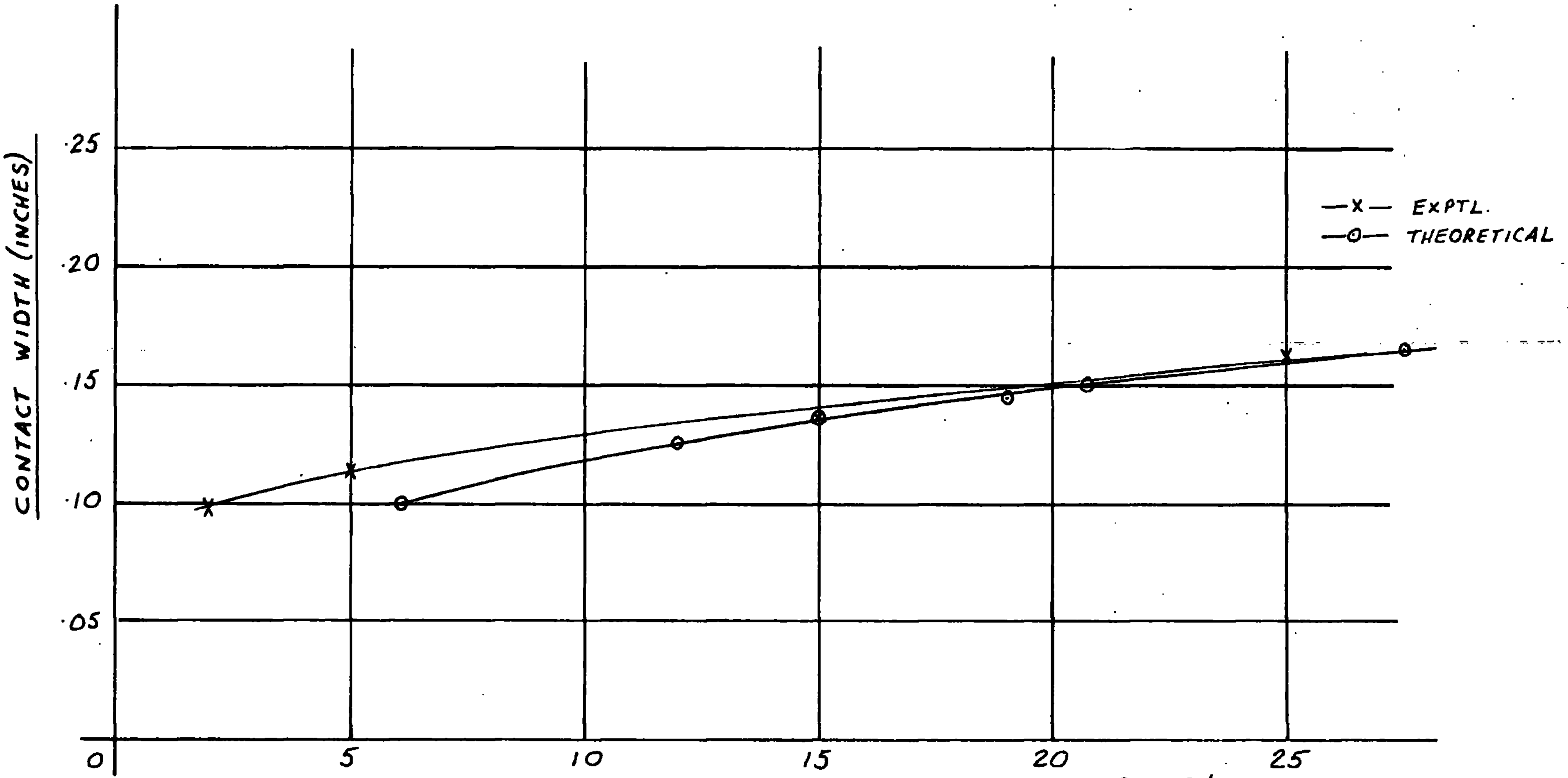

FIG. A.6. COMPARISON OF CONTACT WIDTHS ~ LOAD (THEORETICAL & EXPTL.) FOR ·1" SPEC.

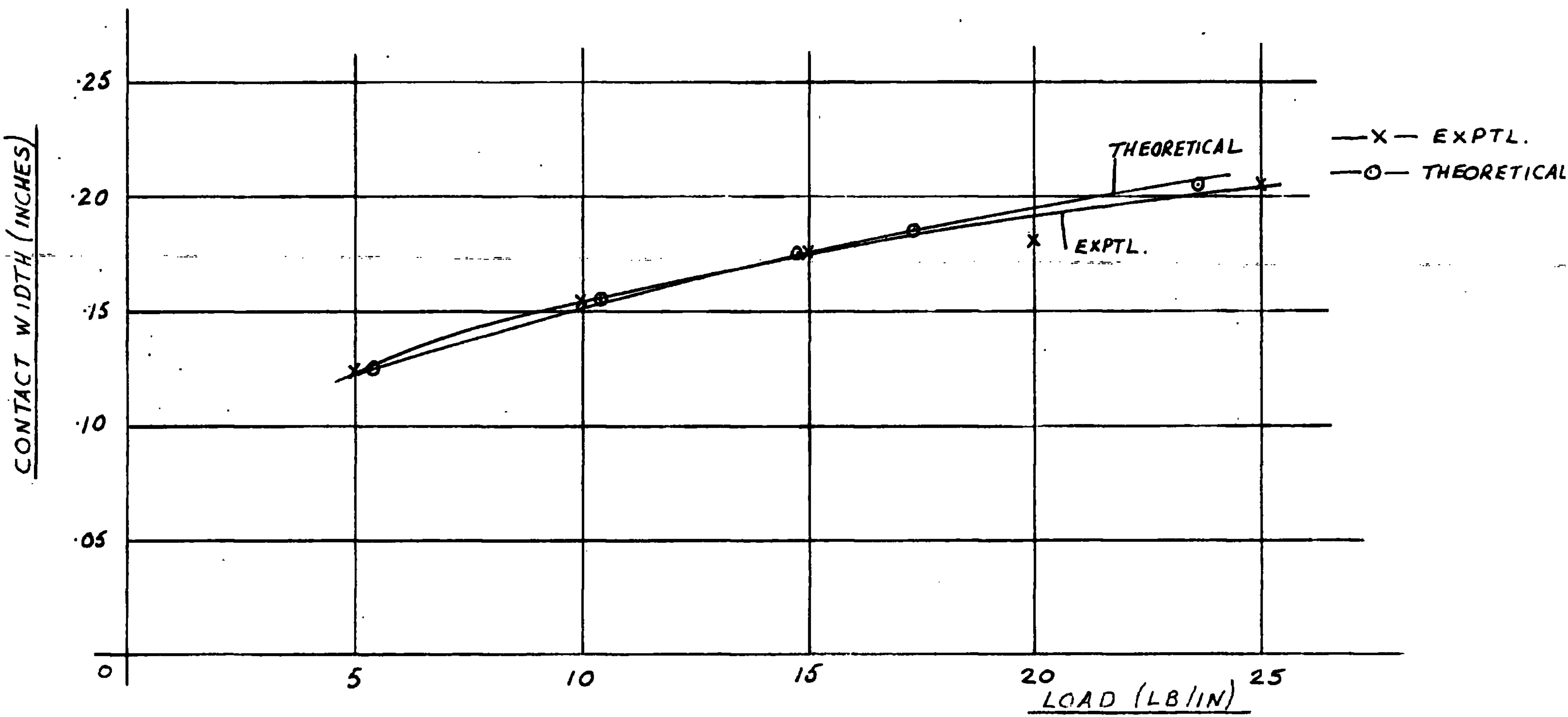

FIG. A. 7. COMPARISON OF CONTACT WIDTHS ~ LOAD (THEORETICAL & EXPTL.) FOR ·2" SPEC.

APPENDIX 5

References

1.	Brighton, D.K., Hooke, C.J. and O'Donoghue, J.P.	1967-68 Proc. I.Mech.E., Vol. 182, 3N.
2.	Cohen, S.C. and Tabor, D.	1966 Proc. Roy. Soc. A 291, 186.
3.	Denny, D.F.	1953 Proc. Phys. Soc. Series B 66,721.
4.	Dowson, D., and Higginson, G.R.	J. Mech. Eng. Science 1959. No. 1.6.
5.	Dowson, D., and Higginson, G.R.	'Elasto-hydrodynamic Lubrication'. 1966. Pergamon Press.
6.	Dowson, D., Longfield, M.D., Walker, P.S., and Wright, V.	Proceedings Inst.Mech.E. 1967-68. Volume 182, Part 3N.
7.	Dowson, D., and Whitaker, A.V.	A.S.L.E. preprint 64. LC-22 Washington Conference. 1964.
8.	Dowson, D., and Whomes, T.L.	Proceedings Inst.Mech.E. 1966-67. Vol. 181, Part 30.
9.	Fogg, A., and Hunswicks, S.A.	1937. I.Mech.E. General Discussion on Lubrication and Lubricants.
10.	Higginson, G.R.	Proceedings Inst. Mech.E. 1965-66. Vol. 180, Part 3B.
11.	Hooke, C.J., Brighton, D.K., and O'Donoghue, J.P.	Proceedings Inst.Mech.E. 1966-67. Vol. 181, Part 3B.
12.	Jagger, E.T.,	Proceedings of Inst.Mech.E. 1967-68. Vol. 182, 3A.
13.	King, R.F., and Tabor, D.	1953. Proc. Phys. Soc. Series B 66,728.
14.	Pascoe, M.W., and Tabor, D.	1956. Proc. Phys. Soc. Series A 235,210.
15.	Watanabe, M., Karasawa, M., and Matsubara, M.	1968. Wear, 12, 185.